Conception et évaluation de systèmes transporteurs de principes actifs hydrophobes à base de polysaccharides modifiés : vers de nouvelles approches pour la thérapie anti-cancéreuse

Jing Jing

UNIVERSITÉ DE GRENOBLE

THÈSE

Pour obtenir le grade de

DOCTEUR DE L'UNIVERSITÉ DE GRENOBLE

Spécialité : **Sciences des polymères**

Arrêté ministériel : 7 août 2006

Présentée par

Jing JING

Thèse dirigée par Rachel AUZELY-VELTY

préparée au sein du Centre de Recherches sur les Macromolécules Végétales (CERMAV-CNRS)
dans l'École Doctorale de Chimie et Science Vivante

Design and evaluation of hydrophobic drug delivery systems based on chemically modified polysaccharides: toward new approaches for anti-cancer therapy

Thèse soutenue publiquement le **« 26 mars 2013 »**,
devant le jury composé de :

M. Denis WOUESSIDJEWE
Professeur UJF, Département de Pharmacochimie Moléculaire, Président
Mme. Min-Hui LI
Directeur de recherche, Institut Curie – CNRS, Rapporteur
M. Benoit FRISCH
Directeur de recherche, Université Louis Pasteur – CNRS, Rapporteur
Mme. Catherine PICART
Professeur INP Grenoble, Laboratoire des matériaux et du génie physique – Minatec, Membre
Mme. Liliane GUERENTE
Maître de conférence UJF, Département de Chimie Moléculaire, Membre
M. Bruno De GEEST
Professeur, Ghent University, Membre
Mme. Rachel AUZELY-VELTY
Professeur UJF, CERMAV – CNRS, Directeur de thèse

Université Joseph Fourier / Université Pierre Mendès France / Université Stendhal / Université de Savoie / Grenoble INP

Acknowledgments

Completing a PhD is truly a marathon event, and I would not have been able to complete this journey without the aid and support of countless people over the past seven years.

First of all, I express my deeply gratitude to my supervisor, Professor Rachel Auzély-Velty. To work with you has been a real pleasure to me. You have been a steady influence throughout my PhD career; you have oriented and supported me with promptness and care, and have always been patient and encouraging in times of new ideas and difficulties. Your ability to select and to approach compelling research problems, your high scientific standards, and your hard work set an example. Above all, you made me feel a friend, which I appreciate from my heart.

Thanks to M. Reduane Borsali for giving me the chance to work in CERMAV.

Furthermore, I am very grateful to Professor Catherine Picart and Professor Bruno De Geest, for their satisfying collaboration in the biological studies. Many of interesting results would not have been possible without your support both in my work and in this thesis.

In addition, I am indebted to many people for spending the time working with me, making these years an unforgettable experience.

I learned a lot from you, Anna Szarpak-Jankowska, about life, research, how to tackle new problems, discuss with you frequently led to key insights.

To Isabelle Pignot-Paintrand, Amandine Durand Terrasson, Marc Block for the help with microscopic techniques. Thank you Isabelle, I admire your seriousness and patience.

To Marie France Marais, thank you for teaching me so clearly to work in sterile conditions.

To Eric Bayma, Martine Morales, Isabelle Caldara, all of your aids allowed me to work in the best conditions.

I am appreciated to Isabelle Jeacomine, Christophe Travelet, and Cyril Bras for their technique supporting in my PhD work. I am also appreciated to Jimmy Mergy and Di Cui for your useful and great help in my thesis.

I am also indebted to all friends of or yet left of CERMAV, Agathe Belime, Talitha Fernandes Stefanello, Emile Hachet, Audrey Fournier, Xia Miao, Hélène Van Den Berghe, Celso Vataru Nakamura… You have been an invaluable support day in, day out, during all these years. Also for my special friends outside of CERMAV Raphaël Guillot, Varvara Gribova, Prathamesh Kharkar, I had the pleasure to work with you.

Finally, I would like to thank Yan Xu for your love and encouragement. And, thank you for your support when I have needed it the most. Thank you with all my heart! And my son, you are the best bonus of my thesis, you gave me so many happy, I love you so much!! Thanks to my mom, dad, and sister for your infinite support throughout everything.

Table of contents

General introduction (en)

Although conventional treatment options of cancer such as chemotherapy, radiation and surgery have experienced significant advances over the past few decades, they remain far from optimal. Nanotechnology, led by the development of nanoparticle-based drug delivery systems and imaging contrast agents, has had an important role in diagnosis, prevention, and treatment of the disease. The use of nanotechnology for cancer therapy and imaging is expected to overcome the limitations of conventional treatments, such as poor drug bioavailability, nonspecific systemic drug distribution, inadequate drug concentrations reaching the tumor and inability to monitor therapeutic responses in real time. Some nanotechnology-based formulations have been already approved by the US Food and Drug Administration, like Doxil®, Abraxane®… However significant challenges remain regarding in particular the methods used to produce sophisticated multifunctional nanoparticles. Most of the procedures developed to date to prepare nanoparticles involve the use of toxic solvents and surfactants, which require intensive postprocessing purification.

Nanoengineered capsules composed of sequentially assembled polymer layers hold promise for a variety of biomedical applications. These capsules are prepared by the layer-by-layer assembly of oppositely charged polyelectrolytes onto a sacrificial colloidal template followed by core removal. The assembly process allows for nanoscale manipulation of the properties of the capsules, including size, composition, permeability, stability, surface functionality as well as sensitivity to chemical or physical stimuli. However, their hydrophilic multilayer shell and their aqueous cavity pose difficulties to incorporate hydrophobic drug molecules. In this context, we proposed to develop an original and versatile approach to selectively encapsulate hydrophobic molecules in the nanoshell of multilayered capsules. We focused on the design of biocompatible and biodegradable multilayer capsules using hyaluronic acid (HA) as the polyanion partner, based on previous work performed in our laboratory showing the ability to prepare multilayer capsules from this natural polysaccharide[1], and to obtain various functional derivatives of HA under mild aqueous conditions[2-4]. Moreover, HA can be specifically recognized by the CD44 receptor that is over-expressed by several cancer cells including human breast epithelial cells[5] and human ovarian tumor cells[6]. This unique property may provide a distinct advantage over other macromolecular building blocks that may be used for the fabrication of drug delivery systems.

In this regard, this polysaccharide has been recently exploited to design nanogels. Nanogels are swollen nanosized networks composed of hydrophilic or amphiphilic polymer chains.

They are developed as carriers for the transport of drugs, and can be designed to spontaneously incorporate biologically active molecules through formation of hydrogen bonds, electrostatic or hydrophobic interactions. One part of this thesis includes the synthesis, the physico-chemical characterization and the investigation of the biological properties of hydrophobic anti-cancer drug loaded nanogels based on HA.

The work presented in this thesis were performed in the group "Structure and Modification of Polysaccharides" of the CERMAV. One of the objectives of the researches performed in this group is to obtain structurally controlled tailor-made biopolymers with potential applications in the cosmetic, pharmaceutical and biomedical fields, in particular. The PhD work were made possible thanks to close collaborations with the Professor Catherine Picart (Laboratory of Materials and Physical Engineering (LMGP)-Minatec, INP Grenoble) and the Professor Bruno De Geest (Ghent University, Belgium) who provided strong scientific support for the physico-chemical and biological characterization of the carrier systems. They were additionally supported by the Agence Nationale de la Recherche ("BIOCAPS" project of the PNANO program).

This thesis manuscript is divided into four sections:

The first chapter overviews the NPs for cancer therapy and imaging, including their general characteristics, their passive and active targeting toward tumors and their controlled drug release properties.

The second chapter describes two types of capsules prepared with alkylated HA derivatives and quaternized chitosan (QCHI) or poly(L-lysine) (PLL). A hydrophobic dye nile red and an anti-cancer drug paclitaxel (PTX) were incorporated individually in the shell of capsules. The amount of the dye or drug entrapped per capsule was determined. The stability of the alkylated HA/QCHI capsules and the alkylated HA/PLL capsules in culture media was also investigated. Finally, we examined the cytotoxic effect of PTX loaded alkylated HA/PLL capsules on breast cancer cells.

In the third chapter, we report on the design of another type of capsules based on HA which can also incorporate water-insoluble molecules in the shell. Our strategy for the design of such capsules was based on the use of a HA derivative possessing pendant β-cyclodextrin molecules (HA-CD) as a polyanion. This derivative can form host-guest complexes with hydrophobic molecules through inclusion in the hydrophobic CD cavity. PTX was thus encapsulated in the capsules and their effective loading and release properties were studied.

Similarly to the capsules based on alkylated HA, we examined the cytotoxic effect of PTX loaded capsules prepared from HA-CD on breast cancer cells.

The last chapter presents self-assembled nanogels based on HA. A thermosensitive copolymer of diethyleneglycolmethacrylate and oligoethyleneglycolmethacrylate was grafted onto HA chains leading to a graft hybrid copolymer (HA-poly(DEGMA-co-OEGMA)). Upon increasing the temperature at the body temperature, HA-poly(DEGMA-co-OEGMA) spontaneously formed nanogels and encapsulated PTX in their hydrophobic nanodomains. The PTX-loaded nanogels exhibited a high selectivity towards cells overexpressing the CD44 receptor for HA on their surface.

Introduction générale (fr)

Malgré les progrès réalisés ces dernières années en chimiothérapie, en radiothérapie et en chirurgie pour traiter le cancer, ces méthodes conventionnelles sont encore loin d'être optimales. Parmi les différentes approches issues des nanotechnologies, l'utilisation de vecteurs nanoparticulaires, cargos de taille nanométrique, s'est imposée comme une des solutions envisageables pour augmenter l'efficacité des traitements existants, tout en réduisant leur toxicité systémique. Ces vecteurs permettent d'outrepasser les limitations des approches conventionnelles non seulement en thérapie mais aussi en imagerie et en diagnostic, en améliorant par exemple la solubilité en milieu aqueux des principes actifs, leur efficacité thérapeutique (en favorisant leur accumulation au niveau du tissu cible), la capacité à évaluer les réponses thérapeutiques. Certaines formulations ont été approuvées par l'agence américaine de réglementation des médicaments et des produits alimentaires (FDA), comme le Doxil®, l'Abraxane®… Néanmoins, ces systèmes nanoparticulaires ne remplissent pas toutes les caractéristiques nécessaires pour pouvoir véhiculer un principe actif sélectivement vers des cellules ou tissus cibles et le libérer de manière contrôlée. Ces caractéristiques constituent des défis importants qui passent par la conception de nanoparticules plus sophistiquées, combinant plusieurs fonctions. Par ailleurs, à ce jour, la plupart des procédés utilisés pour préparer des nanoparticules impliquent l'utilisation de solvants toxiques et/ou des tensioactifs, ce qui impose des étapes de purification et de post-traitement intensifs.

Les capsules préparées par assemblage couche-par-couche de polymères de charges opposées sur un support colloïdal, suivi de sa décomposition, sont apparues comme une nouvelle approche prometteuse pour transporter des principes actifs. Le procédé d'assemblage permet de moduler facilement les propriétés des capsules, notamment leur perméabilité, leur stabilité ainsi que leur leur interaction avec les espèces biologiques via leur fonctionnalités en surface. Cependant, leur paroi hydrophile et la cavité aqueuse engendrent des difficultés pour intégrer des molécules hydrophobes. Dans ce contexte, nous nous sommes proposés de développer des approches originales et modulables pour encapsuler sélectivement des molécules hydrophobes dans la paroi de capsules multicouches. Ces travaux s'appuient sur des études antérieures menées au sein de notre laboratoire et portant sur la conception de capsules biocompatibles et biodégradables à base d'acide hyaluronique (HA)[1], ainsi que de différents dérivés de HA en milieu aqueux.[2-4] Par ailleurs, le HA est un ligand du récepteur protéique CD44 qui est surexprimé par plusieurs cellules cancéreuses, notamment les cellules épithéliales (carcinome) de la glande mammaire[5] et les cellules tumorales ovariennes[6]. Cette propriété unique de HA

offre un avantage distinct par rapport aux autres macromolécules pour l'élaboration de systèmes de vectorisation d'agents anti-cancéreux.
A cet égard, ce polysaccharide a été récemment exploité pour la conception de nanogels. Les nanogels sont des réseaux tridimensionnels de taille nanométrique composés de chaînes de polymères hydrophiles ou amphiphiles. Du fait de leur capacité à incorporer divers types de (macro)molecules actives par formation de liaisons hydrogène, d'interactions électrostatique et/ou hydrophobes, ces systèmes suscitent un intérêt croissant pour transporter des médicaments. Une partie de cette thèse est ainsi consacrée à la synthèse et la caractérisation de nanogels à base de HA capables d'encapsuler des agents anti cancéreux hydrophobes.

Les travaux présentés dans ce manuscrit ont été effectués au sein de l'équipe "Structure et Modification des Polysaccharides" du CERMAV et s'inscrivent parmi les thématiques du groupe visant à développer de nouveaux polysaccharides modifiés en vue d'obtenir des structure contrôlée sur mesure de biopolymères avec des applications potentielles dans les domaines cosmétiques, pharmaceutiques et biomédicales, en particulier. Les travaux de thèse ont été rendus possibles grâce à la collaboration étroite avec le Professeur Catherine Picart (Laboratoire des Matériaux et Génie des Procédés (LMGP)-Minatec, INP Grenoble) et le Professeur Bruno De Geest (Ghent University, Belgique). Le projet est financé par l'Agence Nationale de la Recherche.

Ce manuscrit de thèse est divisé en quatre chapitres :

Le premier chapitre est consacré à un mise au point sur les nanoparticules utilisées pour la traitement du cancer et l'imagerie. Il décrit leurs propriétés générales, leur caractéristiques en termes de ciblage passif et actif vers les tumeurs ainsi que les stratégies de libération contrôlée de médicaments.

Le second chapitre présente deux types de capsules préparées à partir de dérivés alkylés de HA et de dérivés du chitosane quaternisé (QCHI) ou de poly (L-lysine) (PLL). Une sonde fluorescente et un agent anticancéreux hydrophobes (le Nile red et le paclitaxel (PTX), respectivement) ont été incorporés individuellement dans la paroi des capsules. La quantité de molécules hydrophobes encapsulées a été déterminée. La stabilité des capsules HA-alkylé /QCHI et HA-alkylé /PLL dans un milieu de culture a également été étudiée. L'activité biologique des capsules HA-alkylé/PLL vis-à-vis de cellules du cancer du sein (MDA MB 231) a été étudiée.

Dans le troisième chapitre, nous décrivons la synthèse et l'étude d'un autre type de capsules préparées à partir de HA capables également d'incorporer des molécules

hydrophobes dans la paroi. Cette stratégie a été réalisée par greffage de la β -cyclodextrine sur le HA pour conduire à des biopolymères (HA-CD) capables de former des complexes d'inclusion avec des molécule hydrophobes. Le PTX a été encapsulé dans ces capsules. La quantité de PTX incorporé dans la paroi et la libération de PTX ont été étudiées. L'activité biologique des capsules HA-CD /PLL vis-à-vis de cellules du cancer du sein (MDA MB 231) a également été évaluée.

Le dernier chapitre porte sur l'élaboration de nanogels auto-assemblés à base de HA. Un copolymère thermosensible, le diéthylèneglycolméthacrylate - oligoéthylèneglycolméthacrylate (poly(DEGMA-OEGMA)), a été greffé sur des chaînes de HA (HA-poly(DEGMA-OEGMA)). Lors du chauffage à 37 °C, les dérivés HA-poly(DEGMA-co-OEGMA) synthétisés conduisent à la formation de nanogels, dans lesquels le PTX peut être incorporé. Les nanogels chargés en PTX montrent une cytotoxicité importante vis-à-vis de cellules cancéreuses CD44+ (cellules du cancer ovarien SKOV-3, surexprimant le récepteur CD44).

References

(1) Szarpak, A.; Cui, D.; Dubreuil, F.; De, G. B. G.; De, C. L. J.; Picart, C.; Auzely-Velty, R. *Biomacromolecules* **2010**, *11*, 713-720.

(2) Kadi, S.; Cui, D.; Bayma, E.; Boudou, T.; Nicolas, C.; Glinel, K.; Picart, C.; Auzely-Velty, R. *Biomacromolecules* **2009**, *10*, 2875-2884.

(3) Charlot, A.; Auzely-Velty, R. *Macromolecules* **2007**, *40*, 1147-1158.

(4) Charlot, A.; Heyraud, A.; Guenot, P.; Rinaudo, M.; Auzely-Velty, R. *Biomacromolecules* **2006**, *7*, 907-913.

(5) Iida, N.; Bourguignon, L. Y. W. *J. Cell. Physiol.* **1997**, *171*, 152-160.

(6) Bourguignon, L. Y. W.; Zhu, H.; Chu, A.; Iida, N.; Zhang, L.; Hung, M.-C. *J. Biol. Chem.* **1997**, *272*, 27913-27918.

Chapter 1

Nanotechnology for cancer treatment - Bibliography review

1.1. Résumé (fr)

Depuis une quinzaine d'années et les avancées en nanotechnologies, les chercheurs ont eu pour idée d'utiliser des nanoparticules comme moyen de "locomotion" d'agents anti-cancéreux afin d'être plus précis et de n'attaquer que la tumeur. Des spécialités pharmaceutiques à base de vecteurs de médicaments à visée anticancéreuse ont été lancées récemment sur le marché. De ces progrès résultent déjà aujourd'hui une diminution des doses prescrites, une baisse de la toxicité et une meilleure tolérance thérapeutique. L'utilisation de systèmes transporteurs d'agents anti-cancéreux offre également l'espoir d'une approche thérapeutique combinatoire, par l'ingénierie de nanoparticules délivrant plusieurs drogues destinées à neutraliser différentes cibles au sein d'une même tumeur. Par ailleurs, le développement de nouveaux outils pour l'imagerie offre aujourd'hui l'espoir d'un diagnostic précoce et non-invasif du cancer, ce qui devrait permettre de réduire le nombre de cas de cancers évoluant vers un stade terminal. Ainsi, l'application biomédicale des outils issus de la nanotechnologie permet d'envisager l'évolution vers une médecine personnalisée, dans laquelle chaque patient et chaque cancer seront traités comme des cas individuels.

Ce chapitre a ainsi pour but de situer le travail dans son contexte bibliographique en faisant une mise au point sur les stratégies de vectorisation développées à ce jour dans le domaine de la thérapie anti-cancéreuse.

Celles-ci reposent de manière générale sur la mise au point de formulations nanoparticulaires de nature organique (particules constituées de lipides, de polymères, de protéines ou encore de peptides) ou inorganique. Il est important de souligner que grâce à leur taille submicromique, ces systèmes transporteurs s'accumulent préférentiellement dans les tissus tumoraux dont le système vasculaire présente des porosités (400 - 600 nm). Cet effet "EPR" (Enhanced Permeability and Retention) permet ainsi un "ciblage passif" des tumeurs. Couplée à d'autres caractéristiques chimiques, l'utilisation de systèmes nanoparticulaires permettrait également de proposer des stratégies de "ciblage actif" des cellules cancéreuses. La possibilité de fonctionnaliser la surface des particules avec différents agents de ciblage devrait ainsi permettre d'améliorer significativement les propriétés pharmaceutiques de tels systèmes. D'autres stratégies « intelligentes », conçues en guise de ciblage, consistent à exploiter les propriétés caractéristiques des cellules cancéreuses et des tumeurs. En particulier leur métabolisme très actif associé à l'acidification de l'environnement tumoral, à la sécrétion de protéases (métalloprotéases) peut être avantageusement utilisé pour favoriser le ciblage

spécifique des nanoparticules thérapeutiques (présentant un élément activable par le pH ou par clivage protéolytique) vers les cellules cancéreuses. Toutes ces approches passent par la fonctionnalisation chimique adéquate des vecteurs, ce qui peut être un frein au développement à plus ou moins grande échelle de ces systèmes " sur mesure ".

La mise au point de nouveaux vecteurs selon des procédés modulaires, utilisant des molécules biocompatibles est donc un axe de recherche important dans ce domaine. La technique de dépôt couche par couche de polyélectrolytes sur des surfaces solides constitue à ce titre une approche particulièrement intéressante pour concevoir des systèmes transporteurs dont les propriétés peuvent être facilement modulées. Cette technique, basée sur l'adsorption alternée de polyanions et de polycations sur des particules colloïdales sacrificielles, a permis d'obtenir à la fin des années 1990 de nouvelles formes de vecteurs multicompartiments, appelés capsules multicouches. Depuis une dizaine d'années, ces assemblages suscitent une attention considérable liée à la possibilité de conférer à la paroi des fonctionnalités diverses en fonction de sa composition chimique. Selon la nature des polyélectrolytes utilisés, il est ainsi possible de concevoir des capsules pouvant répondre efficacement à des stimuli physiques ou chimiques permettant une libération programmée des principes actifs encapsulés et/ou capables d'interagir sélectivement avec certaines cellules. Bien que la taille de l'ordre de quelques micromètres limite encore les applications in vivo de nouveaux systèmes transporteurs, certaines équipes ont commencé à développer des *nano*capsules.

1.2. Introduction

Cancer causes one in eight deaths worldwide, which represents more deaths than AIDS, tuberculosis, and malaria combined. According to recent World Health Organization projections, cancer has replaced ischemic heart disease as the overall leading cause of death worldwide in 2010. The total cancer deaths in 2008 were 7.6 millions (about 21,000 cancer deaths a day)[1]. Cancer is a generic group of diseases that can affect different parts of the body. Cancer occurs because of mutations in genes that control cell cycles. Four major characteristics of cancer cells are uncontrolled growth (uncontrolled division), invasion of adjacent tissue, metastasis (spreading to other locations in the body), and immortality (protection against programmed cell death).[2] Therefore, the increase in the efficacy of cancer treatment is an essential task for modern medicine.

Although localized tumors can be successfully removed by surgery, the treatment of spreading or metastatic tumors requires high-dose chemotherapy.[3] Current cancer therapies are largely limited by 1) the difficulty to deliver poorly water-soluble drugs; 2) the non-specific delivery and poor biodistribution of drugs; 3) the inability to bypass biological barriers; 4) the drug resistance of cancers and 5) the lack of an effective modality for treatment monitoring.[3-6] The application of nanotechnology to cancer therapy has the potential to overcome these challenges by enabling the engineered nanomedicines to navigate the body in very specific ways. Theranostic nanomedicines, mostly nanoparticles (NPs) carrying therapeutics, are designed to improve current cancer therapies by addressing the specific existing limitations. Nanoparticles may be constructed from a wide range of materials and used to encapsulate or solubilize chemotherapeutic agents for improved delivery in vivo or to provide unique optical, magnetic and electrical properties for imaging and therapy. One major advantage of nanoparticles is their potential to be used as non-invasive diagnostic tools. Another advantage is the capacity to combine multiple modalities in only one system, enabling higher sensitivity to be achieved and deeper insight gained into in vivo processes. The combination of molecular imaging and local treatment of lesions is unique for nano-objects and has the potential to change the current medical paradigm of “see and treat” to “detect and prevent”.[7] Several functional nanoparticles have already been demonstrated, including some clinically approved liposome drug formulations and metallic imaging agents. The next generation of nanoparticle-based research is directed to the consolidation of functions into strategically engineered multifunctional systems, which may ultimately

facilitate the realization of individual therapy. These multiplexed nanoparticles may be capable of identifying malignant cells by means of molecular detection, visualizing their location in the body by providing enhanced contrast in medical imaging techniques, killing diseased cells with minimal side effects through selective drug targeting, and monitoring treatment in real time.

The enhanced permeability and retention (EPR) effect

The term 'cancer' identifies a large group of complex and multifaceted diseases that are characterized by cells that have undergone mutations of their genetic material and whose growth is unregulated. Cancer cells tend to replicate at a higher rate than normal cells. The abnormalities present in the tumor tissue result in extensive leakage of blood plasma components and other macromolecules.[8] The greater permeability of tumor vessels to macromolecules compared with normal vessels, and the impaired clearance of these macromolecules from the interstitial space of the tumor (contributing to longer retention of these molecules), is called enhanced permeability and retention (EPR) effect[9] (**Figure 1.1**).

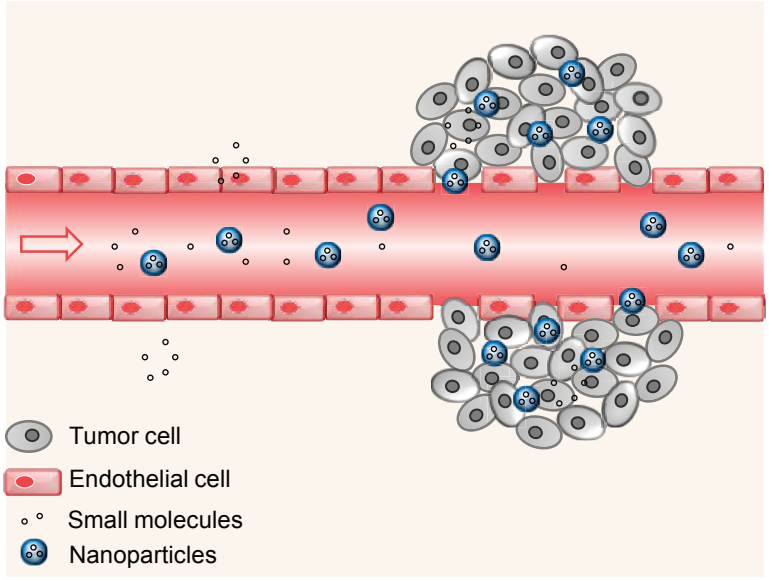

Figure 1. 1. Schematic illustration for enhanced permeability and retention (EPR) effect.

This effect, though not universally accepted, has been described as particularly relevant for particles with diameters greater than 100 nm[10] and will depend on tumor type and stage. The ability of macromolecules and NPs to accumulate specifically in tumor tissue has been studied extensively since Maeda et al.[11] first described the EPR effect twenty years ago. Inspired by

the EPR effect, many passive targeting strategies have been applied to deliver nanoscale drugs, therapeutics and imaging contrast enhancers to the tumor site, in which such agents are injected into the blood stream with the aim of accumulating preferentially at the tumor site. Nowadays, most drug delivery systems for cancer are being designed based on this principle, also with some clinical products.[12]

1.3. Nanoparticles for cancer therapy and imaging

1.3.1. Type of nanoparticles currently applied in cancer therapy

The utility of nanoparticles for the delivery of small molecule chemotherapeutics in vivo is now well established, with various formulations of doxorubicin (DOX), daunorubicin and paclitaxel (PTX) already commercially available (**Table 1.1)**. These drugs are the most potent chemotherapeutic agents used in cancer treatment. They are usually administered at a higher quantitative dosage because of their poor aqueous solubility, which increases the undesirable side effects. In general, nanoparticles are designed to circumvent limitations of conventional drug delivery systems, including nonspecific biodistribution and targeting, low aqueous solubility, poor bioavailability and low therapeutic indices stemming from insufficient drug concentration at disease sites.

Table 1. 1. Selected examples of nanomedicines for cancer treatment (approved or in clinical development).

Carrier type (size)	Active ingredient	Nanomedicine	Approval/clinical testing
Liposome (100 nm) [13]	Doxorubicin	Doxil®	Approved for multiple cancers
Liposome (100 nm) [14]	Daunorubicin	DaunoXome®	Approved for Kaposi's sarcoma
Liposome (100 nm) [15]	Doxorubicin, thermal release	ThermoDox®	Phase III: liver/HCC[a] Phase II: metastatic cancers
Colloidal albumin (123 nm)[16]	Paclitaxel	Abraxane®	Approved for metastatic breast cancer
Polymer-drug conjugate[b,17]	Paclitaxel	CT-2103 (Xyotax)	Phase III: ovarian, NSCLC[c]
PEG-PLA micelle[d,18,19]	Paclitaxel	Genexol-PM	Phase III: brease
Cyclodextrin-PEG micelle (30 nm) [20]	Camptothecin	CRLX-101 (formerly IT-101)	Phase II: lung (NSCLC[c]), ovarian
Cyclodextrin-PEG micelle (100 nm)[21,22]	siRNA (anti-RRM2)	CALAA-01 (Cyclosert)	Phase I: solid tumors
Aminosilane-coated	Magnetic	NanoTherm®	Approved (EU) for

SPIOs[e] (16 nm)[23]	hyperthermia		glioblastomas
Gold nanoparticle (27 nm) [24]	Tumor Necrosis Factor	CYT-6091 (Aurimmune)	Phase I: solid tumors
CM-dextrane[f]-Fe_3O_4 NPs (40-60 nm) [25]	Imaging agent (MRI contrast)	Resovist®	Approved for liver/HCC[a] imaging

[a]HCC: hepatocellular carcinoma. [b]Polymer-drug conjugate: poly(L-glutamic acid)-Paclitaxel. [c]NSCLC: non-small-cell lung cancer, the most common type of lung cancer. [d]PEG-PLA micelle: micelle formed from block copolymers of poly(ethylene glycol) and poly(D,L-lactic acid). [e]SPIO: superparamagnetic iron oxide. [f]CM-dextran: carboxymethyl dextran.

By a general definition, nanoparticles applied as drug delivery systems can include liposomes, other polymeric NPs, and inorganic NPs.

1.3.1.1. Liposomes

Liposomes are composed of natural lipid layers, and are classified according to the number of lipid bilayers as either unilamellar or multilamellar. The one or several lipid bilayers can solubilize hydrophobic drugs. Alternating aqueous compartments can entrap hydrophilic drugs[26,27] (**Figure 1.2**). Liposomes offer several advantages as drug delivery carriers. They are generally non-toxic and biocompatible. They are relatively easy to prepare and prevent accumulation of drugs in normal organs which reduces their toxicity and improves pharmacokinetic effects. Liposome properties such as size, surface charges, membrane rigidity and the phase transitions within the bilayer can be controlled either by selecting appropriate lipid compositions or by changing external conditions such as temperature, pH of the medium or the presence of specific agents[28,29]. When coupled with antibodies, liposomes can be used for active targeting[30-32]. At present, a few liposomal formulations are available in the market for the treatment of AIDS related Kaposi's sarcoma, breast, ovarian and other tumor types[33,34]. These liposomes employ the EPR effect to reach tumors where they act as drug depots. Release in the interstitium occurs mainly via disruption of the liposomal bilayer and through tumor uptake and subsequent drug release.

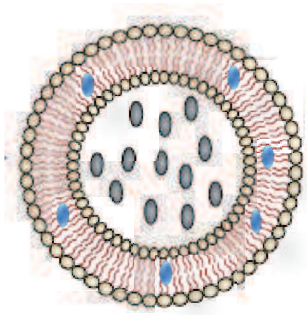

Figure 1. 2. Structure of a carrier liposome. Hydrophilic drugs can be loaded in the liposome interior, while hydrophobic drugs can be loaded between the lipid layers.

Although clinically successful in some applications, liposomes also have limitations. One of the problems with liposomes as drug delivery carriers is their lack of stability in biological fluids and during storage, nonspecific uptake by the mononuclear phagocytic system and rapid drug release profiles in vivo.[35] Consequently, drug molecules leak to normal tissues and cause undesirable side effects.

1.3.1.2. Polymeric nanoparticles

One class of polymeric NPs includes polymeric micelles (**Figure 1.3.a**) consisting of amphiphilic diblock and triblock copolymers, which can self-associate in selective solvents. The core regions of the micelles serve as reservoirs for hydrophobic drugs[36-39], whereas the hydrophilic exterior imparts stability to the carrier in aqueous environments[40,41]. Since their structures are primarily retained by noncovalent interactions, there is a need for further improving the in vivo stability of polymeric micelles. Another class of self-assembled structures of amphiphilic copolymers is that of polymersomes (**Figure 1.3.b**) which are characterized by a high stability and tunable membrane properties as allowing the triggered release of drugs.[42,43] Due to their multicompartment structure, these systems can encapsulate or integrate a broad range of hydrophilic or hydrophobic drugs. Several work focused on the design of polymersomes for targeted drug delivery.[43-45] In particular, the development of stimuli-reponsive polymersomes to further control the release of drugs by switching the stability and permeability of the membrane has attracted a lot of interest.[46-52]

To minimize inherent instability and degradation limitations associated with liposome and micelle formulations, other polymer-based drug carriers were developed. Compared with liposomes and micelles, polymeric systems demonstrate a series of attractive properties as pharmaceutical carriers, including high drug loading capability, prolonged circulation time stemming from higher stability in vivo, and slower rates of dissociation that allow retention of loaded materials for a longer period of time. In addition, the delivery systems can be designed to provide either controlled release or triggered release of the therapeutic molecule. In nanocapsules (**Figure 1.3.c**), the shells are usually filled with an aqueous or oil solution, which can contain water-soluble or oil-soluble drugs. Nanospheres (**Figure 1.3.d**) consist of a solid mass, which may be impregnated with an anticancer agent.[53-55] Drugs can be loaded into polymeric NPs by physical entrapment or chemical conjugation. Finally, nanogels (**Figure 1.3.e**), which are polymeric three-dimensional networks of nanometer size (< 1000 nm) capable of absorbing high amounts of water, are emerging as promising carriers. These soft

particles have unique physicochemical characteristics, including reversible swelling properties, which resemble those of the living tissues[56,57].

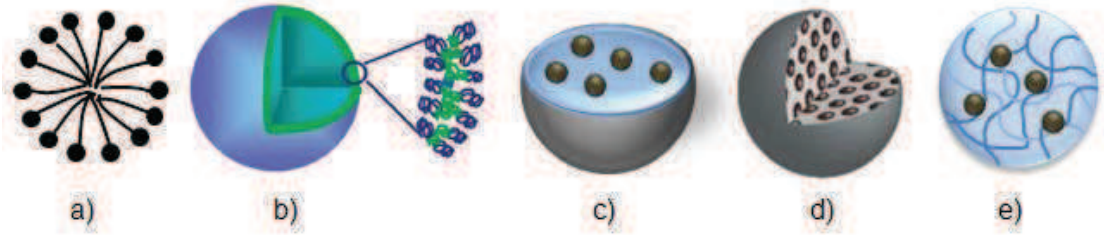

Figure 1. 3. Main types of polymeric NPs. a) Micelles. b)Polymersomes. c) Nanocapsules. d) Nanospheres. e) Nanogels.

The polymers used in these systems can be broadly divided into natural and synthetic materials. Natural polymers that have been investigated for drug delivery applications include polysaccharides such as alginate[58,59], hyaluronic acid[60], dextran[61] and chitosan[62-64] as well as polypeptides such as collagen[65], albumin[66,67], elastin[68], and gelatin[69,70]. These materials are well tolerated in vivo and are available in abundance in nature. Synthetic polymers include polyesters based on lactide, glycolide, caprolactone, and dioxanone, polyanhydrides based on sebacic and adipic acid, as well as polyamides, polycarbonates, polyorthoesters, and phosphate-based polymers, which have been reviewed in detail elsewhere[71-74]. These polymers are often hydrophobic in nature, and are ideally suited for long-term delivery. A significant drawback of synthetic materials is that many form acidic degradation products that can accumulate and cause inflammation at the implant site.

As can be seen from **Table 1.1**, several polymer NPs are now in various states of preclinical and clinical development as carriers of chemotherapeutics. Abraxane®, an albumin-taxol NP for the treatment of metastatic breast cancer have achieved FDA approval for use in cancer therapy. Genexol-PM[19], a micellar vehicle for delivery of paclitaxel is now in Phase II clinical trials. Doxorubicin-conjugated dendrimers were investigated in preclinical studies by Lee et al.[75]. The past decade has seen increasing attention on the development of NPs capable of delivering short RNA duplexes, called small interfering RNA (siRNA), into the cytoplasm of tumor cells as a potential means of combating cancer. CALAA-01[21], a cyclodextrin containing polymeric NP, which was the first ever NP-based siRNA delivery system entered a phase I clinical trial in 2008.

1.3.1.3. Inorganic nanoparticles

Much attention has also been focused on inorganic nanoparticles in cancer treatment applications. Of the wide number of materials available, nanoparticles based on gold, semiconducting metals (quantum dots, QD) and iron oxides are of particular interest owing to their scientific and technological significance in microelectronics, optoelectronics, and cellular imaging. Nanoparticle probes can endow imaging techniques with enhanced signal sensitivity, better spatial resolution, and the ability to relay information about biological systems at the molecular and cellular levels.

Simultaneous imaging, therapy and sensing of the release of a conjugated drug can be achieved by activation of the QD's fluorescence. For example, a QD-aptamer(Apt)-doxorubicin conjugate was prepared for specific delivery of doxorubicin to prostate cancer cells (**Figure 1.4**).[76] The double-stranded A10 prostate specific membrane antigen (PSMA) aptamer intercalates DOX but also recognizes the extracellular domain of the PSMA. When DOX intercalated into the aptamer, quenching of fluorescence from both the QD and DOX was found to occur via a Bi-fluorescence resonance energy transfer (Bi-FRET) mechanism. Binding of DOX to the QD (donor–acceptor) diminished QD fluorescence, while the binding of DOX to the aptamer (donor–quencher) decreased DOX fluorescence. Release of DOX from the NPs by physical dissociation from the conjugate, or biodegradation of the PSMA aptamer by enzymes present in lysosomes, induced recovery of fluorescence from both the QD and drug.[76] Paclitaxel has also been covalently attached to gold NPs with high loading density and in a controlled mode.[77]

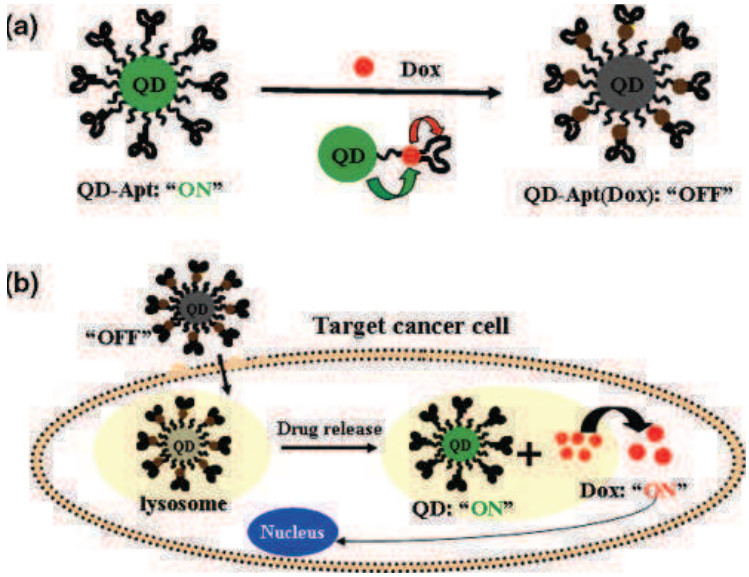

Figure 1. 4. (a) Schematic illustration of QD-Apt(DOX) Bi-FRET system. In the first step, the CdSe/ZnS core-shell QD are surface functionalized with the A10 PSMA aptamer. The intercalation of

DOX within the A10 PSMA aptamer on the surface of QDs results in the formation of the QD-Apt(DOX) and quenching of both QD and DOX fluorescence through a Bi-FRET mechanism: the fluorescence of the QD is quenched by DOX while simultaneously the fluorescence of DOX is quenched by intercalation within the A10 PSMA aptamer resulting in the "OFF" state. (b) Schematic illustration of specific uptake of QD-Apt(DOX) conjugates into target cancer cell through PSMA mediate endocytosis. The release of DOX from the QD-Apt(DOX) conjugates induces the recovery of fluorescence from both QD and DOX ("ON" state), thereby sensing the intracellular delivery of DOX and enabling the synchronous fluorescent localization and killing of cancer cells.[76]

There are concerns about the use of QDs for medical purposes because of their composition of heavy metals (the high toxicity of cadmium and selenium) and their instability to photolysis and oxidative conditions, which could result in dissolution of the QD core. A subsequent study demonstrated that QDs toxicity was reduced after surface modification with *N*-acetylcysteine, while the nonmodified QDs induced lipid peroxidation in the cells.[78] The issue of toxicity has been studied by several groups who have reported that the release of toxic metals might be limited with biocompatible surface coatings, such as poly(ethylene glycol) (PEG) or micelle encapsulation.[79,80] Notwithstanding this, there has been considerable research into the development of cadmium-free QDs, such as CuInS 2[81], as safe and non-toxic probes for biological use.

1.3.2. Main characteristics of nanoparticles used for cancer therapy

Although the EPR effect is the major effect that is exploited for the diagnosis and treatment of cancer using NPs, other properties including size, shape, composition and surface also influence the biodistribution and clearance of NPs from the body and are thus important considerations in NP design.

1.3.2.1. General nanoparticle characteristics

The size of nanoparticle is a key property that affects its biodistribution in vivo and the cellular uptake rate. Particles less than 6 nm will be cleared and filtered from the blood. As the normal endothelium has an average effective pore size of ca. 5 nm, particles smaller than this will rapidly extravasate across the endothelium.[82] Studies have shown that particles with sizes between 10 nm and 5 μm are typically internalized into cells via endocytosis.[83] Endocytosis is an energy-dependent process by which particles are engulfed and encapsulated within a lipid bilayer that isolates them from the cytoplasm of the cell. This process is highly

dependent on cell type, internalization mechanism, and properties of the interacting materials. Typically, endocytosis can be classified into two categories: phagocytosis (cell eating), by which cells internalize only solid material, and pinocytosis (cell drinking), where cells take up a significant amount of liquid from the extracellular environment along with the internalized material. While phagocytosis is generally limited to specialized cells such as macrophages and dendritic cells that interact directly with large material (>250 nm), pinocytosis occurs in almost all cells.[83] The efficiency of particle delivery is often found to vary from one study to another. Experiments using liposomes of different mean sizes suggest that the threshold vesicle size for extravasation into tumors is ~ 400 nm, but other studies have shown that particles with diameters < 200 nm are more effective.[84] The observed range in efficacy has been attributed to the extent of particle extravasation, which depends strongly on the degree of tumor vascularization and angiogenesis.[85] NPs smaller than 200 nm have been suggested to be ideal for cancer therapy[86,87] because of their favorable biodistribution and clearance/accumulation behavior.[88]

Most NPs are easily cleared by the reticuloendothelial system (RES) or mononuclear phagocytic system (MPS).[89] The RES is part of the immune system and consists of phagocytic cells like monocytes and macrophages that are located in the spleen, lymph nodes, and Kupffer cells in the liver. The main functions of the RES are to remove senescent (ageing) cells from the bloodstream and to produce phagocytic cells for immune and inflammatory responses. In order to reduce the premature clearance by the RES, steric stabilization shielding groups have been introduced onto surface of NPs. PEGylation is one preferred method.[34,88-90] PEGylation refers to the process of covering the NPs with PEG or its derivatives by grafting, entrapping, adsorbing or covalently binding these molecules to the NP surface.[91] The most widely accepted theory for this increased circulation time is that PEG reduces the protein interactions on the surface of the NPs and prevents their binding to opsonins.[91] This may be due to the hydrophilicity of PEG and the attraction of water to the surface which repels the protein. One study showed that PEG modified gelatin NPs increased circulation half-life from 3 to 15 h over unmodified NP in total body clearance.[92]

1.3.2.2. Passive and active targeting

Strategies on delivering drug-encapsulated nanoparticles to cancerous tissue have been focused on passive and active targeting (**Figure 1.5**). As previously noted, passive targeting can be achieved by taking advantage of the EPR effect, which allows NPs to access tumors by

way of their leaky vasculature.[87,93] Another passive targeting method exploits the tumor microenvironment (pH and redox potential)[94]; here, pH- or redox-responsive prodrugs are converted into an active drug when they reach the acidic, hypoxic microenvironment of the tumor target. A number of passively targeting nanocarriers were developed in the 1980s and 1990s, and some of them were approved for clinical use. One of the examples is Doxil®, which has shown enhanced circulation time compared to free doxorubicin, good drug retention, and is up to six times more effective than free doxorubicin.[95]

It should be noted that passive targeting can be limited by PEG molecules which are used to prolong the circulation time of nanoparticles. The PEGylated surface can prevent not only the interaction between the NPs and opsonins but also that between the NPs and cell surface.[96-99] The reduced interactions inhibit effective uptake of the payload by the tumor cells.

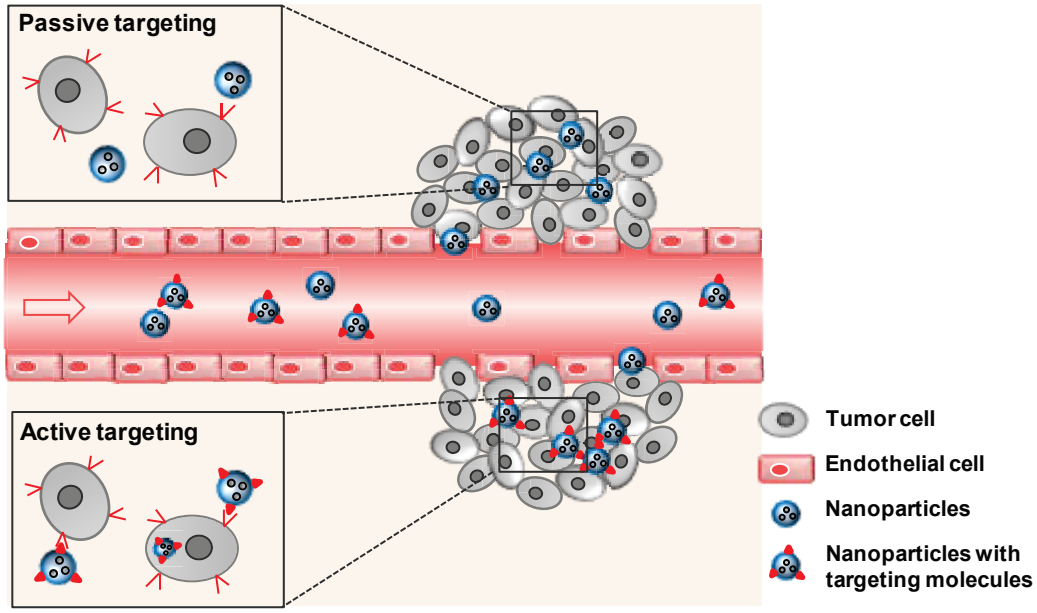

Figure 1. 5. Schematic representation of nanocarriers that passively or actively target tumors. Both types of nanocarriers reach tumors selectively through the leaky vasculature surrounding the tumors. Upon arrival at tumor sites, nanocarriers with targeting molecules can bind to the target tumor cells or enter the cells via specific receptor (cell) – ligand (carrier) interactions, whereas stealth nanocarriers are less efficient in interacting with tumor cells.

To improve targeting efficiency of nanoparticles, the concept of 'active' targeting, that is, the use of biomolecular recognition molecules, has been introduced to provide a greater degree of specificity (**Figure 1.5**).[100,101] Examples of targeting molecules include antibodies, ligands, peptides, nucleic acids, and other molecules that bind directly to a receptor overexpressed on a tumor-cell surface.

- Folate-based targeting molecules

One of the most extensively studied small molecule targeting moieties for drug delivery is folic acid (folate). The high-affinity vitamin is a commonly used ligand for cancer targeting because folate receptor has been frequently associated with the development of malignant tumors.[102] Folate receptors that deliver folic acid into cells have shown 100- to 300- fold overexpression in a wide spectrum of cancer cell.[103] In a recent study, polymer cross-linked liposomes loaded with doxorubicin were modified with folate.[104] It was shown that folate-funtionalized liposomes bound tumor cells differentially as a function of the folate receptor expression levels on the cell membrane.[104] These carriers were shown to be 50-fold more potent than the untargeted agent toward a panel of cancer cells overexpressing the folate receptors in vitro. Recently dendrimer-based targeted anticancer therapeutics using folate have demonstrated promising in vivo efficacy in terms of targeting and specific killing of cancer cells via multivalent interaction.[105]

- Monoclonal antibodies (mAb)

A wide variety of monoclonal antibodies targeting molecules have been assessed for their potential application in cancer therapy.[106,107] Overexpressed tumor-associated molecules used for mAb are growth factor receptors, which include the epidermal growth factor receptor (EGFR) and the human epidermal growth factor receptor 2 (HER2). Except the targeting efficacy, the conjugation of multiple antibodies to each nanocarrier enhances their avidity, and nanocarriers can be surface functionalized with multiple distinct antibodies to overcome tumor heterogeneity. For example, trastuzumab and rituximab have been conjugated to poly(lactic acid) NPs resulting in conjugates that exhibit a 6-fold increase in the rate of particle uptake compared with similar particles lacking the mAb targeting molecules.[108,109] Targeted liposomes using antibody derivatives as the targeting ligand have also been studied. Long-circulating doxorubicin encapsulated immunoliposomes conjugated to human HER2 antibodies have been shown to mediate internalization of targeted liposomes and intracellular drug release.[110]

- Aptamer targeting molecules

Nucleic acid aptamers are single stranded DNA, RNA or unnatural oligonucleotides that fold into unique structures capable of binding to specific targets with high affinity and specificity.[111] Aptamers offer the substantial advantage of synthetic materials that can be produced in preparative scale with high purity and reproductivity. The consideration of such

favorable characteristics of aptamers has resulted in their rapid progress into clinical practice. Farokhzad et al.[112] have developed docetaxel loaded NP functionalized with the A10 aptamer[113], that target the prostate specific membrane antigen (PSMA), a transmembrane protein that is upregulated in a variety of cancers. This formulation was further evaluated in vivo.[114] It was shown that a single intratumoral injection of aptamer modified NPs allowed all the treated mice to survive more than three months in contrast to other controls. This result indicates that the NPs-aptamer is more efficient than nontargeted docetaxel therapy.

- Hyaluronic acid

Active targeting of bioactive molecules by physicochemical association with hyaluronic acid (HA) is an attractive approach in current nanomedicine because HA is biocompatible, non-toxic and non-inflammatory. HA receptor CD44 and RHAMM are overexpressed in many types of tumor cells.[115,116] HA-decorated liposomes with drugs such as DOX[117,118] and mitomycin C[119] were investigated in cancer treatment. In vitro cytotoxicity of the drug-loaded liposomes was examined after incubation with both CD44-positive and CD44-negative cell lines and compared with the non-targeted liposomes. Loading the drug to the HA-coated liposomes resulted in a substantial increase of toxicity against the hyaladherin-overexpressing cells; non-targeted liposomes led to a slight reduction in cell cytotoxicity. El-Dakdouki et al. reported a hyaluronan-coated superparamagnetic iron oxide NPs (HA-SPION).[120] When incubated with cancer cells, HA-SPIONs were rapidly taken up and the internalization of HA-SPION by cancer cells was much higher than the NPs without HA coating. Furthermore, doxorubicin was attached onto the NPs through an acid responsive linker. DOX-HA-SPION was much more potent than free DOX to kill cancer cells.

As mentioned above, recent work comparing non-targeted and targeted NPs has shown that the primary role of the targeting ligands is to enhance cellular uptake into cancer cells and to minimize the accumulation in normal tissue.[87] This behavior suggests that the colloidal properties of NPs will determine their biodistribution, whereas the targeting ligand serves to increase the intracellular uptake in the target tumor. A number of studies found that the targeting ligands did not improve the tumor distribution of nanocarriers.[121-125] A study comparing immunoliposomes and nontargeted liposomes showed that biodistribution of the two liposomes was similar.[122] Epidermal growth factor receptor (EGFR)-targeted immunoliposomes were injected intravenously to mice bearing EGFR-overexpressing tumors, and their biodistribution was compared with that of PEGylated (nontargeted) liposomes.[122]

The antibodies did not increase the amount of liposomes at the tumor site nor did it shorten the time for the nanocarriers to reach the target tissues.[122] Another example shows that HER2-targeted immunoliposomes had no difference in biodistribution or tumor accumulation time versus nontargeted liposomes.[121] Bartlett et al. reported a similar observation.[124] These observations indicate that the biodistribution of the targeted nanocarriers in tumors is mostly governed by the EPR effect rather than the interaction between the targeted nanocarriers and the target cells. Notably, the former group of studies suggests that the targeting molecules play a role *after* the nanocarriers are distributed in the tumor tissues. Although the tumor distributions of targeted and nontargeted nanocarriers were similar, only targeted nanocarriers could efficiently enter the tumor cells from the extracellular space. Studies using colloidal gold-labeled liposomes show that the HER2- targeted immunoliposomes accumulated within tumor cells, whereas nontargeted liposomes were located predominantly in the extracellular matrix.[121] Similarly, the extent to which the EGFR-targeted immunoliposomes were found inside the tumor cells was 6-fold higher than that of nontargeted liposomes.[122] In light of these results, the difference between targeted and nontargeted nanocarriers in tumor distribution observed by other studies,[126-130] can be interpreted alternatively. The superior tumor accumulation of targeted nanocarriers may be another reflection of their efficient entry to the tumor cells following extravasation. A study comparing antitumor effects of intratumorally injected nanoparticles implies that the nontargeted particles could be cleared from the tumor sites unless they were subsequently taken up by the cells.[114]

Active targeting strategy improves the anticancer effect of a drug by facilitating cellular uptake and intracellular retention of the drug carriers. In particular, the active targeting strategy is a promising tool for overcoming the multidrug resistance, for which the passively targeted nanocarriers do not much avail,[85] as the actively targeted nanocarriers can provide an intracellular drug reservoir. On the other hand, tumor distribution of the targeted nanocarriers is largely governed by the same principle as nontargeted nanocarriers (the EPR effect) and the targeting molecules do not seem to play a role until the carriers reach the target tissues. Therefore, an ideal nanocarrier should attain both the EPR effect and the specific and avid interactions between the targeted nanocarriers and tumors, which will lead to maximum tumor distribution and cellular uptake of the nanocarriers, respectively. To this end, it is critical to design a nanocarrier system that is "maximally targeted and maximally stealth."[131]

1.3.2.3. Controlled release strategies

Release cargo can be classified based on the type of stimulus as internally and externally controlled. Internal stimuli include activation by pH, redox potential and enzymes. External stimuli include light, ultrasound, electromagnetic fields or ionizing radiation.[132]

- Internal stimuli

Tumor and inflammatory tissues show differences in pH-levels compared to healthy tissue. Due to their heavy dependence on glycolysis, tumors tend to have lower pH (pH ~ 6.5) values than physiological levels (pH ~ 7.4),[133] opening several avenues for controlling release. One example of pH-responsive system is a micelle based on poly(ethyleneglycol)-b-poly(β-amino ester) block copolymer, in which the methyl ether poly(ethyleneglycol) (MPEG) part forms a hydrophilic shell and the poly(β-amino ester) a hydrophobic core (**Figure 1.6**). Poly(β-amino ester) has a pK_a of ~ 6.5 and allows formation of micelles (diameter ~ 40-60 nm) at pH > 6.9.[134] At pH 6.4 the micelles released > 71% of the drug in 6 h, whereas those at pH 7.4 did not release more than 20 % in 24 h.[134] The in vivo study in B16F10 tumor-bearing mice showed that the ability of the micelles to deliver doxorubicin effectively suppressed tumor growth and prolonged the survival as compared to free doxorubicin.[134]

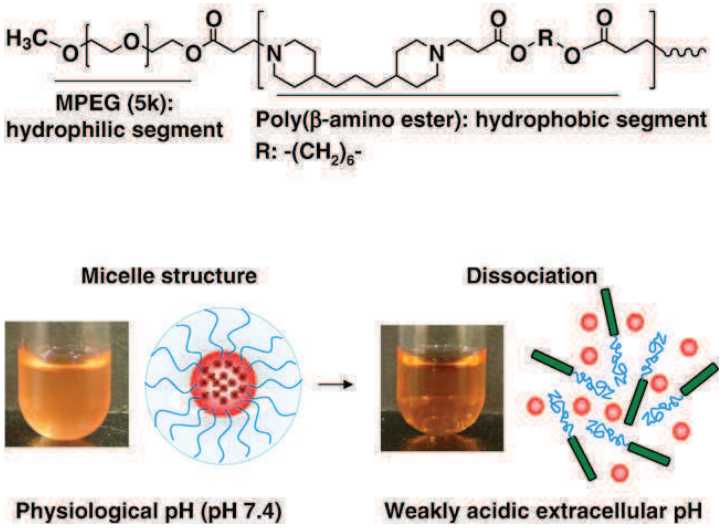

Figure 1. 6. Structure of MPEG-HPAE block copolymer. DOX-loaded MPEG-HAPE micelles under physiological pH were completely dissociated, and rapidly released DOX at weakly acidic pH environments.[134]

Another example of pH-sensitive system is a polymer micelle with a covalently entrapped doxorubicin methacrylamide derivative (DOX-MA, **Figure 1.7**) within the core of poly(ethylene glycol)-b-poly[*N*-(2-hydroxypropyl) methacrylamide-lactate] (PEG-b-

p(HPMAm-Lac_n), **Figure 1.7**) micelles.[135] The structure of the DOX derivative is susceptible to pH-sensitive hydrolysis, enabling controlled release of the drug in acidic conditions. The entire drug payload was released within 24 h incubation at pH 5, whereas only around 5% release was observed at pH 7.4 over the same time period. The micelles showed better anti-tumor activity than free DOX in mice bearing B16F10 tumors.[135] However, whether the pH-responsiveness contributed to the effectiveness is not known, because it was not compared with a pH-insensitive system.

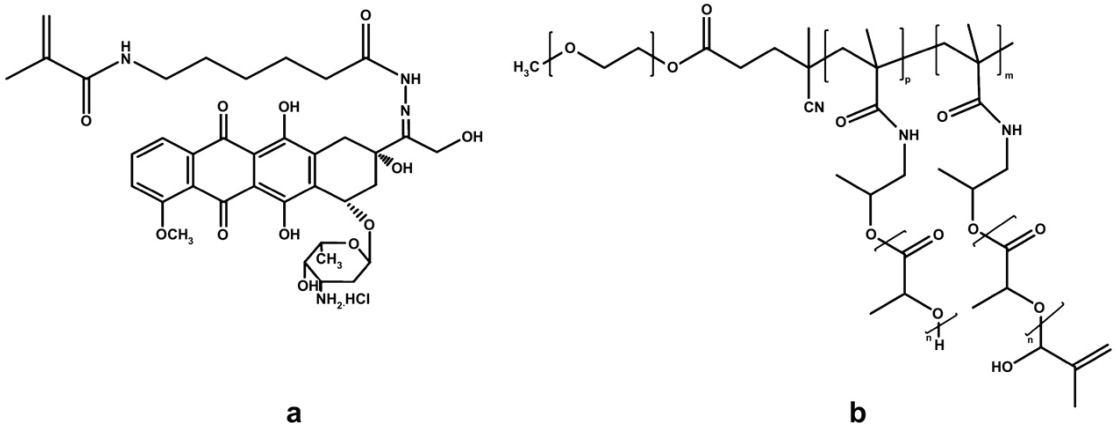

Figure 1. 7. Chemical structures of (a) doxorubicin methacrylamide derivative (DOX-MA) and (b) poly(ethylene glycol)-b-poly[*N*-(2-hydroxypropyl) methacrylamide-lactate] (PEG-b-p(HPMAm-Lac_n).[135]

Sawant et al reported a liposome system including a pH-sensitive linker which could achieve pH-responsive transformation from the stealth liposome to a cell-interactive form (**Figure 1.8**).[136] This system includes a PEG layer attached to the liposome surface via a hydrazone linker, which cleaves at pH 5-6. The liposome surface is also conjugated to TAT peptide, which is shielded by the PEG layer at pH 7.4. At pH 5-6, the PEG layer detaches revealing the TAT peptide as the hydrazone linker hydrolyzes. A preliminary incubation of the pH-sensitive liposomes at pH 5 allowed the liposomes to enter the cells efficiently, whereas the pH-insensitive liposomes were much less efficient.[136] A similar strategy is described by Bae et al in a study concerning a TAT peptide-based micelle system.[137]

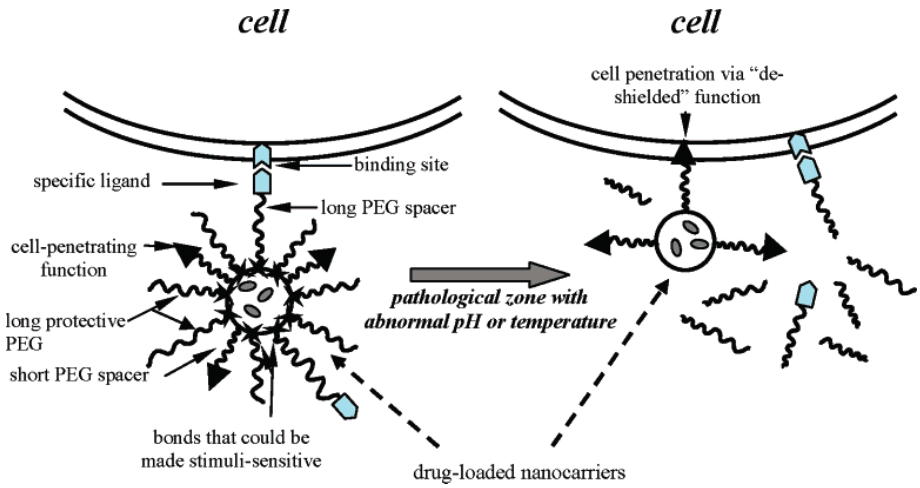

Figure 1. 8. Interaction of the multifunctional pH-responsive pharmaceutical nanocarrier with the target cell. Local stimuli-dependent removal of protecting PEG chains or mAb-PEG moieties allows for the direct interaction of the cell-penetrating peptides (CPP) moiety with the cell membrane.[136]

Polymersomes based on PEG-poly(lactic acid) (PLA) were reported by Ahmed et al.[49] Under acidic conditions, the PLA first underwent hydrolysis, and several hours later, pores formed in the membrane followed by final membrane disintegration. In vivo experiments demonstrated growth arrest and shrinkage of rapidly growing tumors after intravenous injection of the DOX- and PTX-loaded polymersomes.

Redox-sensitivity is another switch functionality of major potential impact in intelligent nanomaterials. In vivo, a large difference in redox potential by factor of 100–1000 between the oxidizing extracellular and reducing intracellular space has been reported.[138,139] Oxidative conditions exist in extracellular fluids and inflamed or tumor tissues, while intracellular compartments are known to be reductive.[140] Zhao et al. have shown successful protein delivery into several human cancer cell lines and release through redox-responsive nanoparticles.[141] They demonstrated effective encapsulation of caspase-3 (CP-3) with positively charged, disulfide containing cross-linker polymers followed by internalization into cancer cells. Subsequent release into the cytosol induced cancer cell apoptosis due to active CP-3 in HeLa, MCF-7 and U 87MG cells. Kim et al. demonstrated a similar gate-keeping effect using mesoporous silica NPs covalently linked through disulfide bridges with cyclodextrin instead of polymers and loaded with DOX.[142,143] Cyclodextrin blocked the pores and inhibited undesired DOX release. In vitro studies using A549 cancer cells showed reduced cancer cell survival after incubation with DOX loaded mesoporous silica nanoparticles as a result of glutathione-induced controlled drug release.[143] Liposomes are also under investigation for redox-sensitive drug delivery.[133,144,145]

The use of enzymes can also be exploited for triggered release of drugs from NPs in a tumor-specific manner. Perhaps the most exploited enzymes are matrix metalloproteinases (MMP), which are often overexpressed at tumor sites as well as in many cardiovascular diseases. The stealth PEG coating on liposomes can include a MMP cleavage site.[146] The PEG was removed upon exposure to MMP. The MMP-sensitive liposomes showed significantly higher gene transfection efficiency than MMP-insensitive liposomes in in vitro cell models overexpressing MMP. In an in vivo study, the MMP-sensitive liposomes showed three times higher gene transfection efficiency than the MMP-insensitive ones which indicates that the MMP overexpressed in the tumor extracellular matrix successfully removed the PEG from the liposomes and facilitated cellular uptake of the liposomes.[146] A disadvantage of enzyme triggered release is that no enzyme is solely expressed in the targeted region; therefore nonspecific release occurs throughout the body.

- External stimuli

Temperature sensitive NPs are made of temperature-sensitive polymers which possess a lower critical solution temperature (LCST) in aqueous solution. This means that these polymers are soluble in water below the LCST and turn into a collapsed state due to an increase of their hydrophobic character above the LCST. This feature has been used in anti-cancer therapy. Some tumor cells are more sensitive to heat-induced damage than normal cells, rendering a combination of tumor hyperthermia and heat responsive nanomaterials promising.[12] Liposomes and dendrimers have been rendered temperature sensitive by incorporation of LCST polymers. Upon an increase in temperature above the LCST, the polymers collapse, the liposomal membrane bursts and a drug can be released.[147,148] Another example is a nanogel synthesized by light cross-linking from poly(L-lysine)-g-poly(ethylene glycol) (PLL-g-PEG)/oligo(L-lactic acid)-b-pluronic F127-b-oligo(L-lactic acid).[149] The nanogels exhibited reversible size transition from ~ 150 nm at 37 °C to ~ 1.4 μm at 15 °C. The abrupt and dramatic intracellular volume expansion of the nanogels upon the brief cold-shock treatment severely damaged sub-cellular self-assembled network architectures and physically ruptured cellular membrane structures, resulting in necrotic cell death. To further enhance the extent of cell death, various targeting ligands recognizable by specific cells could be conjugated on the surface for guiding specific intracellular delivery.

Light-responsive materials can be built through covalent incorporation of specific light-sensitive chemical groups with the aim to release a payload by illumination.[150] Cabane et al. have reported the synthesis of a photocleavable amphiphilic block copolymer. They used an

o-nitrobenzyl linker as a photosensitive molecule, which they incorporated between the hydrophobic and hydrophilic blocks. Through self-assembly of the copolymers in buffer media, the formation of vesicles and micelles could be achieved. Rapid structural changes in size of the vesicles were observed in electron microscopy and dynamic light scattering after irradiation with UV-light, demonstrating successful photocleavage.[151] UV damage to the surrounding tissue is however a major limitation to broad clinical application of this chemistry. Na et al. reported a hyaluronic acid-bearing photosensitizer nanogel as a new type of photodynamic therapy agent.[152] After incubation of the HA/photosensitizer conjugate nanogels with cells, the degradation of the HA by enzymes in endosomes and lysosomes was monitored as a dissipation of the autoquenching behavior. The nanogels also exhibited HA-induced tumor-homing properties, resulting in a rapid internalization rate. Moreover, the nanogels indicated high cytotoxicity against cancer cells under light emission, which was comparable with the free photosensitized, but very low cytotoxicity without light.

Ultrasound is another method of triggered release of drugs from NPs. The mechanism relies on the ability of ultrasound to produce free radicals that degrade polymers, increase local temperatures, and permeabilize cell membranes.[153] Schroeder and coworkers recently demonstrated ultrasound-triggered drug release of cisplatin from liposomes in vivo.[154] Liposomes were injected intraperitoneally into mice bearing J6456 lymphomas, followed by administration of low frequency ultrasound 1 h later. Results show that approximately 70% of cisplatin was released following ultrasound, compared with approximately 3% without ultrasound. In the tumors receiving ultrasound, cisplatin levels were nearly three-fold higher than those in tumors receiving no ultrasound. In C-26 colon tumors in the footpad of mice, liposomes were injected intravenously, followed by ultrasound irradiation 24 h later. Findings demonstrate that tumor growth in the footpad was significantly suppressed in mice receiving cisplatin-containing liposomes and ultrasound when compared with free cisplatin with and without ultrasound after 29 days.

Other external stimuli systems, such as electromagnetically sensitive[155,156], radiation sensitive[157,158] NPs have also been investigated for cancer treatment. A key challenge in externally controlled nanomaterials is tissue penetration and avoidance of undesired tissue damage. They require particular care in design of materials with optimal sensitivity to allow reduction of transmitted energy.

1.3.3. Nanoparticles in cancer imaging

Tumor imaging plays a fundamental role in cancer therapy, from informing the diagnosis and consequent choice of treatment, to the pinpointing of diseased areas during treatments (e.g., radiotherapy), and extending to post-treatment monitoring. The ability to monitor treatment in real-time will allow physicians to adjust the type and dosing of drug for each patient, to prevent overtreatment that would result in harmful side-effects, or undertreatment that would lead to incomplete cancer remission. The ability to see when a drug reaches a maximum tolerable concentration in offtarget organs and a sufficient concentration in the tumor would be a significant advantage over current treatments. NPs can enable treatment monitoring by either attaching different imaging moieties or taking advantage of the intrinsic properties of some NP materials (e.g., super paramagnetism for magnetic resonance imaging (MRI)). While these theranostic NP formulations are more complex to develop, their potential clinical utility substantiates the investment required at the front-end.

Many different types of nanomaterials have been developed to provide contrast in medical imaging, including liposomes and micelles, polymers and dendrimers, noble metals, semiconductors, carbon nanotubes and fullerenes, transition metal oxides, metal-organic frameworks, and lanthanide series.[7,159,160] Some of these materials incorporate an imaging moiety into their design, while others provide contrast as a result of their intrinsic material properties. Multiple imaging modalities can also be implemented into a single nanotheranostic design by incorporating multiple moieties to provide a more complete picture of the disease. Molecular imaging can identify tumor cell location within the body, and aims to provide information such as metabolism, expression profile, and stage of the disease.[161] Furthermore, molecular imaging can reveal early tumor response to therapy that will aid in improving treatment regimens.[4]

1.4. Polyelectrolyte multilayer capsules in drug delivery

Polyelectrolyte microcapsules have been extensively explored for their physicochemical properties since their advent in the late 1990s[162], and more recently they have attracted attention for drug delivery applications[163-171].

Polyelectrolyte multilayer capsules are synthesized by the layer-by-layer (LbL)[162] technique consisting in the consecutive deposition of polymers that can interact through electrostatic interactions, or hydrogen bonding, or other covalent interactions on a particle template. Their size can range from 10 nm to several microns[172,173]. After the LbL adsorption process, the cores can be successfully removed to obtain hollow and stable capsules (**Figure 1.9**) whose inner cavity and polymer wall can be loaded with a variety of substances such as molecular dyes, drugs, nanoparticles and biomolecules. The hollow capsules usually have a wall thickness between a few tens and several hundred of nanometers[174] and a diameter ranging from hundred of nanometers to several micrometers depending on the size of the original core template. Microcapsules have a higher payload capacity than smaller nanoparticles, and can accommodate multiple types of drug molecules. The layered nature of the assembly makes surface modification relatively simple for inclusion of targeting or stealth properties. It also makes it possible to include different degradation mechanisms within a single film. When all of these properties are combined, LbL assembled microcapsules are an ideal multifunctional platform for delivery of different therapeutic agents.

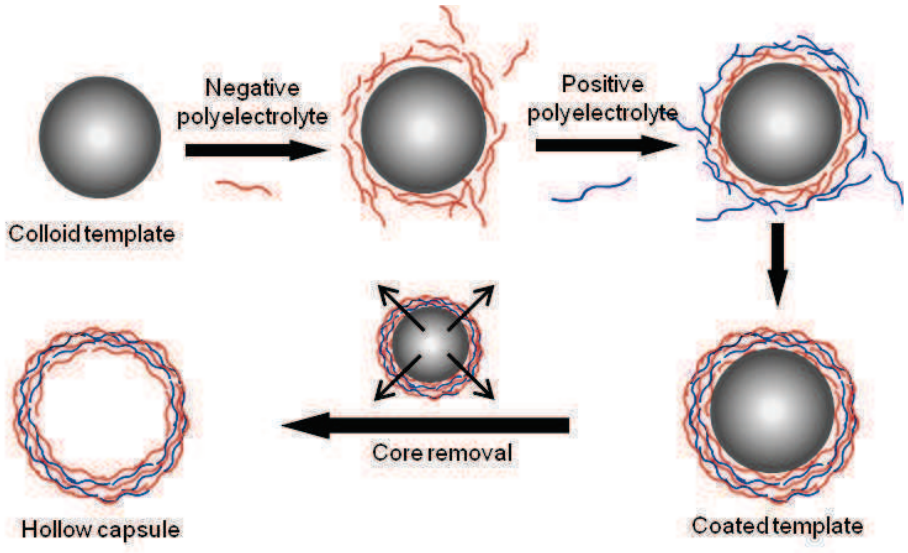

Figure 1. 9. Schematic representation of polyelectrolyte capsule fabrication by layer-by-layer (LbL) assembly. a) Initial electrostatic adsorption of a negatively charged polymer onto a positively charged

template core. b) Second adsorption of positively charged polymer onto the now negatively charged template. c) Multilayer growth via alternating adsorption of oppositely charged polymers. d) Removal of the template by dissolution to obtain a capsule with an empty cavity.

1.4.1. Size and surface chemistry

The size of capsules depends on the size of original core template. It can directly influence the mechanism for internalization. Due to the LbL method used for their preparation, the size of the capsules remain in the micron range which is much larger than the range of sizes that are generally considered to be optimal for internalization by endocytosis. Although early studies showed that particles must be less than 500 nm to undergo cellular internalization by phagocytosis,[175] more recent investigations have shown that the internalization of much larger particles is possible.[176] For example, LbL capsules of 1 μm,[177] 3 μm,[178] and even 6 μm[179] diameter have all been observed inside the cell. However, for chemotherapeutic delivery which requires the particles extravasate from bloodstream and enter tumor tissue through the EPR effect, the size of capsules should be rather below 200 nm. Gold nanoparticles (AuNPs) are attractive substrates for LbL assembly to fabricate capsules with a diameter below 100 nm. [180,181]

The surface of the delivery carriers is one of the most important aspects for designing drug carriers as it is generally the only interaction point with the body. It is important to functionalize the surface to ensure that it is processed in the desired way. As mentioned above, PEG was also used for the modification of the multilayer capsules surface to prevent non-specific protein adsorption and improve blood circulation half-life. Several factors contribute to reduced adsorption of proteins on PEG coated polyelectrolyte capsules. The hydrophilic character of PEG avoids hydrophobic interactions with proteins. Additionally, PEG shields charges of the capsules thereby minimizing potential electrostatic interactions with proteins and flexible PEG chains provide steric repulsion.[182] Heuberger et al. functionalized poly(acrylic acid) (PAH)/poly(styrene sodium sulfate) (PSS) capsules with poly(L-lysine) (PLL)-g-PEG. The PEG functionalized capsules exhibited a severe reduction of protein adsorption compared to PAH/PSS capsules.[182] Lipids may also be used to alter the surface chemistry of delivery vehicles. A lipid coating mimics the cellular membrane, and it may either enhance or reduce the interaction of the delivery vehicle with a cell. A lipid coating decreases the permeability of the capsule, allowing the entrapment of small molecules without conjugation.[183] Moreover, the use of capsules predefines the size of the lipid coating,

resulting in monodisperse populations.[184] Hammond et al. recently reported in vivo applications of AuNP (size ~ 20 nm) and quantum dots (size ~ 20 nm) templated polyelectrolyte capsules.[185] These templates were not removed after capsules preparation and used as a tracer for in vivo studies. Degradable biopolyelectrolytes (PLL, dextran (DEX) and HA) were used as layer components. It was found that HA as outermost layer strongly enhanced the circulation time (~9 h) and minimized accumulation (~10-15% recovered fluorescence/g) in the liver, whereas using PLL or DEX as terminal layers strongly provoked accumulation of particles in the liver and spleen. Furthermore, the non-fouling properties of HA allowed the capsules to accumulate in xenografted tumors by virtue of the EPR effect.[185]

1.4.2. Anti-cancer drug loaded capsules

The delivery of anticancer drugs by LbL capsules has been investigated by several research groups. As many potent anticancer agents are hydrophobic molecules, the development of LbL capsules for delivering such drugs has received significant attention. These drugs include doxorubicin, daunorubicin, paclitaxel, 5-fluorouracil, polyphenols (**Figure 1.10**).[180,186-188] Short interfering RNA (siRNA) as hydrophilic anticancer drug has been encapsulated into LbL capsules.[189,190]

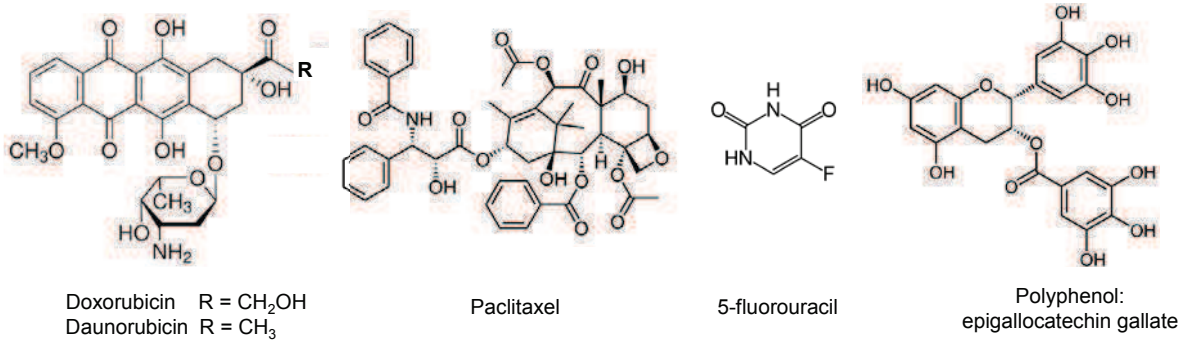

Figure 1. 10. Structures of doxorubicin, daunorubicin, paclitaxel, 5-fluorouracil, and an example of polyphenol, epigallocatechin gallate.

Four main strategies have been proposed for loading water-insoluble compounds into LbL capsules. The first method consists of filling the cavity of pre-formed hollow capsules with an oil phase containing the drug.[187,191,192] The capsules were dehydrated in ethanol and dispersed in a drug/oleic acid mixture to allow infiltration of the oil phase through the semi-permeable walls of the polymer capsules and filling of the capsules. FDA-approved oleic acid was chosen as an oil phase to solubilize two model chemotherapy drugs: doxorubicin and 5-

fluorouracil. The excess drug/oleic acid mixture was removed by centrifugation. This final preparation was dispersed in phosphate buffer , giving monodispersed drug-loaded oleic acid emulsions stabilized within polymer capsules.[191]

The second approach is to embed a reservoir of hydrophobic drug into the LbL assembly. The reservoir could be polymeric micelles[193] or liposomes[194]. The latter was termed capsosomes by Caruso group. Manna et al. used a micellar solution of pyrene in sodium dodecyl sulfate (SDS) as a model drug to exploit electrostatic interaction between chitosan and SDS to form LbL capsules.[193] In the case of capsosomes, polymer membrane was subsequently assembled by the alternating adsorption of poly(N-vinyl pyrrolidone) (PVPON) and thiol-modified poly(methacrylic acid) (PMASH) onto the preadsorbed layer of liposomes (**Figure 1.11**). Upon removal of the silica template, stable capsosomes encapsulating the enzyme luciferase or b-lactamase within their liposomal sub-compartments were obtained.[194] This approach allowed stable encapsulation of both hydrophilic macromolecules (e.g. enzymes[194]) and hydrophobic molecules (e.g. anticancer drugs) within the liposomal compartments of the capsosomes.

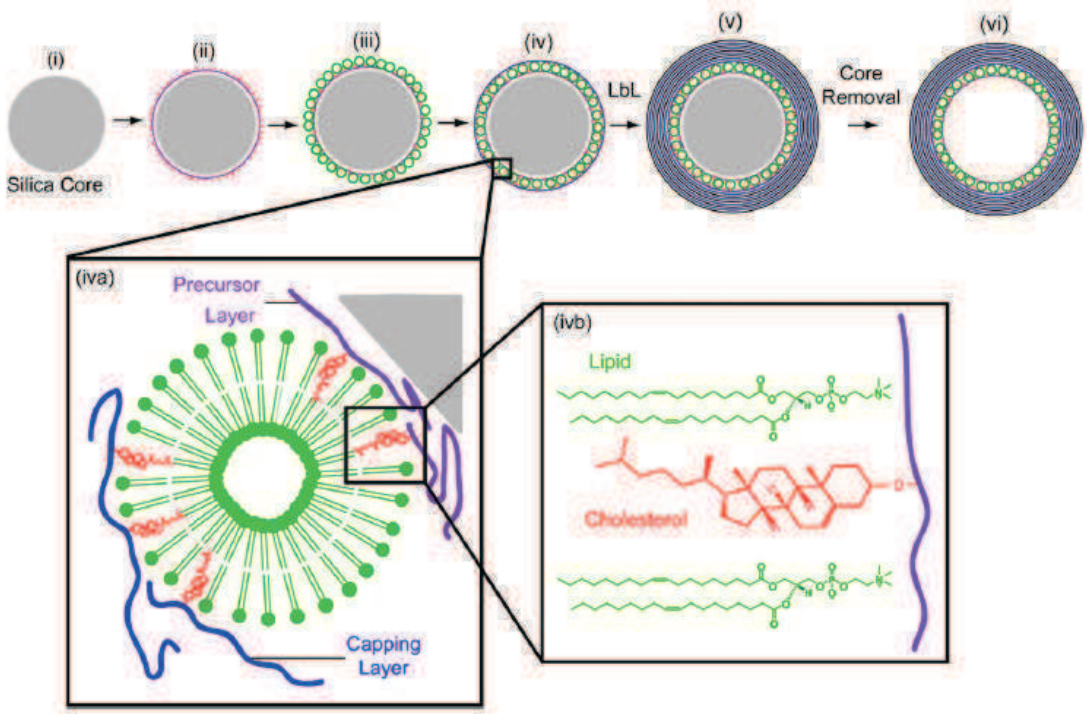

Figure 1. 11. Schematic illustration of capsosome assembly. A silica particle (i) is coated with a cholesterol-functionalized polymer precursor layer (ii), liposomes (iii), and a cholesterol-functionalized polymer capping layer (iv), followed by subsequent polymer layering (v), and removal of the silica template core (vi). Liposomes are adsorbed onto the polymer surface non-covalently with cholesterol-modified polymers (iva). Cholesterol is spontaneously incorporated into the lipid membrane (ivb).[194]

The third strategy consists in conjugating drugs to a polymer used as a chemotherapeutic prodrug and then incorporating into a multilayered film. Using this approach, Schneider and co-workers synthesized doxorubicin loaded LbL capsules.[180] They used ten nanometer sized gold nanoparticles (AuNPs) as template, which were LbL coated with a $(PAH/PSS)_2PAH$ multilayer film and were subsequently functionalized with a layer of a macromolecular prodrug based on doxorubicin. The latter is a *N*-(2-hydroxypropyl)methacrylamide) (HPMA) copolymer carrying oligopeptide spaced doxorubicin side groups.[195] The DOX was linked to the polymer via an oligopeptide spacer that was a substrate for lysosomal enzymes (**Figure 1.12**). Caruso et al. aslo reported doxorubicin loaded capsules. The drug was conjugated to alkyne-functionalized poly(L-glutamic acid) (PGA_{Alk}) via amide bond formation ($PGA_{Alk+DOX}$).[196,197] PGA_{Alk} and $PGA_{Alk+DOX}$ were assembled via hydrogen bonding with poly(*N*-vinyl pyrrolidone) (PVPON) on silica templates. The films were subsequently covalently stabilized using diazide cross-linkers, and PVPON was released from the multilayers by altering the solution pH to disrupt hydrogen bonding. After removal of the sacrificial template, single-component PGA_{Alk} capsules were obtained.

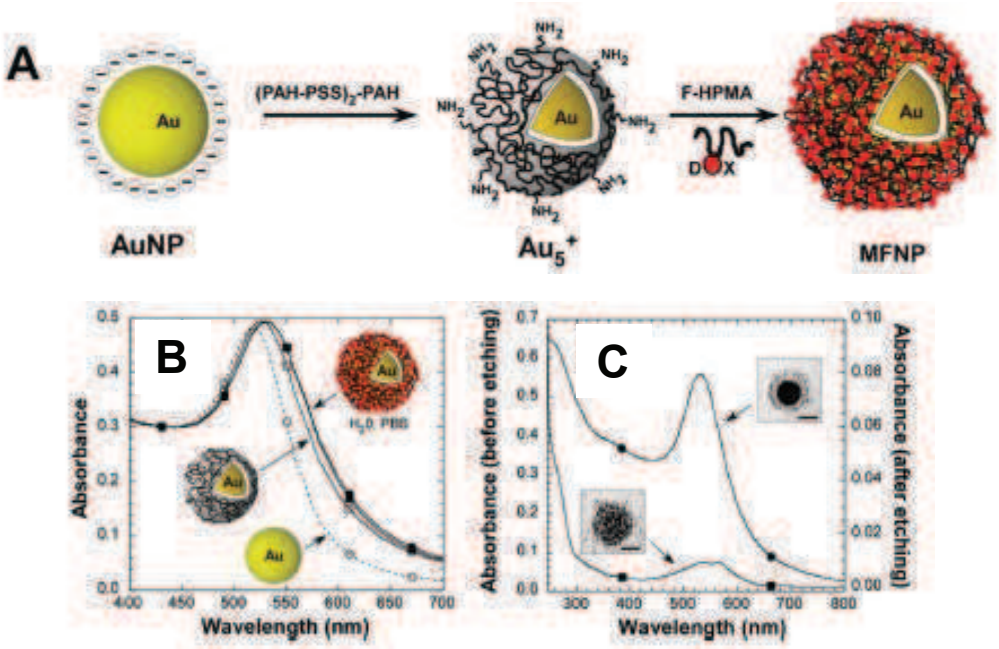

Figure 1. 12. (A) From left to right: 13 nm sized AuNPs as obtained after synthesis, stabilized by adsorbed sodium citrate; AuNPs coated with five primer layers of PAH and PSS (i.e., Au_5^+:Au/$(PAH/PSS)_2$/PAH, the number "5" refers to the total number of layers and the charge "+" refers to the charge of the outer layer); Au_5^+ further coated with a external layer of F-HPMA (yielding MFNP). The red circles represent doxorubicin moieties (DOX) and are at scale with respect to the size of DOX molecules and the density of DOX moieties on the nanoparticle surface. (B) UV-vis spectra of native AuNPs dispersed in pure water (○, dotted line), Au_5^+ dispersed in pure water (□),

multifunctional nanoparticles dispersed in pure water (●) and in PBS (■); (●) and (■) are undistinguishable. All spectra were normalized to yield the same absorbance value at the wavelength of 440 nm. (C) UV-vis spectra of MFNP before (●) and after (■) the dissolution of Au cores by an excess of potassium cyanide solution (KCN). Insets are TEM micrographs of MFNP before and after the dissolution of the cores.[180]

The last approach entails encapsulation of water-insoluble drug into LbL capsules through their template. It can be achieved by using templates formed with therapeutic crystals.[198] Another approach consists in using interaction of template/drugs to encapsulate hydrophobic drug. Shutava et al. synthesized gelatin NPs template capsules in which they encapsulated polyphenols by hydrophobic association.[188] Natural polyphenols with previously demonstrated anticancer potential, epigallocatechin gallate (EGCG), tannic acid, curcumin, and theaflavin, were encapsulated into gelatin-based 200 nm nanoparticles consisting of a soft gel-like interior and a surrounding LbL shell of polyelectrolytes (**Figure 1.13**).[188] Decomposable mesoporous silica templates[199] were used as another mean to encapsulate hydrophobic drugs. After removal of the silica particles, the water-insoluble small compounds agglomerate into clusters, and are retained in the polymer capsules.

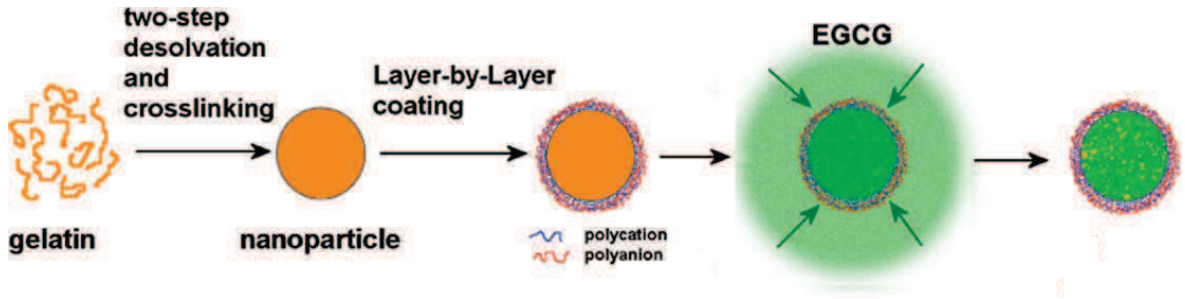

Figure 1. 13. Schematic presentation of preparation of LbL-coated gelatin nanoparticles containing EGCG.[188]

Elbakry and co-wokers demonstrated that siRNA could be incorporated directly in multilayer assemblies onto AuNPs containing hyperbranched poly(ethyleneimine) (PEI) as polycation.[190] siRNA was not expected to easily wrap around small AuNPs because it is a stiff, rodlike molecule. To obtain well-defined particles onto which the polyelectrolyte can be adsorbed with high yield and to avoid interparticle bridging and flocculation, it was important to choose the appropriate polyelectrolyte concentration and ionic strength. Caruso et al. described the delivery of siRNA using LbL microcapsules.[189] The microcapsules are based on negatively charged poly(methacrylic acid) thin films containing cross-linking disulfide bonds. One system is polycation-free and another contains PLL for siRNA complexation in the microcapsule core (**Figure1.14**). Receptor specific siRNA delivery mediated by AuNPs was

demonstrated by Lee et al. via functionalization of AuNPs with HA.[200] siRNA was encapsulated onto a cysteamine modified AuNPs.

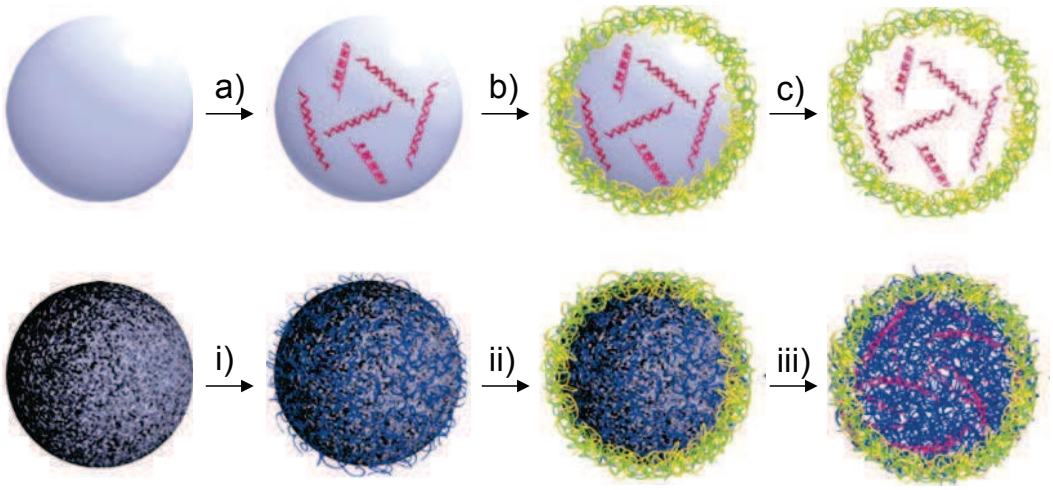

Figure 1. 14. Schematic representation of siRNA loading methods. Preloaded microcapsules: (a) siRNA is adsorbed onto amine-functionalized silica particles; (b) LbL assembly of film is performed around the siRNA coated particles; (c) the film is cross-linked and the core removed. Postloaded microcapsules: (i) mesoporous silica particles are infiltrated with the polycation PLL; (ii) LbL assembly of film is performed around the polymer filled particles; (iii) following core removal, the siRNA is infiltrated into the particles and sequestered by the polycation core.[189]

1.4.3. Interaction of capsules and living cells

1.4.3.1. Cytotoxicity

To evaluate the potential of polyelectrolyte capsules for cancer treatment it is important to understand their interactions with living cells. One of the most important issues is cytotoxicity because the uptake of large amounts of polyelectrolyte capsules could be toxic for cell. Several research groups have assessed it by performing in vitro cell-viability assays such as the 3-(4,5-dimethylthiazol-2-yl)-2,5-diphenyltetrazolium bromide (MTT) test or Trypan Blue. Generally, no severe toxicity was observed at moderate capsule concentrations. The main sources for toxicity come obviously from the polyelectrolytes composing the wall as well as from the functionalities embedded in the cavity and/or in the wall.[201] In this regard, a reduction of the cytotoxicity could be obtained by using materials that are biocompatible and biodegradable. The magnitude of the cytotoxic effect of the capsules is primarily concentration-dependent.[174,202] De Geest[174] et al. showed that cell viability was reduced by 80 % after incubation with dextran sulphate and poly(L-arginine) (DEXS/PARG) capsules in a capsules to dendritic cell (DC) ratio of ~ 10^3. For a capsule/cell ratio of 125 and below, more

than 60 % the cells survive. For a capsule/cell ratio of 30, cytotoxicity was low and approximately 80 % of the dendritic cells remained viable. Reduced toxicity was attributed to the reduction of aggregation of the capsules on the top of the cells. Additionally, it has been reported that polycationic polymers decrease cell viability.[203,204] Fisher et al. showed that the cytotoxicity of polycations is depends on their molecular weight, their cationic charge density and the flexibility of their structure.[205] However, some work demonstrated that capsules with a positively charged outer layer were ingested more than negatively charged ones. Thus, in the case of alginate (ALG)/chitosan (CHI) capsules, Wang et al. found that the positively charged outer layer of capsules was the key pathway to enhance the uptake efficiency of capsules via electrostatic interactions with MCF-7 cells membrane.[192]

1.4.3.2. Mechanisms of capsules uptake by living cells

In general, microcapsule internalization appears not only to be dependent on capsule intrinsic factors (size, composition, charge…) but also on the cell type taking up the particles. LbL capsules are readily internalized not only by professional phagocytes (DCs[206-208] and macrophages[209]), but also by numerous other cell types including breast cancer cells, hepatoma cells, fibroblasts,[210] epithelial kidney cells… De Koker et al. demonstrated that, during the association of DEXS/PARG capsules with bone marrow mice dendritic cells (BM-DCs), the cell membrane extends over the capsules, forming large cytoplasmatic extrusions to engulf polyelectrolyte microcapsules (**Figure 1.15.a**).[206] They proposed macropinocytosis as the mechanism of uptake of capsules by DCs. This hypothesis was further confirmed using a set of uptake inhibitors (**Figure 1.15.c**). Microcapsule uptake was inhibited by cytochalasin D, an inhibitor of actin polymerization that is known to block both phagocytosis and macropinocytosis, and blocked by incubation with rottlerin, a recently identified selective inhibitor of macropinocytosis.[211] Remarkably, both genistein and filipin III,[212,213] two known inhibitors of caveolae-mediated endocytosis, but not chlorpromazine,[214] an inhibitor of the clathrin pathway of endocytosis, inhibited microcapsule internalization. Caveolae-mediated uptake of polyelectrolyte microcapsules by tumor cells has been described recently,[215] indicating DCs and tumor cells might internalize polyelectrolyte microcapsules by similar mechanisms.

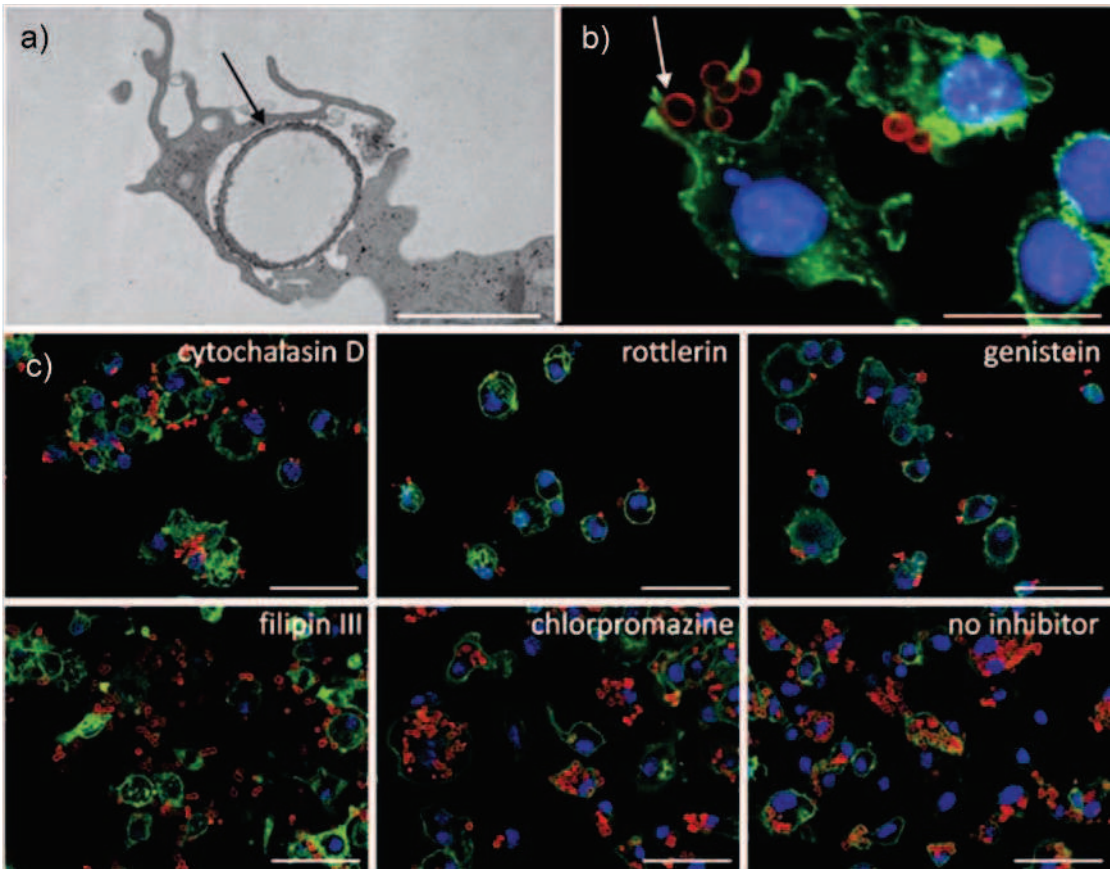

Figure 1. 15. Images of bone-marrow-derived dendritic cells (BM-DCs) taking up dextran sulfate/poly-L-arginine microcapsules. The TEM image a) shows a BM-DC forming cytoplasmic protrusions to engulf the microcapsules (black arrow), which are visible as hollow disks with a dark, electron dense wall. Scale bar: 3 mm. b) Confocal microscopy images showing the formation of actin-rich protrusions. The actin cytoskelet was stained with alexa 488 phalloidin (green). Microcapsules were labelled red by incorporation of RITC-poly-L-arginine. Nuclei were stained blue with Hoechst 33258. Scale bar: 10 mm. c) Confocal images of the effects of cytochalasin D, rottlerin, filipin III and chlorpromazine on microcapsule uptake by BM-DCs. Scale bars: 50 mm.[206]

Similarly, Yan et al. observed the formation of plasma membrane protrusions in human colorectal cancer cells when interacting with thiolated poly(methacrylic acid) (PMA_{SH}) capsules, confirming that macropinocytosis and phagocytosis are the predominant routes for cellular uptake of capsules.[187] It has also been shown that the internalized LbL capsules are deformed and located in membrane-enclosed compartments, which further mature to late endosomes or lysosomes.

Several groups have focused these researches on the intracellular fate of the capsules and have observed a substantial deformation of the capsules. Complete destruction and intracellular degradation were demonstrated by De Geest et al. by using degradable poycation.[215] Co-incubation of cancer cells with capsules results in their internalization and gradual

disintegration over a period of 60 h, after which no intact capsules could be observed.[215] This process appears to be much faster for PLL/HA capsules which promptly deform and rupture upon cellular internalization.[209] The deformation of capsules may be due to an enzymatic or/and mechanic degradation. De Geest, Parak, and coworkers entrapped a nonactive prodrug, a self-quenched fluorescence-labeled protein, which needs to be enzymatically cleaved in order to become active in biodegradable LbL capsules.[216] Upon capsule uptake by living cells, the multilayer shells were actively degraded and digested by intracellular proteases. Shell degradation enabled intracellular proteases to reach the protein cargo in the cavity of the capsules. Enzymatic fragmentation of the fluorescence-labeled protein led to individual fluorescence-labeled peptides. In this case, only pro-drugs inside the capsules reaching cells are activated and those in capsules in an extracellular environment cannot be activated. In addition, they compared the accessibility of encapsulated proteins for proteases with non-degradable PSS/PAH capsules in which the protein remained intact. This study clearly showed the importance of using degradable polymers which can be eroded and cleaved by intracellular proteases (**Figure 1.16**).

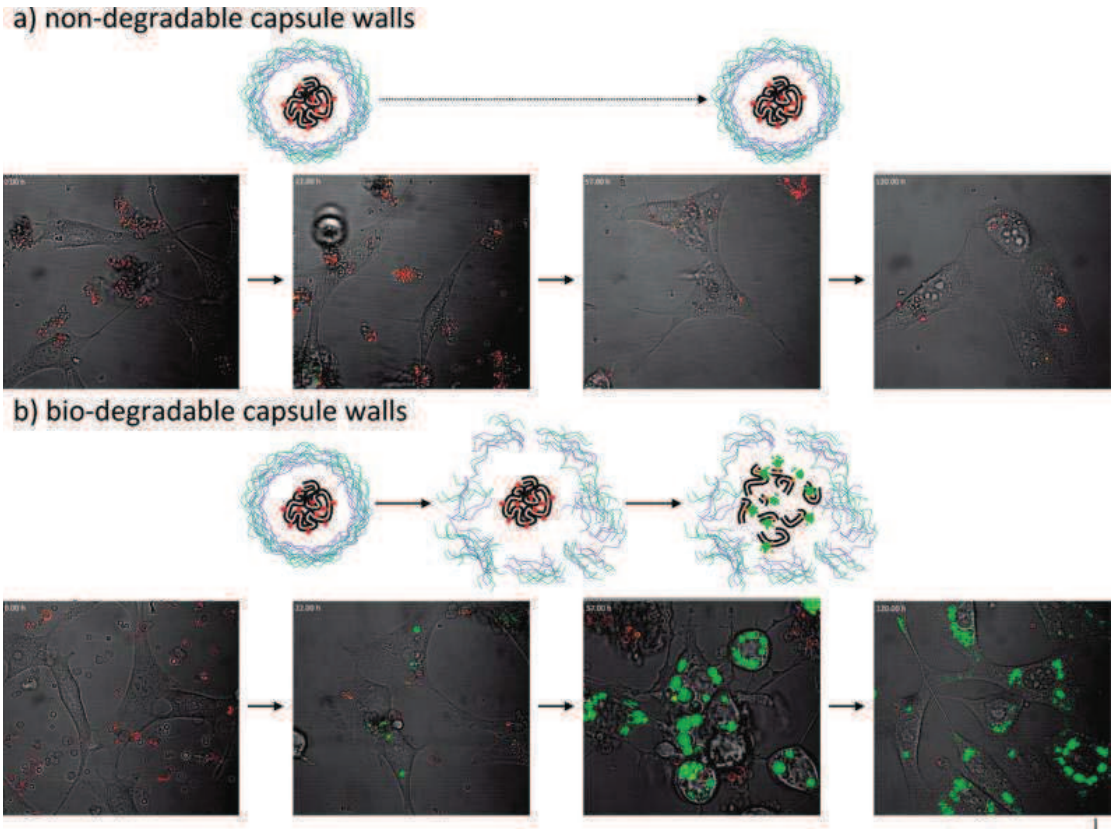

Figure 1. 16. Enzymatic cleavage of protein cargo. Embryonic NIH/3 T3 fibroblasts were incubated with a) non-degradable PSS/PAH or b) degradable DEXS/PARG capsules filled with the fluorogenic protein cargo, DQ-ovalbumine (DQ-OVA). Images were taken immediately after addition of the

capsules (t) 0 h) over time up to 120 h with a confocal microscope in different channels, green, red, and transmission. An overlay of the different channels is presented in the figures.[216]

1.4.3.3. Targeting capsules

To enhance the cellular uptake, drug loaded polyelectrolyte microcapsules were functionalized with cell-targeting structures which allow delivery of the cargo to a cell type of interest avoiding unwanted uptake. In this way, high drug concentration can be obtained in the target tissue using a minimum amount of drug loaded carriers. For targeting to a specific cell type, polyelectrolytes microcapsules have been functionalized with monoclonal antibodies, or magnetic particles. Cortez et al. described the functionalization of PSS/PAH microcapsules with human A33 monoclonal antibodies, which bind to the human A33 antigen expressed by 95 % of all human colorectal cancer cells. This functionalization resulted in an enhanced uptake of capsules by cancer cells containing the A33 antigen compared to non functionalized microcapsules.[217] Magnetic drug targeting has been suggested as a method to locally accumulate drugs. It has been shown in vitro that polyelectrolyte capsules of which the shells are functionalized with magnetic nanoparticles, in a magnetic field gradient accumulated and followed internalization by breast cancer cells.[218]

In the literature, there is few work involved in the cell targeting. This is because most of studies of capsules with cells remain in the in vitro stage. Biospecific interactions between capsules and cells are more important when capsules are applicated in vivo. Up to date, few papers have explored the in vivo behavior of LbL capsules.

1.4.3.4. *In vivo* studies

A first detailed in vivo study was reported by De Koker et al. They subcutaneously injected biodegradable microcapsules composed of dextran sulfate/poly(L-arginine) (DEXS/PARG) in mice.[174] These capsules induced moderate inflammation, similar to adjuvants used for human vaccination such as aluminum hydroxide. Within sixteen days after injection, most of the microcapsules are internalized by the cells and start to get degraded, presumably due to the interplay of mechanical forces and enzymatic action exerted by the phagocyting cells (**Figure 1.17**). Furthermore, the tissue response after pulmonary delivery of DEXS/PARG capsules was also addressed.[207] The capsules became relatively fast (timeframe of 1-2 days)

internalized by alveolar macrophages and dendritic cells, which transported the capsules to the draining lymph nodes. Only capsules debris remained after 2 weeks post-instillation. Although these findings clearly demonstrated that capsules degradation also takes place in vivo there is so far no data on the long term fate of these capsules with respect to clearance from the body.

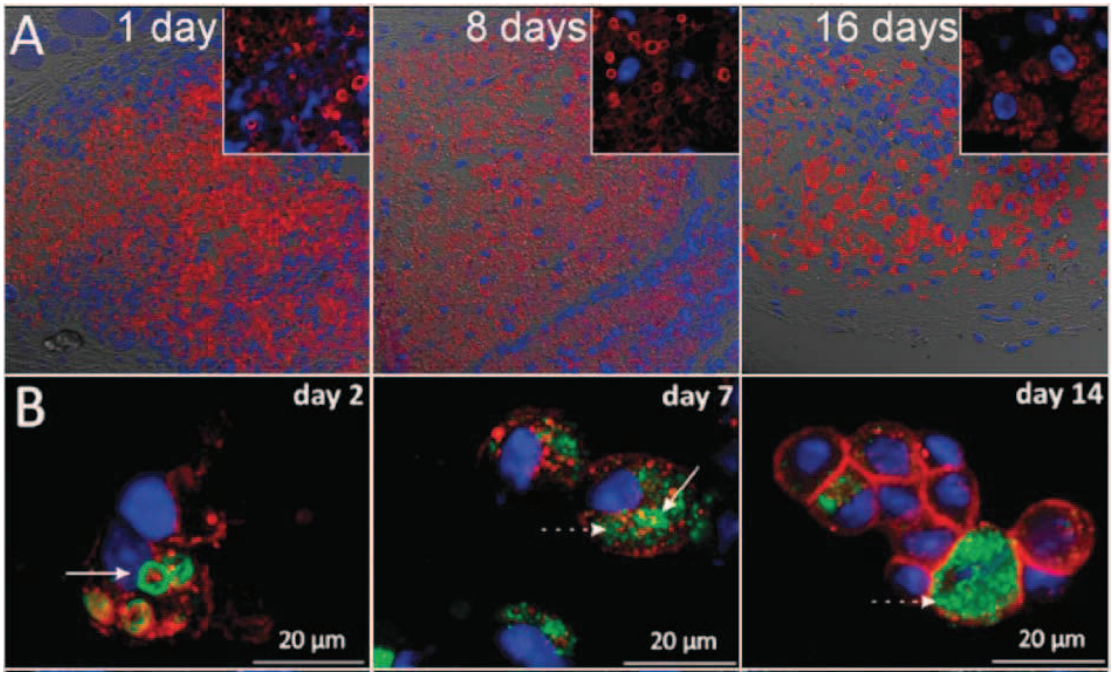

Figure 1. 17. Confocal microscopy images recorded at different time points of (A) tissue section from mice that were subcutaneously injected with degradable DEXS/PARG capsules, (B) cyotospins of alveolar macrophages and dendritic cells of mice that received capsules via pulmonary administration.[174]

Recently, Hammond et al. reported in vivo pH sensitive quantum dots (used in the study to allow in vivo florescence imaging and can easily be replaced by non-toxic templates when intended for therapeutic purposes) templated capsules to target acidified tissue induced by tumor hypoxia.[219] QDs were first coated with a PLL layer modified with iminobiotin (PLLib) followed by a layer of the complementary protein neutravidin (nav) and finally capped with a layer of biotin end-functionalized PEG. The iminobiotin-neutravidin interaction is a pH dependent affinity bond, which is stable at pH 8-12 but decomposes at pH 4-6. The obtained capsules consisted of an acid removable PEG layer, revealing a cationic PLL surface that should enhance cellular uptake by electrostatic interactions. In mice with an implanted tumor, the PEG layer allowed prolonged retention of the capsules in the bloodstream while the pH sensitive capsules (QD/PLLib/nav/PEG) strongly accumulated in the tumor, compared to pH insensitive control capsules using PLL functionalized with biotin (PLLb)

(QD/PLLb/nav/PEG). Moreover, immunohistochemistry revealed that the capsules were indeed located in hypoxic regions (acidic tumor microenvironment) of the solid tumor as shown in **Figure 1.18**.

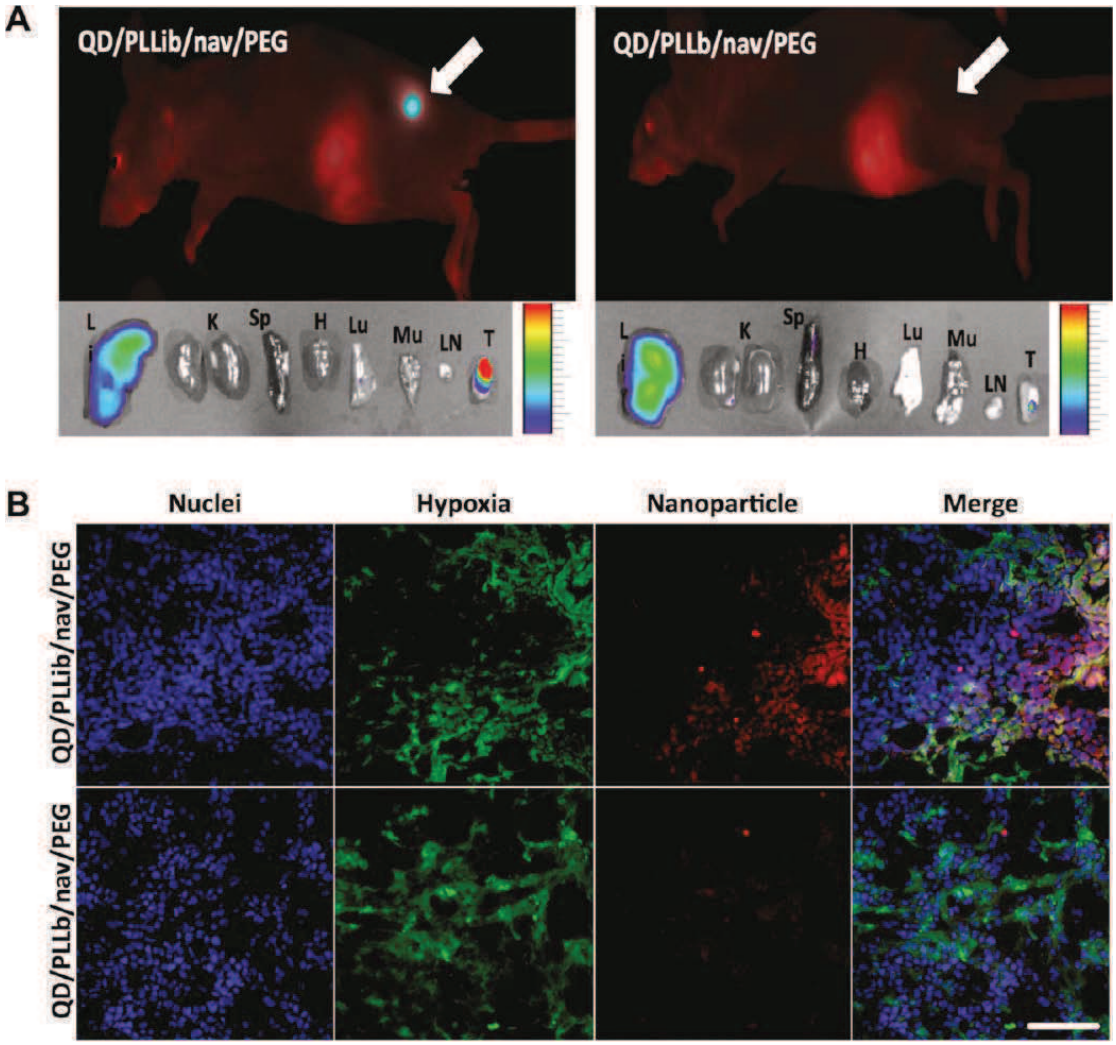

Figure 1. 18. (A) Spectrally unmixed lateral scan of representative MDA-MB-435 mice model and biodistribution of nanoparticles in organs 48 h after administration. QD/PLLib/nav/PEG nanoparticle fluorescence was still present in tumors at 48 h, which suggests significant nanoparticle uptake by tumor cells. Red = tissue and food autofluorescence; teal = nanoparticle fluorescence. Li = liver; K = kidney; Sp = spleen; H = heart; Lu = lungs; Mu = muscle; LN = lymph nodes; T = tumor. Image is spectrally unmixed to separate the nanoparticle fluorescence from tissue autofluorescence. (B) Tumor sections (20×) from mice given QD/PLLib/nav/PEG or QD/PLL/nav/PEG. In tumors given QD/PLLib/nav/PEG treatments, a co-localization between nanoparticle and HIF-1R positive regions was found. Nanoparticle presence was not significant in tumors given QD/PLL/nav/PEG. Red = LbL nanoparticle; green = hypoxia; blue = nuclei. Scale bar = 50 μm.[219]

1.4.4. Cargo release

Most polyelectrolyte capsules can be considered stimulus-responsive. For internal stimuli, changes in the pH value and/or ionic strength could evidently modify the interactions between the successive layers, and induce the release of encapsulated material in the core of capsules. Besides ionic strength and pH value, temperature, solvent polarity, glucose and oxidation have also been used to modify the permeability of capsules. In most of these capsules, however, the release of encapsulated drugs was a rapid "burst" release due to a rapid and large change in the capsule permeability induced by physiological triggers. For example, Sukhorukov and coworkers reported that encapsulated peroxidase was completely released from dextran sulfate/protamine capsules within 1 h by a change in pH.[220] Caruso and co-workers reported that catalase was released from PLL/poly(L-glutamic acid) capsules within 30 min by pH and ion strength changes.[221] Thus, it has been difficult to achieve sustained release of encapsulated drugs from hollow capsules. In addition, these parameters are non-physiological triggers, which often hamper their in-vivo applications.

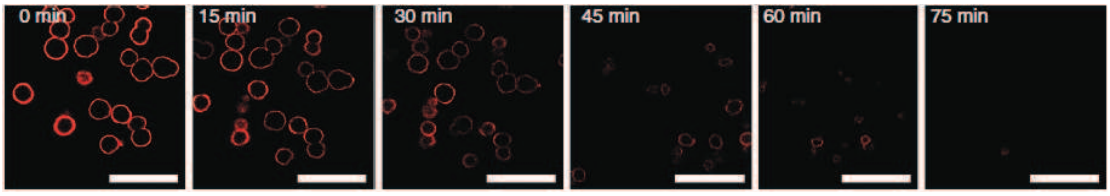

Figure 1. 19. Confocal microscopy snapshots taken during the enzymatic degradation of dextran sulfate/ poly(L-arginine) capsules in the presence of pronase, incubated at physiological conditions. The scale bar represents 10 μm.[215]

De Geest and coworkers demonstrated enzymatic release microcapsules. This type of capsules formed with dextran sulfate and poly(L-arginine).[215] **Figure 1.19** shows a series of confocal microscopy snapshots of the microcapsules incubated in a pronase solution at 37°C. Pronase is a mixture of enzymes able to quasi-cleave every peptide bond. As a function of time, the capsules slightly shrink, crumple and disassemble. Using the enzymatic degradation of the capsule membrane, the membrane thickness and the permeability of the capsule can be expected to be gradually changed. Therefore, sustained release can be accomplished by optimizing the conditions of the enzymatic degradation of capsule membranes. Enzymatically degradable capsules are generally made from polypeptides or polysaccharides, and they rely on the presence of appropriate enzymes for their degradation. This is a useful technique as proteases and nucleases are present in many specific areas of the body, which provides control over the timing or location of degradation. With similar strategy, other research groups

reported later enzymatic degradable capsules.[222,223] It was also shown that the wall properties of capsules can be readily changed upon varying enzyme concentrations.

Disulfide bonds are readily formed by oxidation of thiol groups and are cleaved by the reverse process, reduction. Reducing environments occur at specific locations in the body, the cytosol of the cell and the colon;[224] whereas other locations are comparatively oxidizing, like the blood stream. Thus, redox-activated release is triggered on cellular internalization. Caruso et al. developed capsules using oxidative cross-linking of the thiol moieties in the shell.[225,226] The obtained capsules were broken down in vitro under reductive conditions. This technology was applied by the same group to encapsulate oligonucleotides, peptides, and low-molecular-weight anticancer drugs.[227]

Additionally, release from polyelectrolyte capsules might also be achieved by applying external stimuli. This has mainly been accomplished by incorporating metal nanoparticles or light-responsive dyes into the walls of the capsules.[228] By embedding gold, silver and magnetic NPs into the capsule walls, the release of encapsulated drug molecules from the cavities can be achieved upon exposure to an external physical trigger.[229-232] **Figure 1.20** shows the mechanism of photoactivated release of cargo from the cavity of a polyelectrolyte capsule containing gold NPs in the walls: laser irradiation leads to local heating of the metal AuNPs and subsequent opening of small pores within the capsule wall.[233] Alternatively to laser irradiation methods, high-frequency magnetic field (HFMF) has been proven to trigger the release of drugs from microcapsules prepared by loading ferromagnetic gold-coated cobalt NPs into the walls.[234] In addition, ultrasound has also been used to trigger release from multilayered capsules by mechanically disintegrate the capsule walls.[235]

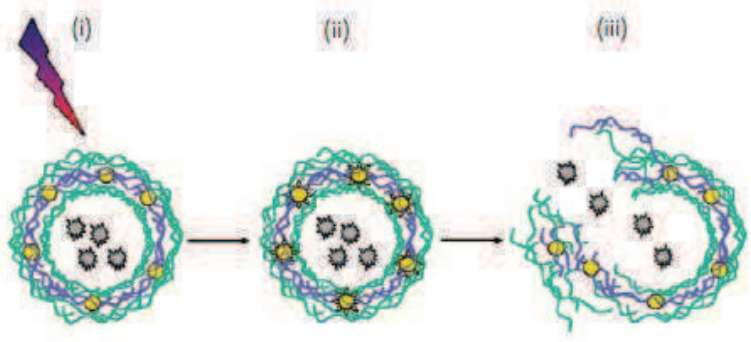

Figure 1. 20. Controlled-release of cargo with light-responsive capsules. (i) Laser irradiation of AuNPs-functionalized capsules leads to (ii) local heating of the metal NPs, and (iii) subsequent rupture of the capsule wall.

All these release studies were performed in vitro. For in vivo studies, biocompatible and biodegradable nanocapsules are required to investigate their pharmacokinetics.

1.5. Conclusion

Although a vast amount of research has increased our knowledge of cancer biology and therapy, which has improved survival of cancer patients, the disease remains lethal. The limitations in current cancer therapies signal the need for novel therapies that attack these specific issues. Nanotechnology provides a unique opportunity to combat cancer on the molecular scale through careful engineering of nanomedicines to specifically interact with cancer cells and inhibit cancer cell function. Various NP formulations have already made their way into the clinic and have become the standard of care in some cancer patients. It should be evident that there is no magical formulation for a nanocarrier, as each needs to be specifically designed for its application. A constant theme throughout nanoparticle mediated drug delivery is extension of circulation time to allow for extravasation across vasculature and into tissue; stable particles with a long circulation half-life are ideal. Additionally, achieving high specificity of nanoparticle accumulation in the area of interest is also optimal. Then, engineering a triggered release functionality with spatial and temporal specificity is also crucial for optimizing delivery. Lastly, the residue of nanoparticle after release of their cargo should degrade without aggregation in tissues.

Polyelectrolyte capsules have emerged as promising carriers for various drugs. Perhaps the biggest advantage of this approach is its versatility. Each application requires particular specifications, and the LbL technique allows the surface chemistry, size, permeability, and degradability to be altered to suit the application. Highly specialized films have been created in recent years. Many different types of drugs can be efficiently encapsulated, either into the film or into the cavity of the carrier. The surface chemistry can be easily altered by adding layers of different polymers or attaching targeting moieties. The degradation and cargo release can be finely controlled by a variety of mechanisms. However, capsules with diameters below 1 μm are required for intravenous administration, and studies of their biodistribution and biocompatibility are also needed to accelerate progress in developing LbL-engineered capsules for biomedicine.

References

(1) Jemal, A.; Bray, F.; Center, M. M.; Ferlay, J.; Ward, E.; Forman, D. *CA: A Cancer Journal for Clinicians* **2011**, *61*, 69.

(2) Carmeliet, P.; Jain, R. K. *Nature* **2000**, *407*, 249.

(3) Mehlen, P.; Puisieux, A. *Nat Rev Cancer* **2006**, *6*, 449.

(4) Brindle, K. *Nat Rev Cancer* **2008**, *8*, 94.

(5) Szakacs, G.; Paterson, J. K.; Ludwig, J. A.; Booth-Genthe, C.; Gottesman, M. M. *Nat Rev Drug Discov* **2006**, *5*, 219.

(6) Farokhzad, O. C.; Langer, R. *ACS Nano* **2009**, *3*, 16.

(7) Barreto, J. A.; O'Malley, W.; Kubeil, M.; Graham, B.; Stephan, H.; Spiccia, L. *Advanced Materials* **2011**, *23*, H18.

(8) Iyer, A. K.; Khaled, G.; Fang, J.; Maeda, H. *Drug Discovery Today* **2006**, *11*, 812.

(9) Ruoslahti, E. *Nat Rev Cancer* **2002**, *2*, 83.

(10) Brigger, I.; Dubernet, C.; Couvreur, P. *Advanced Drug Delivery Reviews* **2002**, *54*, 631.

(11) Maeda, H.; Matsumura, Y. *Crit. Rev. Ther. Drug Carrier Syst.* **1989**, *6*, 193.

(12) Ganta, S.; Devalapally, H.; Shahiwala, A.; Amiji, M. *Journal of Controlled Release* **2008**, *126*, 187.

(13) Barenholz, Y. *Journal of Controlled Release* **2012**, *160*, 117.

(14) Petre, C. E.; Dittmer, D. P. *Int. J. Nanomed.* **2007**, *2*, 277.

(15) Landon, C. D.; Park, J.-Y.; Needham, D.; Dewhirst, M. W. *Open Nanomed. J.* **2010**, *3*, 38.

(16) Green, M. R.; Manikhas, G. M.; Orlov, S.; Afanasyev, B.; Makhson, A. M.; Bhar, P.; Hawkins, M. J. *Annals of Oncology* **2006**, *17*, 1263.

(17) Feng, Z.; Zhao, G.; Yu, L.; Gough, D.; Howell, S. B. *Cancer Chemother. Pharmacol.* **2010**, *65*, 923.

(18) Kim, T.-Y.; Kim, D.-W.; Chung, J.-Y.; Shin, S. G.; Kim, S.-C.; Heo, D. S.; Kim, N. K.; Bang, Y.-J. *Clinical Cancer Research* **2004**, *10*, 3708.

(19) Kim, D.-W.; Kim, S.-Y.; Kim, H.-K.; Kim, S.-W.; Shin, S. W.; Kim, J. S.; Park, K.; Lee, M. Y.; Heo, D. S. *Annals of Oncology* **2007**, *18*, 2009.

(20) Davis, M. E. *Advanced Drug Delivery Reviews* **2009**, *61*, 1189.

(21) Davis, M. E. *Molecular Pharmaceutics* **2009**, *6*, 659.

(22) Davis, M. E.; Zuckerman, J. E.; Choi, C.-H. J.; Seligson, D.; Tolcher, A.; Alabi, C. A.; Yen, Y.; Heidel, J. D.; Ribas, A. *Nature (London, United Kingdom)* **2010**, *464*, 1067.

(23) Maier-Hauff, K.; Ulrich, F.; Nestler, D.; Niehoff, H.; Wust, P.; Thiesen, B.; Orawa, H.; Budach, V.; Jordan, A. *J Neurooncol* **2011**, *103*, 317.

(24) Libutti, S. K.; Paciotti, G. F.; Byrnes, A. A.; Alexander, H. R.; Gannon, W. E.; Walker, M.; Seidel, G. D.; Yuldasheva, N.; Tamarkin, L. *Clinical Cancer Research* **2010**, *16*, 6139.

(25) Reimer, P.; Balzer, T. *Eur Radiol* **2003**, *13*, 1266.

(26) Perrie, Y.; Frederik, P. M.; Gregoriadis, G. *Vaccine* **2001**, *19*, 3301.

(27) Lasic, D. D.; Templeton, N. S. *Advanced Drug Delivery Reviews* **1996**, *20*, 221.

(28) Babincová, M.; Čičmanec, P.; Altanerová, V.; Altaner, Č.; Babinec, P. *Bioelectrochemistry* **2002**, *55*, 17.

(29) Huynh, N. T.; Passirani, C.; Saulnier, P.; Benoit, J. P. *Int. J. Pharm.* **2009**, *379*, 201.

(30) Kaneda, Y. *Advanced Drug Delivery Reviews* **2000**, *43*, 197.

(31) Pinto-Alphandary, H.; Andremont, A.; Couvreur, P. *International Journal of Antimicrobial Agents* **2000**, *13*, 155.

(32) Andresen, T. L.; Jensen, S. S.; Jorgensen, K. *Prog. Lipid Res.* **2005**, *44*, 68.

(33) Park, J. W. *Breast Cancer Res.* **2002**, *4*, 95.

(34) Gabizon, A.; Shmeeda, H.; Barenholz, Y. *Clinical Pharmacokinetics* **2003**, *42*, 419.

(35) Woodle, M. C. *Advanced Drug Delivery Reviews* **1995**, *16*, 249.

(36) Oerlemans, C.; Bult, W.; Bos, M.; Storm, G.; Nijsen, J. F. W.; Hennink, W. E. *Pharmaceutical Research* **2010**, *27*, 2569.

(37) Kwon, G. S. *Crit. Rev. Ther. Drug Carrier Syst.* **2003**, *20*, 357.

(38) Gao, Z. G.; Lee, D. H.; Kim, D. I.; Bae, Y. H. *Journal of Drug Targeting* **2005**, *13*, 391.

(39) Koziara, J. M.; Whisman, T. R.; Tseng, M. T.; Mumper, R. J. *Journal of Controlled Release* **2006**, *112*, 312.

(40) Jones, M.-C.; Leroux, J.-C. *European Journal of Pharmaceutics and Biopharmaceutics* **1999**, *48*, 101.

(41) Upadhyay, K. K.; Le, M. J. F.; Misra, A.; Voisin, P.; Bouchaud, V.; Ibarboure, E.; Schatz, C.; Lecommandoux, S. *Biomacromolecules* **2009**, *10*, 2802.

(42) Lee, J. S.; Feijen, J. *Journal of Controlled Release* **2012**, *161*, 473.

(43) Discher, D. E.; Ortiz, V.; Srinivas, G.; Klein, M. L.; Kim, Y.; Christian, D.; Cai, S.; Photos, P.; Ahmed, F. *Progress in Polymer Science* **2007**, *32*, 838.

(44) Lin, J. J.; Ghoroghchian, P. P.; Zhang, Y.; Hammer, D. A. *Langmuir* **2006**, *22*, 3975.

(45) Meng, F.; Zhong, Z. *J. Phys. Chem. Lett.* **2011**, *2*, 1533.

(46) Kang, S. W.; Li, Y.; Park, J. H.; Lee, D. S. *Polymer*, Ahead of Print.

(47) Li, M.-H.; Keller, P. *Soft Matter* **2009**, *5*, 927.

(48) Mabrouk, E.; Cuvelier, D.; Brochard-Wyart, F.; Nassoy, P.; Li, M.-H. *Proc. Natl. Acad. Sci. U. S. A.* **2009**, *106*, 7294.

(49) Ahmed, F.; Pakunlu, R. I.; Srinivas, G.; Brannan, A.; Bates, F.; Klein, M. L.; Minko, T.; Discher, D. E. *Molecular Pharmaceutics* **2006**, *3*, 340.

(50) Meng, F.; Zhong, Z.; Feijen, J. *Biomacromolecules* **2009**, *10*, 197.

(51) Amstad, E.; Kim, S.-H.; Weitz, D. A. *Angewandte Chemie International Edition* **2012**, *51*, 12499.

(52) Onaca, O.; Enea, R.; Hughes, D. W.; Meier, W. *Macromolecular Bioscience* **2009**, *9*, 129.

(53) Cegnar, M.; Kristl, J.; Kos, J. *Expert Opin. Biol. Ther.* **2005**, *5*, 1557.

(54) Vauthier, C.; Bouchemal, K. *Pharmaceutical Research* **2009**, *26*, 1025.

(55) Mora-Huertas, C. E.; Fessi, H.; Elaissari, A. *Int. J. Pharm.* **2010**, *385*, 113.

(56) Hamidi, M.; Azadi, A.; Rafiei, P. *Adv. Drug Delivery Rev.* **2008**, *60*, 1638.

(57) Chacko, R. T.; Ventura, J.; Zhuang, J.; Thayumanavan, S. *Advanced Drug Delivery Reviews* **2012**, *64*, 836.

(58) Liu, X.; Heng, W. S.; Paul; Li, Q.; Chan, L. W. *Journal of Controlled Release* **2006**, *116*, 35.

(59) Bouhadir, K. H.; Alsberg, E.; Mooney, D. J. *Biomaterials* **2001**, *22*, 2625.

(60) Al-Ghananeem, A.; Malkawi, A.; Muammer, Y.; Balko, J.; Black, E.; Mourad, W.; Romond, E. *AAPS PharmSciTech* **2009**, *10*, 410.

(61) Gerber, D. E.; Gallia, G. L.; Tyler, B. M.; Eberhart, C. G.; Royer, G.; Grossman, S. A. *Journal of Biomedical Materials Research Part A* **2011**, *99A*, 479.

(62) Li, X.; Kong, X.; Zhang, J.; Wang, Y.; Wang, Y.; Shi, S.; Guo, G.; Luo, F.; Zhao, X.; Wei, Y.; Qian, Z. *Journal of Pharmaceutical Sciences* **2011**, *100*, 232.

(63) Ampollini, L.; Sonvico, F.; Barocelli, E.; Cavazzoni, A.; Bilancia, R.; Mucchino, C.; Cantoni, A. M.; Carbognani, P. *European Journal of Cardio-Thoracic Surgery* **2010**, *37*, 557.

(64) Vassileva, V.; Grant, J.; Souza, R.; Allen, C.; Piquette-Miller, M. *Cancer Chemother Pharmacol* **2007**, *60*, 907.

(65) Davidson, B. S.; Izzo, F.; Cromeens, D. M.; Stephens, L. C.; Siddik, Z. H.; Curley, S. A. *The Journal of surgical research* **1995**, *58*, 618.

(66) Almond, B. A.; Hadba, A. R.; Freeman, S. T.; Cuevas, B. J.; York, A. M.; Detrisac, C. J.; Goldberg, E. P. *Journal of Controlled Release* **2003**, *91*, 147.

(67) Kakinoki, S.; Taguchi, T. *European Journal of Pharmaceutics and Biopharmaceutics* **2007**, *67*, 676.

(68) McDaniel, J. R.; Callahan, D. J.; Chilkoti, A. *Advanced Drug Delivery Reviews* **2010**, *62*, 1456.

(69) Konishi, M.; Tabata, Y.; Kariya, M.; Suzuki, A.; Mandai, M.; Nanbu, K.; Takakura, K.; Fujii, S. *Journal of Controlled Release* **2003**, *92*, 301.

(70) Stuart, K.; Stokes, K.; Jenkins, R.; Trey, C.; Clouse, M. *Cancer* **1993**, *72*, 3202.

(71) Hoffman, A. S. *Journal of Controlled Release* **2008**, *132*, 153.
(72) Moses, M. A.; Brem, H.; Langer, R. *Cancer Cell* **2003**, *4*, 337.
(73) Langer, R. *Pharmacology & Therapeutics* **1983**, *21*, 35.
(74) De Souza, R.; Zahedi, P.; Allen, C. J.; Piquette-Miller, M. *Drug Delivery* **2010**, *17*, 365.
(75) Lee, C. C.; Gillies, E. R.; Fox, M. E.; Guillaudeu, S. J.; Fréchet, J. M. J.; Dy, E. E.; Szoka, F. C. *Proceedings of the National Academy of Sciences* **2006**, *103*, 16649.
(76) Bagalkot, V.; Zhang, L.; Levy-Nissenbaum, E.; Jon, S.; Kantoff, P. W.; Langer, R.; Farokhzad, O. C. *Nano Letters* **2007**, *7*, 3065.
(77) Gibson, J. D.; Khanal, B. P.; Zubarev, E. R. *Journal of the American Chemical Society* **2007**, *129*, 11653.
(78) Choi, A.; Cho, S. J.; Desbarats, J.; Lovric, J.; Maysinger, D. *Journal of Nanobiotechnology* **2007**, *5*, 1.
(79) Smith, A.; Ruan, G.; Rhyner, M.; Nie, S. *Ann Biomed Eng* **2006**, *34*, 3.
(80) Dubertret, B. P. D. J. N. V. A. H. L. A. *Science* **2002**, *298*, 1759.
(81) Pons, T.; Pic, E.; Lequeux, N.; Cassette, E.; Bezdetnaya, L.; Guillemin, F.; Marchal, F.; Dubertret, B. *ACS Nano* **2010**, *4*, 2531.
(82) Rao, J. *ACS Nano* **2008**, *2*, 1984.
(83) Doherty, G. J.; McMahon, H. T. *Annual Review of Biochemistry* **2009**, *78*, 857.
(84) Yuan, F.; Dellian, M.; Fukumura, D.; Leunig, M.; Berk, D. A.; Torchilin, V. P.; Jain, R. K. *Cancer Research* **1995**, *55*, 3752.
(85) Bae, Y. H. *Journal of Controlled Release* **2009**, *133*, 2.
(86) Davis, M. E.; Chen, Z.; Shin, D. M. *Nat Rev Drug Discov* **2008**, *7*, 771.
(87) Gullotti, E.; Yeo, Y. *Molecular Pharmaceutics* **2009**, *6*, 1041.
(88) Alexis, F.; Pridgen, E.; Molnar, L. K.; Farokhzad, O. C. *Molecular Pharmaceutics* **2008**, *5*, 505.
(89) Sunderland, C. J.; Steiert, M.; Talmadge, J. E.; Derfus, A. M.; Barry, S. E. *Drug Development Research* **2006**, *67*, 70.
(90) Shutava, T. G.; Arapov, K. A.; Pattekari, P. P.; Lvov, Y. M.; Levchenko, T. S.; Sawant, R. R.; Torchilin, V. P. *MRS Online Proceedings Library* **2012**, *1416*, null.
(91) Owens Iii, D. E.; Peppas, N. A. *International Journal of Pharmaceutics* **2006**, *307*, 93.
(92) Vlerken, L.; Vyas, T.; Amiji, M. *Pharmaceutical Research* **2007**, *24*, 1405.
(93) Cho, K.; Wang, X.; Nie, S.; Chen, Z.; Shin, D. M. *Clinical Cancer Research* **2008**, *14*, 1310.
(94) Sinha, R.; Kim, G. J.; Nie, S.; Shin, D. M. *Molecular Cancer Therapeutics* **2006**, *5*, 1909.
(95) Gabizon, A. A. *Cancer Investigation* **2001**, *19*, 424.
(96) Mishra, S.; Webster, P.; Davis, M. E. *European Journal of Cell Biology* **2004**, *83*, 97.
(97) Gryparis, E. C.; Hatziapostolou, M.; Papadimitriou, E.; Avgoustakis, K. *European Journal of Pharmaceutics and Biopharmaceutics* **2007**, *67*, 1.
(98) Romberg, B.; Hennink, W.; Storm, G. *Pharmaceutical Research* **2008**, *25*, 55.
(99) Hong, R.-L.; Huang, C.-J.; Tseng, Y.-L.; Pang, V. F.; Chen, S.-T.; Liu, J.-J.; Chang, F.-H. *Clinical Cancer Research* **1999**, *5*, 3645.
(100) Lee, R. J.; Low, P. S. *Journal of Biological Chemistry* **1994**, *269*, 3198.
(101) Loomis, K.; McNeeley, K.; Bellamkonda, R. V. *Soft Matter* **2011**, *7*, 839.
(102) Antony, A. *Blood* **1992**, *79*, 2807.
(103) Low, P. S.; Henne, W. A.; Doorneweerd, D. D. *Accounts of Chemical Research* **2007**, *41*, 120.
(104) Lee, S.-M.; Chen, H.; O'Halloran, T. V.; Nguyen, S. T. *Journal of the American Chemical Society* **2009**, *131*, 9311.
(105) Kukowska-Latallo, J. F.; Candido, K. A.; Cao, Z.; Nigavekar, S. S.; Majoros, I. J.; Thomas, T. P.; Balogh, L. P.; Khan, M. K.; Baker, J. R. *Cancer Research* **2005**, *65*, 5317.
(106) Maynard, J.; Georgiou, G. *Annual Review of Biomedical Engineering* **2000**, *2*, 339.
(107) Weiner, L. M.; Adams, G. P. *Oncogene* **2000**, *19*, 6144.
(108) Nobs, L.; Buchegger, F.; Gurny, R.; Allémann, E. *European Journal of Pharmaceutics and Biopharmaceutics* **2004**, *58*, 483.

(109) Nobs, L.; Buchegger, F.; Gurny, R.; Allemann, E. *Bioconjugate Chem.* **2006**, *17*, 139.

(110) Nellis, D. F.; Ekstrom, D. L.; Kirpotin, D. B.; Zhu, J.; Andersson, R.; Broadt, T. L.; Ouellette, T. F.; Perkins, S. C.; Roach, J. M.; Drummond, D. C.; Hong, K.; Marks, J. D.; Park, J. W.; Giardina, S. L. *Biotechnology Progress* **2005**, *21*, 205.

(111) Nimjee, S. M.; Rusconi, C. P.; Sullenger, B. A. *Annu. Rev. Med.* **2005**, *56*, 555.

(112) Farokhzad, O. C.; Jon, S.; Khademhosseini, A.; Tran, T.-N. T.; LaVan, D. A.; Langer, R. *Cancer Research* **2004**, *64*, 7668.

(113) Lupold, S. E.; Hicke, B. J.; Lin, Y.; Coffey, D. S. *Cancer Research* **2002**, *62*, 4029.

(114) Farokhzad, O. C.; Cheng, J.; Teply, B. A.; Sherifi, I.; Jon, S.; Kantoff, P. W.; Richie, J. P.; Langer, R. *Proceedings of the National Academy of Sciences* **2006**, *103*, 6315.

(115) Day, A. J.; Prestwich, G. D. *Journal of Biological Chemistry* **2002**, *277*, 4585.

(116) Hua, Q.; Knudson, C. B.; Knudson, W. *Journal of Cell Science* **1993**, *106*, 365.

(117) Eliaz, R. E.; Szoka, F. C. *Cancer Research* **2001**, *61*, 2592.

(118) Peer, D.; Margalit, R. *Neoplasia (Ann Arbor, MI, U. S.)* **2004**, *6*, 343.

(119) Peer, D.; Margalit, R. *International Journal of Cancer* **2004**, *108*, 780.

(120) El-Dakdouki, M. H.; Zhu, D. C.; El-Boubbou, K.; Kamat, M.; Chen, J.; Li, W.; Huang, X. *Biomacromolecules* **2012**, *13*, 1144.

(121) Kirpotin, D. B.; Drummond, D. C.; Shao, Y.; Shalaby, M. R.; Hong, K.; Nielsen, U. B.; Marks, J. D.; Benz, C. C.; Park, J. W. *Cancer Research* **2006**, *66*, 6732.

(122) Mamot, C.; Drummond, D. C.; Noble, C. O.; Kallab, V.; Guo, Z.; Hong, K.; Kirpotin, D. B.; Park, J. W. *Cancer Research* **2005**, *65*, 11631.

(123) Gabizon, A. A.; Shmeeda, H.; Zalipsky, S. *Journal of Liposome Research* **2006**, *16*, 175.

(124) Bartlett, D. W.; Su, H.; Hildebrandt, I. J.; Weber, W. A.; Davis, M. E. *Proceedings of the National Academy of Sciences* **2007**, *104*, 15549.

(125) Xiong, X.-B.; Huang, Y.; Lu, W.-L.; Zhang, X.; Zhang, H.; Nagai, T.; Zhang, Q. *Journal of Pharmaceutical Sciences* **2005**, *94*, 1782.

(126) ElBayoumi, T. A.; Torchilin, V. P. *Mol. Pharmaceutics* **2009**, *6*, 246.

(127) ElBayoumi, T. A.; Torchilin, V. P. *Clinical Cancer Research* **2009**, *15*, 1973.

(128) Hu, Z.; Luo, F.; Pan, Y.; Hou, C.; Ren, L.; Chen, J.; Wang, J.; Zhang, Y. *Journal of Biomedical Materials Research Part A* **2008**, *85A*, 797.

(129) Yang, T.; Choi, M.-K.; Cui, F.-D.; Lee, S.-J.; Chung, S.-J.; Shim, C.-K.; Kim, D.-D. *Pharmaceutical Research* **2007**, *24*, 2402.

(130) Yoo, H. S.; Park, T. G. *Journal of Controlled Release* **2004**, *96*, 273.

(131) Gu, F.; Zhang, L.; Teply, B. A.; Mann, N.; Wang, A.; Radovic-Moreno, A. F.; Langer, R.; Farokhzad, O. C. *Proceedings of the National Academy of Sciences* **2008**, *105*, 2586.

(132) Lehner, R.; Wang, X.; Wolf, M.; Hunziker, P. *Journal of Controlled Release* **2012**, *161*, 307.

(133) Lee, E. S.; Gao, Z.; Bae, Y. H. *Journal of Controlled Release* **2008**, *132*, 164.

(134) Ko, J.; Park, K.; Kim, Y.-S.; Kim, M. S.; Han, J. K.; Kim, K.; Park, R.-W.; Kim, I.-S.; Song, H. K.; Lee, D. S.; Kwon, I. C. *Journal of Controlled Release* **2007**, *123*, 109.

(135) Talelli, M.; Iman, M.; Varkouhi, A. K.; Rijcken, C. J. F.; Schiffelers, R. M.; Etrych, T.; Ulbrich, K.; van Nostrum, C. F.; Lammers, T.; Storm, G.; Hennink, W. E. *Biomaterials* **2010**, *31*, 7797.

(136) Sawant, R. M.; Hurley, J. P.; Salmaso, S.; Kale, A.; Tolcheva, E.; Levchenko, T. S.; Torchilin, V. P. *Bioconjugate Chem.* **2006**, *17*, 943.

(137) Lee, E. S.; Gao, Z.; Kim, D.; Park, K.; Kwon, I. C.; Bae, Y. H. *Journal of Controlled Release* **2008**, *129*, 228.

(138) Koo, H.; Jin, G.-w.; Kang, H.; Lee, Y.; Nam, K.; Zhe Bai, C.; Park, J.-S. *Biomaterials* **2010**, *31*, 988.

(139) Li, Y.; Dong, H.; Wang, K.; Shi, D.; Zhang, X.; Zhuo, R. *Sci. China Chem.* **2010**, *53*, 447.

(140) Tew, K. D.; Ali-Osman, F. *Current Opinion in Pharmacology* **2007**, *7*, 353.

(141) Sánchez, M.; Aranda, F. J.; Teruel, J. A.; Ortiz, A. *Chemistry and Physics of Lipids* **2011**, *164*, 16.

(142) Kim, D.; Lee, E. S.; Oh, K. T.; Gao, Z. G.; Bae, Y. H. *Small* **2008**, *4*, 2043.

(143) Kim, H.; Kim, S.; Park, C.; Lee, H.; Park, H. J.; Kim, C. *Advanced Materials* **2010**, *22*, 4280.

(144) Huang, Z.; Li, W.; MacKay, J. A.; Szoka, F. C. *Mol Ther* **2005**, *11*, 409.

(145) Gabizon, A. A.; Tzemach, D.; Horowitz, A. T.; Shmeeda, H.; Yeh, J.; Zalipsky, S. *Clinical Cancer Research* **2006**, *12*, 1913.

(146) Hatakeyama, H.; Akita, H.; Kogure, K.; Oishi, M.; Nagasaki, Y.; Kihira, Y.; Ueno, M.; Kobayashi, H.; Kikuchi, H.; Harashima, H. *Gene Ther* **2006**, *14*, 68.

(147) Torchilin, V. *European Journal of Pharmaceutics and Biopharmaceutics* **2009**, *71*, 431.

(148) Kojima, C. *Expert Opinion on Drug Delivery* **2010**, *7*, 307.

(149) Lee, Y.; Park, S. Y.; Kim, C.; Park, T. G. *Journal of Controlled Release* **2009**, *135*, 89.

(150) Fomina, N.; McFearin, C.; Sermsakdi, M.; Edigin, O.; Almutairi, A. *Journal of the American Chemical Society* **2010**, *132*, 9540.

(151) Cabane, E.; Malinova, V.; Meier, W. *Macromolecular Chemistry and Physics* **2010**, *211*, 1847.

(152) Li, F.; Bae, B.-c.; Na, K. *Bioconjugate Chemistry* **2010**, *21*, 1312.

(153) Mitragotri, S. *Nat Rev Drug Discov* **2005**, *4*, 255.

(154) Schroeder, A.; Honen, R.; Turjeman, K.; Gabizon, A.; Kost, J.; Barenholz, Y. *Journal of Controlled Release* **2009**, *137*, 63.

(155) Al-Deen, F. N.; Ho, J.; Selomulya, C.; Ma, C.; Coppel, R. *Langmuir* **2011**, *27*, 3703.

(156) Pouponneau, P.; Leroux, J.-C.; Soulez, G.; Gaboury, L.; Martel, S. *Biomaterials* **2011**, *32*, 3481.

(157) Shirakawa, M.; Yamamto, T.; Nakai, K.; Aburai, K.; Kawatobi, S.; Tsurubuchi, T.; Yamamoto, Y.; Yokoyama, Y.; Okuno, H.; Matsumura, A. *Applied Radiation and Isotopes* **2009**, *67*, S88.

(158) Ueno, M.; Ban, H. S.; Nakai, K.; Inomata, R.; Kaneda, Y.; Matsumura, A.; Nakamura, H. *Bioorganic & Medicinal Chemistry* **2010**, *18*, 3059.

(159) Rozhkova, E. A. *Advanced Materials* **2011**, *23*, H136.

(160) Minelli, C.; Lowe, S. B.; Stevens, M. M. *Small* **2010**, *6*, 2336.

(161) Weissleder, R.; Pittet, M. J. *Nature* **2008**, *452*, 580.

(162) Decher, G. *Science* **1997**, *277*, 1232.

(163) Sukhorukov, G. B.; Rogach, A. L.; Zebli, B.; Liedl, T.; Skirtach, A. G.; Koehler, K.; Antipov, A. A.; Gaponik, N.; Susha, A. S.; Winterhalter, M.; Parak, W. J. *Small* **2005**, *1*, 194.

(164) De Geest, B. G.; De Koker, S.; Sukhorukov, G. B.; Kreft, O.; Parak, W. J.; Skirtach, A. G.; Demeester, J.; De Smedt, S. C.; Hennink, W. E. *Soft Matter* **2009**, *5*, 282.

(165) De Geest, B. G.; Sanders, N. N.; Sukhorukov, G. B.; Demeester, J.; De Smedt, S. C. *Chemical Society Reviews* **2007**, *36*, 636.

(166) De, K. S.; Hoogenboom, R.; De, G. B. G. *Chemical Society Reviews* **2012**, *41*, 2867.

(167) De Koker, S.; De Cock, L. J.; Rivera-Gil, P.; Parak, W. J.; Auzély Velty, R.; Vervaet, C.; Remon, J. P.; Grooten, J.; De Geest, B. G. *Advanced Drug Delivery Reviews* **2011**, *63*, 748.

(168) del, M. L. L.; Rivera-Gil, P.; Abbasi, A. Z.; Ochs, M.; Ganas, C.; Zins, I.; Soennichsen, C.; Parak, W. J. *Nanoscale* **2010**, *2*, 458.

(169) De Cock, L. J.; De Koker, S.; De Geest, B. G.; Grooten, J.; Vervaet, C.; Remon, J. P.; Sukhorukov, G. B.; Antipina, M. N. *Angewandte Chemie International Edition* **2010**, *49*, 6954.

(170) De Geest, B. G.; Sukhorukov, G. B.; Moehwald, H. *Expert Opinion on Drug Delivery* **2009**, *6*, 613.

(171) Becker, A. L.; Johnston, A. P. R.; Caruso, F. *Small* **2010**, *6*, n/a.

(172) Sukhorukov, G. B.; Donath, E.; Lichtenfeld, H.; Knippel, E.; Knippel, M.; Budde, A.; Möhwald, H. *Colloids and Surfaces A: Physicochemical and Engineering Aspects* **1998**, *137*, 253.

(173) Peyratout, C. S.; Dähne, L. *Angewandte Chemie International Edition* **2004**, *43*, 3762.

(174) De Koker, S.; De Geest, B. G.; Cuvelier, C.; Ferdinande, L.; Deckers, W.; Hennink, W. E.; De Smedt, S.; Mertens, N. *Advanced Functional Materials* **2007**, *17*, 3754.

(175) Aderem, A.; Underhill, D. M. *Annual Review of Immunology* **1999**, *17*, 593.

(176) Aderem, A. *Cell* **2002**, *110*, 5.

(177) Cortez, C.; Tomaskovic-Crook, E.; Johnston, A. P. R.; Radt, B.; Cody, S. H.; Scott, A. M.; Nice, E. C.; Heath, J. K.; Caruso, F. *Advanced Materials* **2006**, *18*, 1998.

(178) Reibetanz, U.; Claus, C.; Typlt, E.; Hofmann, J.; Donath, E. *Macromolecular Bioscience* **2006**, *6*, 153.

(179) Saurer, E. M.; Jewell, C. M.; Kuchenreuther, J. M.; Lynn, D. M. *Acta Biomaterialia* **2009**, *5*, 913.

(180) Schneider, G. F.; Subr, V.; Ulbrich, K.; Decher, G. *Nano Letters* **2009**, *9*, 636.

(181) Gittins, D. I.; Caruso, F. *Advanced Materials* **2000**, *12*, 1947.

(182) Heuberger, R.; Sukhorukov, G.; Vörös, J.; Textor, M.; Möhwald, H. *Advanced Functional Materials* **2005**, *15*, 357.

(183) Moya, S.; Donath, E.; Sukhorukov, G. B.; Auch, M.; Baeumler, H.; Lichtenfeld, H.; Moehwald, H. *Macromolecules* **2000**, *33*, 4538.

(184) Katagiri, K.; Caruso, F. *Macromolecules* **2004**, *37*, 9947.

(185) Poon, Z.; Lee, J. B.; Morton, S. W.; Hammond, P. T. *Nano Letters* **2011**, *11*, 2096.

(186) Liu, X.; Gao, C.; Shen, J.; Mohwald, H. *Macromolecular Bioscience* **2005**, *5*, 1209.

(187) Yan, Y.; Johnston, A. P. R.; Dodds, S. J.; Kamphuis, M. M. J.; Ferguson, C.; Parton, R. G.; Nice, E. C.; Heath, J. K.; Caruso, F. *ACS Nano* **2010**, *4*, 2928.

(188) Shutava, T. G.; Balkundi, S. S.; Vangala, P.; Steffan, J. J.; Bigelow, R. L.; Cardelli, J. A.; O'Neal, D. P.; Lvov, Y. M. *ACS Nano* **2009**, *3*, 1877.

(189) Becker, A. L.; Orlotti, N. I.; Folini, M.; Cavalieri, F.; Zelikin, A. N.; Johnston, A. P. R.; Zaffaroni, N.; Caruso, F. *ACS Nano* **2011**, *5*, 1335.

(190) Elbakry, A.; Zaky, A.; Liebl, R.; Rachel, R.; Goepferich, A.; Breunig, M. *Nano Letters* **2009**, *9*, 2059.

(191) Sivakumar, S.; Bansal, V.; Cortez, C.; Chong, S.-F.; Zelikin, A. N.; Caruso, F. *Advanced Materials (Weinheim, Germany)* **2009**, *21*, 1820.

(192) Wang, K.; He, Q.; Yan, X.; Cui, Y.; Qi, W.; Duan, L.; Li, J. *Journal of Materials Chemistry* **2007**, *17*, 4018.

(193) Manna, U.; Patil, S. *The Journal of Physical Chemistry B* **2008**, *112*, 13258.

(194) Chandrawati, R.; Städler, B.; Postma, A.; Connal, L. A.; Chong, S.-F.; Zelikin, A. N.; Caruso, F. *Biomaterials* **2009**, *30*, 5988.

(195) Kopecek, J.; Kopeckova, P.; Minko, T.; Lu, Z. R.; Peterson, C. M. *Journal of Controlled Release* **2001**, *74*, 147.

(196) Ochs, C. J.; Such, G. K.; Yan, Y.; van, K. M. P.; Caruso, F. *ACS Nano* **2010**, *4*, 1653.

(197) Yan, Y.; Ochs, C. J.; Such, G. K.; Heath, J. K.; Nice, E. C.; Caruso, F. *Advanced Materials (Weinheim, Germany)* **2010**, *22*, 5398.

(198) Trau, D.; Yang, W.; Seydack, M.; Caruso, F.; Yu, N.-T.; Renneberg, R. *Analytical Chemistry* **2002**, *74*, 5480.

(199) Wang, Y.; Yan, Y.; Cui, J.; Hosta-Rigau, L.; Heath, J. K.; Nice, E. C.; Caruso, F. *Advanced Materials* **2010**, *22*, 4293.

(200) Lee, M.-Y.; Park, S.-J.; Park, K.; Kim, K. S.; Lee, H.; Hahn, S. K. *ACS Nano* **2011**, *5*, 6138.

(201) Gil, P. R.; del Mercato, L. L.; del_Pino, P.; Muñoz_Javier, A.; Parak, W. J. *Nano Today* **2008**, *3*, 12.

(202) Kirchner, C.; Javier, A. M.; Susha, A. S.; Rogach, A. L.; Kreft, O.; Sukhorukov, G. B.; Parak, W. J. *Talanta* **2005**, *67*, 486.

(203) Hunter, A. C. *Advanced Drug Delivery Reviews* **2006**, *58*, 1523.

(204) Moghimi, S. M.; Symonds, P.; Murray, J. C.; Hunter, A. C.; Debska, G.; Szewczyk, A. *Mol. Ther.* **2005**, *11*, 990.

(205) Fischer, D.; Li, Y.; Ahlemeyer, B.; Krieglstein, J.; Kissel, T. *Biomaterials* **2003**, *24*, 1121.

(206) De Koker, S.; De Geest, B. G.; Singh, S. K.; De Rycke, R.; Naessens, T.; Van Kooyk, Y.; Demeester, J.; De Smedt, S. C.; Grooten, J. *Angewandte Chemie, International Edition* **2009**, *48*, 8485.

(207) De Koker, S.; Naessens, T.; De Geest, B. G.; Bogaert, P.; Demeester, J.; De Smedt, S.; Grooten, J. *The Journal of Immunology* **2010**, *184*, 203.

(208) De, R. R.; Zelikin, A. N.; Johnston, A. P. R.; Sexton, A.; Chong, S.-F.; Cortez, C.; Mulholland, W.; Caruso, F.; Kent, S. J. *Advanced Materials (Weinheim, Germany)* **2008**, *20*, 4698.

(209) Szarpak, A.; Cui, D.; Dubreuil, F.; De, G. B. G.; De, C. L. J.; Picart, C.; Auzely-Velty, R. *Biomacromolecules* **2010**, *11*, 713.

(210) Javier, A. M.; Kreft, O.; Semmling, M.; Kempter, S.; Skirtach, A. G.; Bruns, O. T.; del Pino, P.; Bedard, M. F.; Raedler, J.; Kaes, J.; Plank, C.; Sukhorukov, G. B.; Parak, W. J. *Advanced Materials (Weinheim, Germany)* **2008**, *20*, 4281.

(211) Sarkar, K.; Kruhlak, M. J.; Erlandsen, S. L.; Shaw, S. *Immunology* **2005**, *116*, 513.

(212) Schnitzer, J. E.; Oh, P.; Pinney, E.; Allard, J. *The Journal of Cell Biology* **1994**, *127*, 1217.

(213) Orlandi, P. A.; Fishman, P. H. *The Journal of Cell Biology* **1998**, *141*, 905.

(214) Wang, L. H.; Rothberg, K. G.; Anderson, R. G. *The Journal of Cell Biology* **1993**, *123*, 1107.

(215) De Geest, B. G.; Vandenbroucke, R. E.; Guenther, A. M.; Sukhorukov, G. B.; Hennink, W. E.; Sanders, N. N.; Demeester, J.; De Smedt, S. C. *Advanced Materials (Weinheim, Germany)* **2006**, *18*, 1005.

(216) Rivera-Gil, P.; De Koker, S.; De Geest, B. G.; Parak, W. J. *Nano Letters* **2009**, *9*, 4398.

(217) Cortez, C.; Tomaskovic-Crook, E.; Johnston, A. P. R.; Scott, A. M.; Nice, E. C.; Heath, J. K.; Caruso, F. *ACS Nano* **2007**, *1*, 93.

(218) Zebli, B.; Susha Andrei, S.; Sukhorukov Gleb, B.; Rogach Andrey, L.; Parak Wolfgang, J. *Langmuir* **2005**, *21*, 4262.

(219) Poon, Z.; Chang, D.; Zhao, X.; Hammond, P. T. *ACS Nano* **2011**, *5*, 4284.

(220) Balabushevich, N. G.; Tiourina, O. P.; Volodkin, D. V.; Larionova, N. I.; Sukhorukov, G. B. *Biomacromolecules* **2003**, *4*, 1191.

(221) Yu, A.; Wang, Y.; Barlow, E.; Caruso, F. *Advanced Materials (Weinheim, Germany)* **2005**, *17*, 1737.

(222) Itoh, Y.; Matsusaki, M.; Kida, T.; Akashi, M. *Biomacromolecules* **2006**, *7*, 2715.

(223) Lee, H.; Jeong, Y.; Park, T. G. *Biomacromolecules* **2007**, *8*, 3705.

(224) Saito, G.; Swanson, J. A.; Lee, K.-D. *Advanced Drug Delivery Reviews* **2003**, *55*, 199.

(225) Zelikin, A. N.; Becker, A. L.; Johnston, A. P. R.; Wark, K. L.; Turatti, F.; Caruso, F. *ACS Nano* **2007**, *1*, 63.

(226) Zelikin, A. N.; Li, Q.; Caruso, F. *Angewandte Chemie, International Edition* **2006**, *45*, 7743.

(227) Wang, Y.; Bansal, V.; Zelikin, A. N.; Caruso, F. *Nano Letters* **2008**, *8*, 1741.

(228) Bédard, M. F.; De Geest, B. G.; Skirtach, A. G.; Möhwald, H.; Sukhorukov, G. B. *Advances in Colloid and Interface Science* **2010**, *158*, 2.

(229) Skirtach, A. G.; Antipov, A. A.; Shchukin, D. G.; Sukhorukov, G. B. *Langmuir* **2004**, *20*, 6988.

(230) Angelatos, A. S.; Radt, B.; Caruso, F. *Journal of Physical Chemistry B* **2005**, *109*, 3071.

(231) Skirtach, A. G.; Dejugnat, C.; Braun, D.; Susha, A. S.; Rogach, A. L.; Parak, W. J.; Moehwald, H.; Sukhorukov, G. B. *Nano Letters* **2005**, *5*, 1371.

(232) Skirtach, A. G.; Karageorgiev, P.; Bedard, M. F.; Sukhorukov, G. B.; Mohwald, H. *Journal of the American Chemical Society* **2008**, *130*, 11572.

(233) Skirtach, A. G.; Muñoz Javier, A.; Kreft, O.; Köhler, K.; Piera Alberola, A.; Möhwald, H.; Parak, W. J.; Sukhorukov, G. B. *Angewandte Chemie International Edition* **2006**, *45*, 4612.

(234) Lu, Z.; Prouty, M. D.; Guo, Z.; Golub, V. O.; Kumar, C. S. S. R.; Lvov, Y. M. *Langmuir* **2005**, *21*, 2042.

(235) De, G. B. G.; Skirtach, A. G.; Mamedov, A. A.; Antipov, A. A.; Kotov, N. A.; De, S. S. C.; Sukhorukov, G. B. *Small* **2007**, *3*, 804.

Chapter 2

Hydrophobic shell loading of biopolyelectrolyte capsules based on alkylated hyaluronic acid

2.1. Résumé (fr)

Ce chapitre décrit la synthèse de capsules biocompatibles et biodégradables élaborées par dépôt couche-par-couche de biopolymères sur un support colloïdal, suivi de sa décomposition dans des conditions douces. Ces capsules sont destinées à la vectorisation de principes actifs hydrophobes incorporés sélectivement dans leur paroi. La paroi des capsules est formée d'un film multicouche comportant des nanodomaines hydrophobes, qui se forment grâce à l'appariement de dérivés alkylés d'acide hyaluronique (HAC10) et de dérivés du chitosane quaternisés (QCHI). La synthèse de ces dérivés a été mise au point lors de travaux antérieurs au sein du laboratoire[1]. Dans cette étude, nous montrons que la stabilité des capsules est fortement affectée par le degré de substitution (DS, nombre moyen de substituants par unité de répétition) des polysaccharides modifiés. Des capsules stables sont obtenues à partir de HAC10 ayant un DS de 0.2 (HA20C10, 20 = 100 × DS) et de chitosane quaternisé de DS = 1.1. Le film multicouche à base de HA20C10/$QCHI_{DS=1.1}$ présente également une forte capacité d'incorporation d'une sonde fluorescente hydrophobe, le Nile Red (NR), par comparaison avec les films préparés à partir de dérivés de polysaccharides possédant des DS plus faibles.

L'incorporation sélective du NR dans la paroi des capsules (HA20C10/$QCHI_{DS=1.1}$)$_5$ a été mise en évidence par microscopie confocale. Nous avons pu estimer la quantité de NR incorporée dans les capsules par spectroscopie UV après extraction du NR des capsules avec de l'éthanol. La quantité dans chaque capsule déduite de la courbe de calibration du NR dans l'éthanol est de l'ordre de 0.17 pg. Ceci correspond à une concentration "effective" dans la paroi de la capsule de ~ 64 mM (diamètre de capsules : 5 μm, et l'épaisseur de capsules : 110 nm), c'est-à-dire environ 6400 fois la concentration du nile red dans la solution aqueuse initiale de HA20C10 ($C_{Nile\ Red}$ = 10 μM). L'analyse de la quantité de NR libérée par les capsules HA20C10/ $QCHI_{DS=1.1}$ en fonction du temps met en évidence une libération lente sur plusieurs jours et ce, bien que le milieu aqueux environnant soit changé deux fois par jour. Ce résultat montre ainsi une affinité élevée de la molécule hydrophobe vis-à-vis de la paroi multicouche. Ceci démontre le potentiel de ces systèmes multicouches comme vecteur de principes actifs hydrophobes dans la mesure où pour qu'un tel vecteur soit efficace, la libération du médicament doit être négligeable avant d'atteindre la cible.

Afin d'analyser le comportement des capsules en présence de cellules, nous avons examiné leur stabilité dans le milieu de culture. Celle-ci s'est avérée dépendre fortement de la présence de protéines dans le milieu. En présence de protéines, un gonflement des capsules est observé. En revanche, les capsules dont la paroi est constituée d'un film réticulé de HA20C10 et de poly(L-lysine) (PLL), ne présentent aucun déformation quelles que soient les conditions de milieu.

Sur la base de ces résultats, nous avons préparé des capsules HA20C10/PLL en remplaçant le NR par le paclitaxel (PTX) qui est un agent anti-cancéreux hydrophobe puissant, utilisé pour le traitement de cancers du sein, de l'ovaire et du poumon. L'activité biologique des capsules vis-à-vis de cellules du cancer du sein (MDA MB 231) a été étudiée dans une deuxième phase. La viabilité de ces cellules s'est avérée être fortement réduite en présence de capsules chargées en PTX et ce, de façon dose-dépendante. L'ensemble de ces travaux a ainsi montré le potentiel de capsules à base de HA alkylé contenant des nanodomaines hydrophobes comme systèmes de délivrance de médicaments peu solubles dans l'eau.

2.2. Introduction

The aim of this work was to synthesize multilayer capsules which were able to encapsulate water-insoluble molecules in the nanoshell. The multilayer capsules are prepared by the layer-by-layer assembly of oppositely charged polyelectrolytes on a colloidal template, followed by its decomposition. Previous work in our laboratory showed the ability to prepare stable capsules containing hyaluronic acid (HA) as a negatively charged polysaccharide using $CaCO_3$ particles as a template under mild conditions.[2] In order to encapsulate hydrophobic molecules, HA was chemically modified with alkyl chains. Our previous work showed the very high affinity of hydrophobic molecules for the hydrophobic nanodomains formed by alkylated derivatives of HA in aqueous solution or in multilayer films.[3] Among all of alkylated HA derivatives, the HA20C10 (derivative with alkyl chains having 10 carbon atoms and degrees of substitution 20 per 100 disaccharide repeating units) showed the strongest ability to trap the dye into hydrophobic nanodomains. Therefore, we investigated the preparation of capsules able to entrap poorly water-soluble molecules in the polyelectrolyte shell based on the HA20C10 derivative.

In this chapter, we describe two types of capsules to selectively encapsulate a water-insoluble molecule in the nanoshell based on HA20C10, using a chitosan derivative which is water-soluble at physiological pH (QCHI)[4] and a polypeptide poly(L-lysine) (PLL) as components of the nanoshell. Contrary to HA20C10/QCHI capsules, the HA20C10/PLL capsules require shell cross-linking to maintain the stable form.

Incorporation of a hydrophobic dye, Nile Red (NR), in the nanoshell of HA20C10/QCHI capsules was demonstrated. The amount of NR loaded in the wall and its release were also investigated. We further showed that the hydrophobic molecule can be delivered intracellularly in dendritic cells. This part of work has been reported in Advanced Materials[5].

Then we compared the ability of incorporating of NR in the nanoshell of HA20C10/QCHI capsules and HA20C10/PLL capsules.

In order to analyze the behavior of these two capsules in the presence of cells, we examined their stability in the culture medium. In the culture medium, swelling behavior of HA20C10/QCHI capsules was observed. However, HA20C10/PLL capsules whose the wall consists of a crosslinked film did not show any destabilization whatever the environmental conditions.

Based on these results, we chose HA20C10/PLL capsules to solubilize the anti-cancer agent, paclitaxel, which is used for the treatment of breast, ovarian and lung cancer. The cytotoxicity of PTX-loaded capsules was examined on breast cancer cells (MDA MB 231). This part of work has been reported in Journal of Controlled Release[6].

2.3. Article[5]

Hydrophobic Shell Loading of Biopolyelectrolyte Capsules

Cui, D.; Jing, J.; Boudou, T.; Pignot-Paintrand, I.; De Koker, S.; De Geest, B. G.; Picart, C.; Auzély-Velty, R. *Advanced Materials* **2011**, Volume 23, Issue 24, p. H200-H204.

Cf :

http://onlinelibrary.wiley.com/doi/10.1002/adma.201100600/pdf

2.4. Supporting information

Submitted to ADVANCED MATERIALS

Supporting Information

Hydrophobic shell loading of biopolyelectrolyte capsules

By Di Cui, Jing Jing, Thomas Boudou, Isabelle Pignot-Paintrand, Stefaan De Koker, Bruno G. De Geest, Catherine Picart,* and Rachel Auzély-Velty*

Films characterization by quartz crystal microbalance with dissipation monitoring. The $(QCHI/HA20C10)_i$ film buildup (where i denotes the number of layer pairs) was followed by *in situ* quartz crystal microbalance (QCM with dissipation monitoring, D300, Qsense, Sweden). The gold-coated quartz crystal was excited at its fundamental frequency (about 5 MHz, $\nu = 1$) as well as at the third, fifth and seventh overtones ($\nu = 3$, 5 and 7 corresponding to 15, 25 and 35 MHz, respectively). Changes in the resonance frequencies Δf and in the relaxation of the vibration once the excitation is stopped ΔD were measured at the four frequencies.

Atomic force microscopy. AFM images of the dried microcapsules were carried out in air with a PicoPlus AFM in tapping mode using tetrahedral tips (OMCL-AC240TM-E tip from Olympus) with a resonance frequency of 75 kHz and a spring constant of 2 N m^{-1}. Capsules deposited on a mica substrate were imaged at line rates of 1 Hz. For surface roughness analysis, 1 × 1 μm^2 AFM images were obtained and the arithmetic average roughness R_a was calculated according to:

$$R_a = \frac{1}{N_x N_y} \sum_{i=1}^{N_x} \sum_{j=1}^{N_y} \left| z_{ij} - z_{mean} \right| \quad (1)$$

where z_{ij} is the height of a given pixel, z_{mean} is the average height of the pixels, and $N_x = N_y = 512$ are the number of pixels in the x and y directions.

Submitted to ADVANCED MATERIALS

Measurement of NR release from capsules over time. The suspension of capsules (5 mL) in PBS was divided in 5 samples, corresponding to 5 different time periods from 0 to 8 days, noted D0, D2, D4, D6, and D8 respectively). The D0 sample, consisting in 200 µL of capsules suspension freshly prepared, was treated as described in the experimental section to determine the amount of NR incorporated. This process was performed in duplicate in order to confirm the values.

The D2, D4, D6 and D8 samples (each consisting of 1 mL of capsules suspension) were introduced in Spectra/Por® dialysis membranes (6-8 kDa cutoff) and the samples were immersed in PBS (200 mL). Each sample was washed four times with PBS (200 mL) during 2 days. For each sample (D2, D4, D6 and D8), 200 µL of capsules suspension were taken up and underwent a treatment similar to the D0 sample for determination of the amount of NR in the capsules. These processes were performed in duplicate.

The analysis of NR contained in the capsules as a function of time demonstrates only a minor release of the dye in spite of the washing steps with PBS, as shown in **Fig. SI 4**. This demonstrates the high stability of the entrapment of the hydrophobic molecule in the nanoshell.

Submitted to ADVANCED MATERIALS

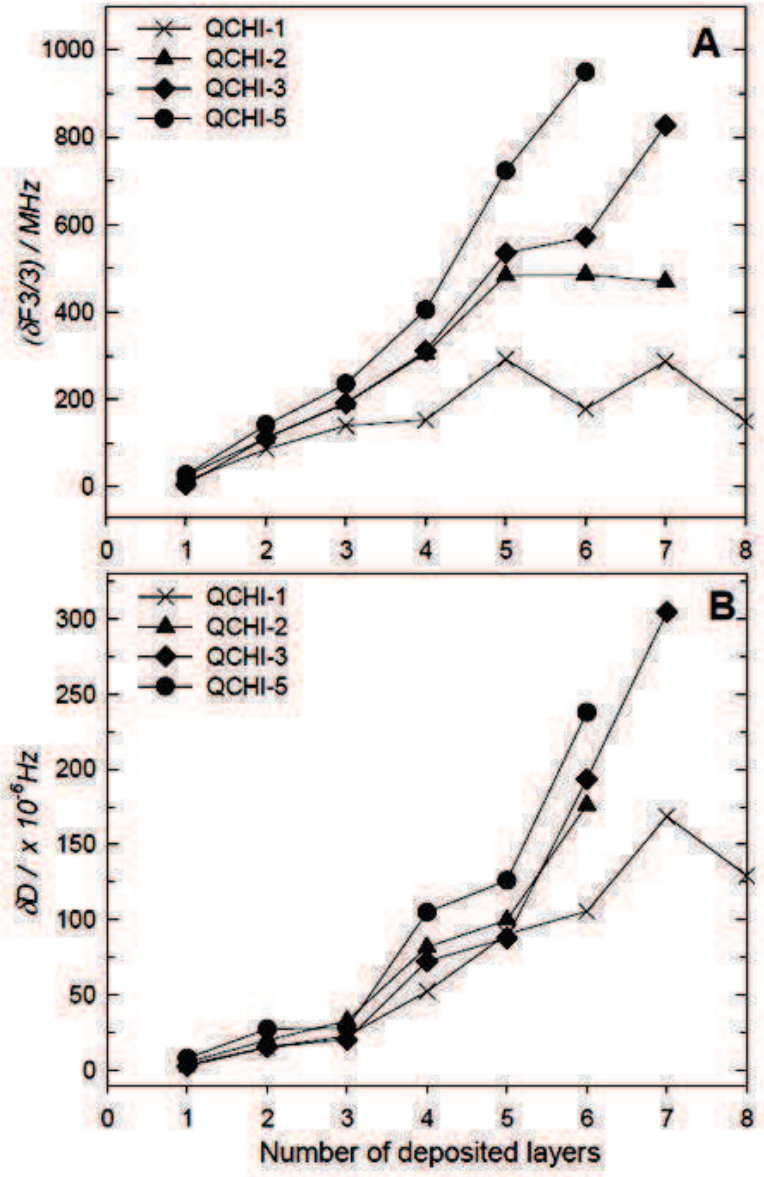

Figure SI 1 : (QCHI/HA20C10) film growth in PBS (pH 7.4) as measured by QCM-D on gold coated crystals. Differences in the QCM frequency shifts (A) and in the dissipation (B) measured at 15 MHz are represented as a function of the number of deposited layers. All QCHI concentrations and HA20C10 were of 2 mg/mL.

Submitted to ADVANCED MATERIALS

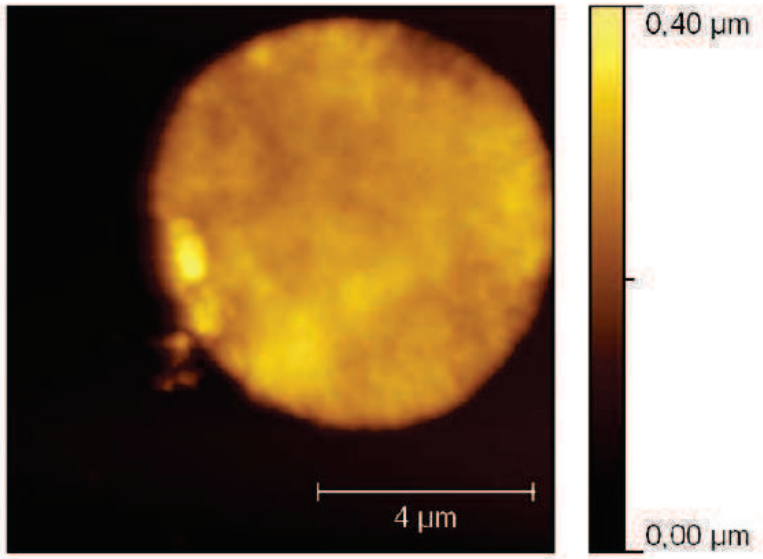

Figure SI 2. AFM topographical image of a microcapsule made of 4.5 layer pairs of (QCHI-4/HA20C10)$_{4.5}$ layers. Image size is 10 × 10 µm^2.

Submitted to ADVANCED MATERIALS

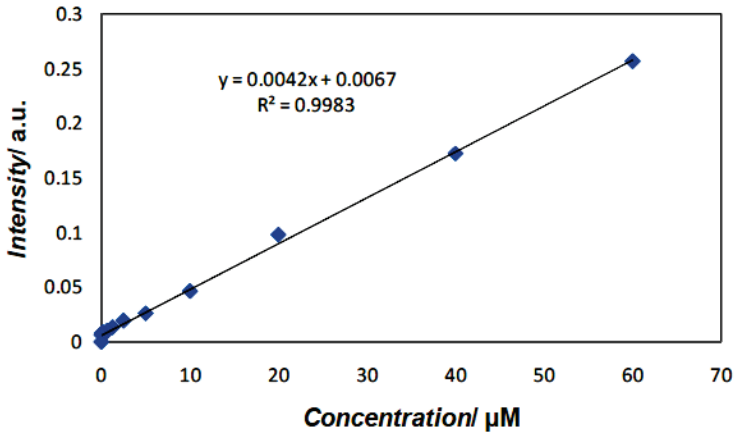

Figure SI 3. Calibration curve for the absorbance of Nile Red in ethanol (measured at 590 nm) as a function of its concentration in solution.

Submitted to ADVANCED MATERIALS

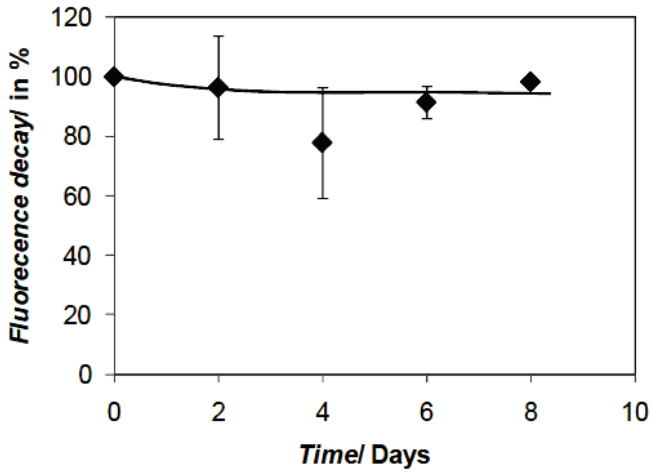

Figure SI 4. Fluorescence intensity measurements of NR intensity remaining in $(HA20C10/QCHI\text{-}4)_5$ microcapsules over a 8 day period of immersion in PBS. The minor decrease in fluorescence indicates that the stability of NR in the hydrophobic nanodomains is very high.

2.5. Complementary results

2.5.1. Replacement of quaternized chitosan (QCHI) as a polycationic partner of alkylated HA by poly(L-lysine) (PLL)

Previous work demonstrated the synthesis of various alkylamino hydrazide derivatives of HA and their ability to form planar polyelectrolyte multilayers with quaternized chitosan (QCHI) and a polypeptide, poly(L-lysine).[3] Based on these results, we prepared capsules using PLL as a polycation. Compared to HA20C10/QCHI capsules, the HA20C10/PLL capsules are not stable after core decomposition. Shell crosslinking is thus required to reinforce the mechanical property of the shell, allowing to obtain stable capsules after core decomposition. Crosslinking was performed by an amine-acid coupling reaction using the water-soluble carbodiimide 1-ethyl-3-(3-dimethylaminopropyl)carbodiimide (EDC, 400 mM) and *N*-hydroxysulfosuccinimide (sNHS, 100 mM). Comparison of the fluorescence intensity of the HA20C10/QCHI and HA20C10/PLL capsules, prepared by LbL assembly of HA20C10 pre-incubated with the same amount of Nile Red (NR) revealed a lower fluorescence intensity for the HA20C10/PLL capsules (**Figure CR 2.1**).

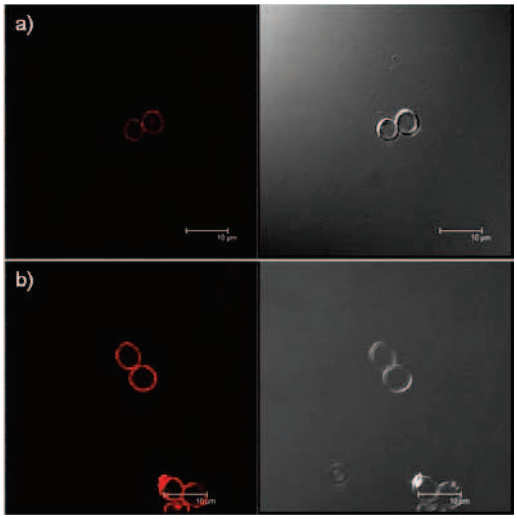

Figure CR 2. 1. Confocal microscopy images of a) crosslinked $(HA20C10/PLL)_{4.5}$ capsules; b) $(HA20C10/QCHI)_{4.5}$ capsules exhibiting a highly localized red fluorescence in their nanoshell due to the specific entrapment of Nile Red molecules in hydrophobic nanodomains. Scale bars: 10 µm.

We quantified the amount of NR loaded in the nanoshell by UV-visible spectrometry using a fluorescence microplate reader (Infinite 1000, Tecan, Austria) after extraction of NR from the

capsules with ethanol. Using a calibration curve for NR in ethanol, we deduced a mean NR mass per capsule. The number of capsules per mL of suspension was determined using a Petroff-Hausser counting chamber. The results are presented in **Table CR 2.1**.

Table CR 2. 1. Effective loading of NR in the hydrophobic nanoshell of capsules.

Capsule	Amount inserted per capsule (pg/cap.)
HA20C10/QCHI	0.17 ± 0.06
HA20C10/PLL	0.09 ± 0.04

The results shown in **Table CR 2.1.** confirmed the CLSM observations : the amount of NR loaded in the HA20C10/PLL capsules is lower than that in the HA20C10/QCHI. This may be related to shell crosslinking which could squeeze out some NR molecules from the shell. In addition, the semi-rigid character of QCHI and its high molar mass (compared to PLL) may result in the formation of nanoshells with many entanglements which can stabilize the hydrophobic molecule in the nanoshell.

2.5.2. Stability of the capsules in culture media

We investigated the stability of HA20C10/QCHI and HA20C10/PLL capsules in culture medium (RPMI 1640 Gibco with or without 10% fetal bovine serum provided by Bertin pharma). **Figure CR 2.2** gives an overview of the HA20C10/QCHI capsules behavior in different conditions (temperature, presence of proteins or hydrophilic molecules).

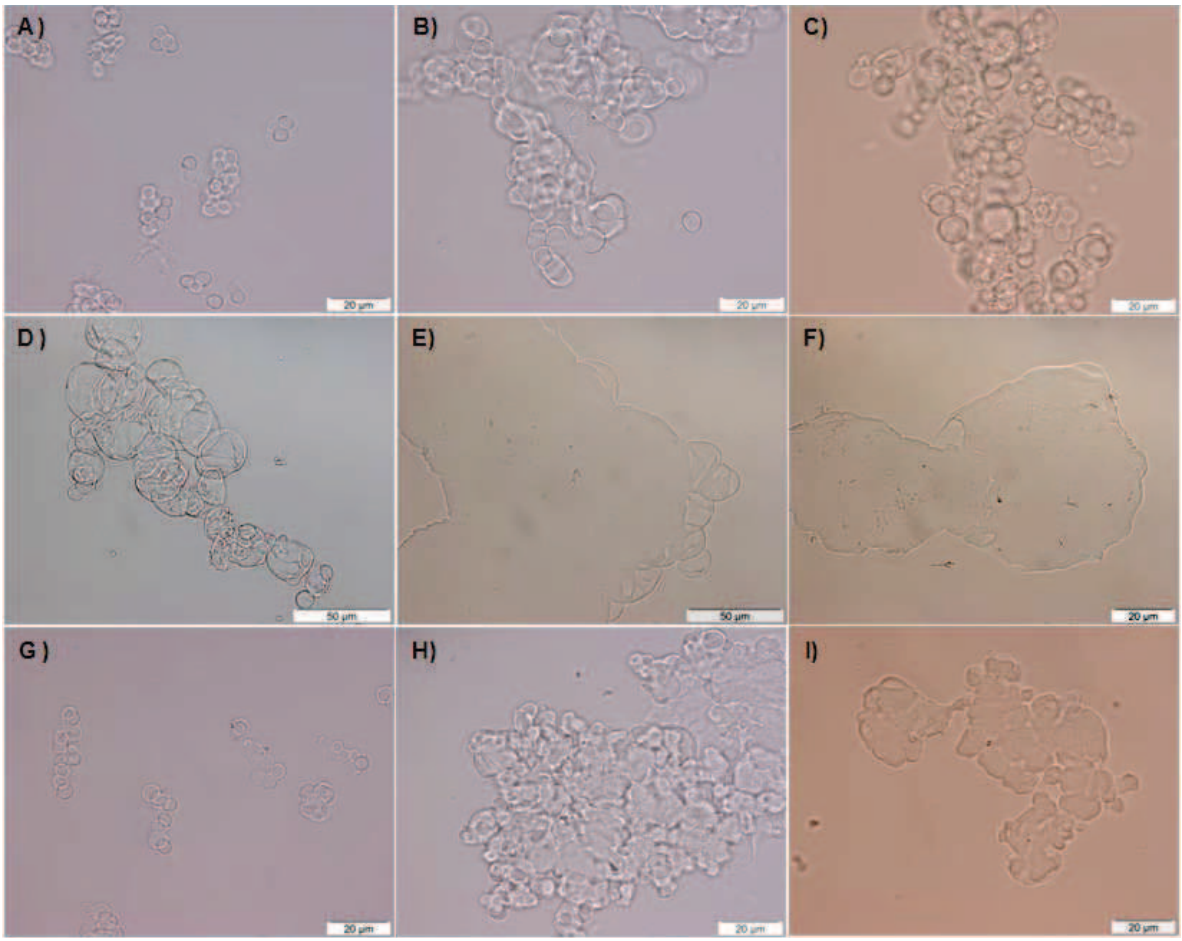

Figure CR 2. 2. Deformation of $(HA20C10/QCHI)_5$ capsules (A) in culture medium without fetal bovine serum at 22°C; (B) one day after incubation in culture medium with fetal bovine serum at 22°C; (C) 4 days after incubation in culture medium with fetal bovine serum at 22°C; (D) in phosphate buffer saline (PBS) containing albumin from bovine serum (BSA) on 10 g/L at 22°C; (E) in PBS buffer containing BSA on 35 g/L at 22°C; (F) loaded with Nile Red in the nanoshell in PBS buffer containing BSA on 35 g/L at 22°C; (G) loaded with Nile Red in the nanoshell in PBS buffer containing dextran on 35 g/L at 22°C;(H) one day after incubation in culture medium with fetal bovine serum at 37°C; (I) 4 days after incubation in culture medium with fetal bovine serum at 37°C. BSA: Mw=66000 g/mol; dextran: Mw=70000 g/mol.

First, when $(HA20C10/QCHI)_5$ capsules were immersed in the culture medium containing fetal bovine serum at 22°C, we observed, after one day, the swelling of some capsules (**Figure CR 2.2.B and C**) contrary to the same capsules in the culture medium without serum (**Figure CR 2.2.A**). We attributed this phenomenon to a destabilization of interactions between the biopolyelectrolytes due to the formation of new hydrophobic and/or electrostatic interactions between the proteins and the biopolyelectrolytes. To verify this hypothesis, we immersed the capsules in phosphate buffer saline (PBS) containing only one protein, albumin from bovine serum (BSA), at a concentration of 10 g/L (**Figure CR 2.2.D**). The capsules were found to swell in such conditions. At a BSA concentration of 35 g/L, the capsules

decomposed upon swelling (**Figure CR 2.2.E**). A similar behavior was observed when NR was incorporated within the wall (**Figure CR 2.2.F**). In order to confirm the mechanism responsible for the swelling of the capsules, we analyzed the effect of addition of the hydrophilic polymer dextran (Mw = 70000 g/mol) at the same concentration of BSA (35 g/L) in the solution. In this case, no swelling of the capsule was observed at 22 °C (**Figure CR 2.2.G**). This result thus supported our hypothesis suggesting disruption of the multilayer shell due to hydrophobic and/or electrostatic interactions between the proteins and the biopolyelectrolytes. Moreover, we observed strong uncontrolled deformation of the capsule walls at higher temperature (37°C) (**Figure CR 2.2.H and I**). We assumed that at higher temperature, the chains mobility could increase as well as the hydrophobic interactions between the multilayer and the proteins, resulting in the decomposition of the shells.

In contrast, HA20C10/PLL capsules maintained their morphology and size in all conditions, which demonstrated the significant mechanical reinforcement of the shell by chemical crosslinking the layers.

As HA20C10 used above was prepared from a HA sample of 200 000 g/mol (HA200), we then prepared an alkylated derivative from a HA sample of 350 000 g/mol (HA350) to assess the impact of the HA molar mass on the capsule stability. **Figure CR 2.3** shows that in the same external conditions, capsules prepared from alkylated HA350 deformed less than capsules containing alkylated HA200, suggesting more cohesive interactions in the former case.

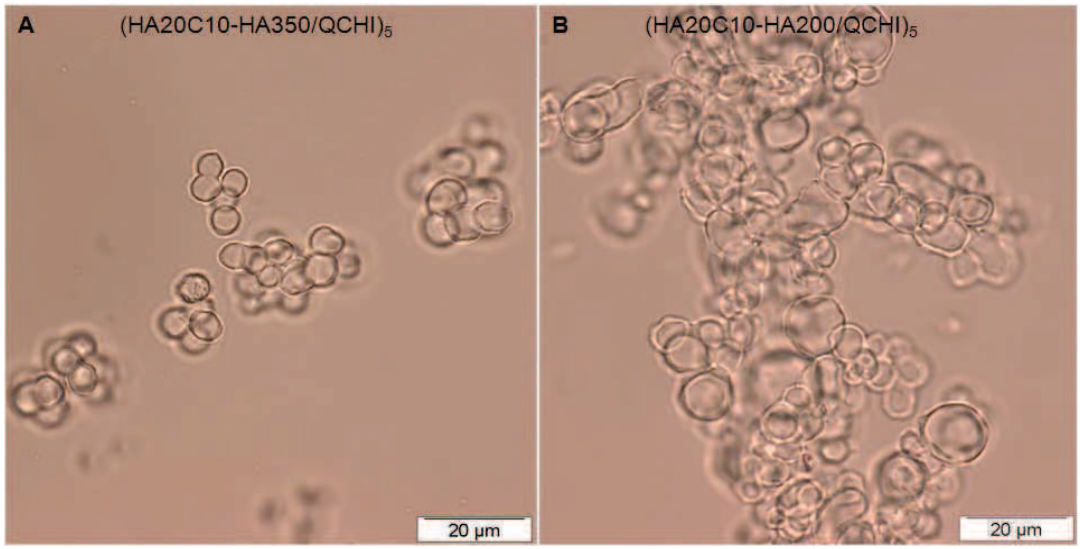

Figure CR 2. 3. Deformation of (A) $(HA20C10\text{-}HA350/QCHI)_5$ capsules and (B) $(HA20C10\text{-}HA200/QCHI)_5$ in culture medium with fetal bovine serum at 22°C. Scale bars: 20 µm.

In order to have a deeper insight into the role of the molar mass on the behavior of alkylated HA in aqueous solution, we compared the viscoelastic properties of the two derivatives by dynamic rheological measurements. **Figure CR 2.4** shows the variation of the storage, G', and loss, G'', moduli as a function of the frequency for the two samples at 10 g/L in phosphate buffer saline.

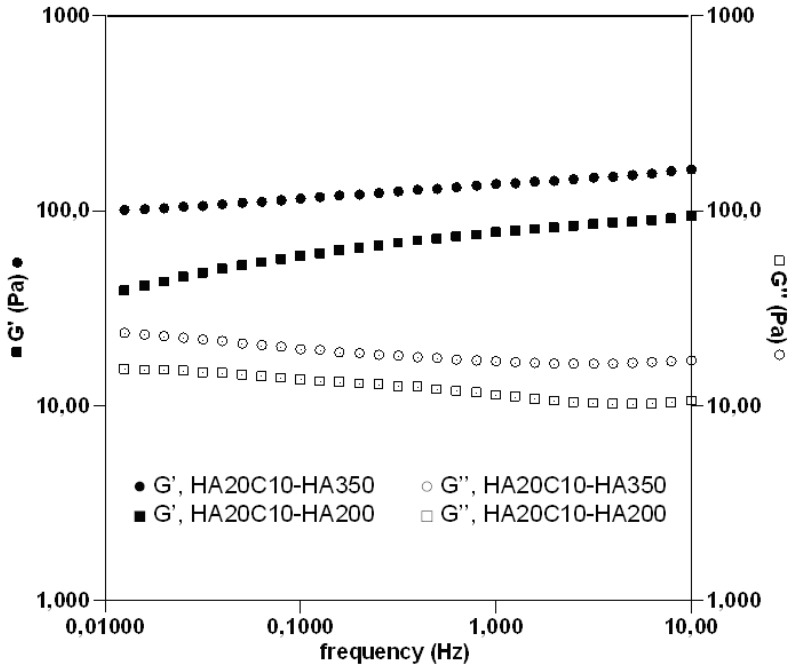

Figure CR 2. 4. Comparison of the storage and loss modulus as a function of frequency for solution of HA20C10-HA200 and HA20C10-HA350 derivatives (10 g/L in PBS (pH 7.4)) at 25°C.

As can be observed from this figure, the storage modulus is higher than the loss modulus, over the entire range of frequencies covered, indicating that the 2 solutions behave like a highly elastic physical gel. When the molar mass is increased, the values of the G' and G'' modulus appear to increase. These data thus support our hypothesis suggesting the presence of more cohesive interactions in the former case of capsules formed with HA20C10-350.

Moreover, in order to determine the critical concentration required for gel formation from these derivatives, we measured the dynamic moduli as a function of frequency for different polymer concentrations. The dynamic mechanical behavior at gel point for chemically crosslinking systems is characterized by a scaling relationship between the dynamic moduli and the frequency ($G'(\omega) \sim G''(\omega)$) as well as a frequency independent loss angle ($\tan\delta_c = G''/G' = \tan(n\pi/2)$).[7] This relationship may be applied to physically cross-linking systems.[8,9] Based on these theoretical aspects, we determined the gel point for these two derivatives by

the observation of a frequency-independent value of delta (δ) as a function of the polymer concentration (**Figure CR 2.5**). As expected, we found that the gel point of HA20C10-350 is lower than that of HA20C10-HA200.

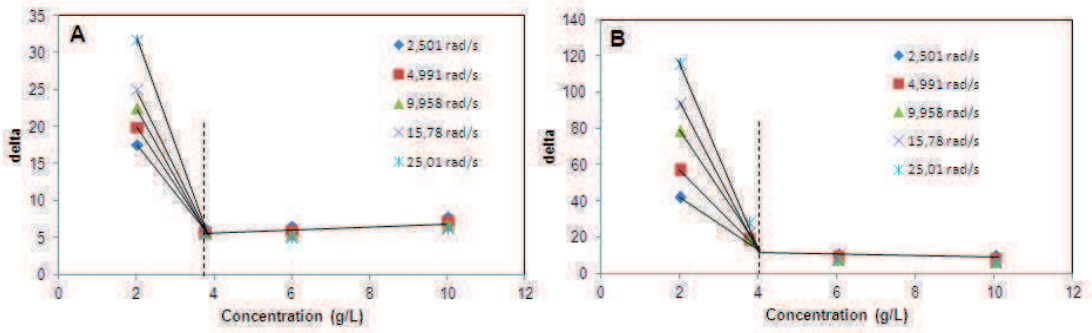

Figure CR 2. 5. Determination of the gelation concentration of (A) HA20C10-HA350 and (B) HA20C10-HA200.

2.5.3. Drug loading in HA20C10/PLL capsules

Using the hydrophobic nanoshell based on HA20C10 and PLL, we replaced the model hydrophobic dye of NR by the hydrophobic anti-cancer drug paclitaxel (PTX) to form a drug loaded capsules. The result with breast cancer cells was reported in an article (Annexes)[6].

We used Oregon green labeled paclitaxel (OG-PTX) as a tracer, which was added at fixed concentration (1/20) to PTX solutions. To estimate the absolute OG-PTX concentration, a calibration curve for the fluorescence of OG-PTX as a function of its concentration was acquired. The effective concentration of PTX in the capsules was calculated knowing the amount of OG-PTX incorporated in the capsules by fluorescence intensity measurements by Tecan instrument after extraction of OG-PTX from capsules with methanol. We used indirect method to determine the quantity of PTX, because PTX adsorb at 230 nm, this is the limit of Tecan instrument. We also used high-performance liquid chromatographic (HPLC) procedures for the PTX quantitative determination. Because of the very low concentration in solution, it was difficult to obtain a reliable value from this method.

After the measurements of fluorescence intensity of OG-PTX, we found that the effective concentration of PTX was to be of 17 fg (10^{-15} g) per capsules. This value was taken as positive reference for the tests with cancer cell using PTX in solution. Unloaded and PTX-loaded capsules were added to MDA-MB-231 cell culture and observed over 3 days. The

cytotoxicity of the capsules was evaluated by counting the cell number and by measuring the cell viability using a MTT assay. The PTX-loaded microcapsules were found to decrease the viability and proliferation of MDA MB 231 breast cancer cells, while unloaded microcapsules did not impact cell viability.

2.6. Conclusion

In order to encapsulate hydrophobic molecules, we have synthesized two types of capsules based on HA20C10 which present hydrophobic nanodomains in aqueous solution. With QCHI, stable capsules could be obtained after core removal. In contrary, HA20C10/PLL needed chemical crosslinking of multilayer shell to maintain the stable form. Comparison of the ability of incorporating Nile Red in these two capsules, HA20C10/QCHI capsules loaded more NR than HA20C10/PLL capsules. But, the study of stability of the capsules in culture media showed that the HA20C10/PLL capsules maintained their morphology and size in all experimental conditions, which demonstrated the significant mechanical reinforcement of the shell by chemical crosslinking. Finely, we chose HA20C10/PLL capsules to encapsulate an anti-cancer agent, paclitaxel. The PTX-loaded capsules were found to decrease the viability and proliferation of MDA MB 231 breast cancer cells, and the empty microcapsules did not impact cell viability. Our results highlight the potential of capsules based on alkylated-HA containing hydrophobic nanodomains for hydrophobic drug delivery.

References

(1) Cui, D., 2011.
(2) Szarpak, A.; Pignot-Paintrand, I.; Nicolas, C.; Picart, C.; Auzely-Velty, R. *Langmuir* **2008**, *24*, 9767.
(3) Kadi, S.; Cui, D.; Bayma, E.; Boudou, T.; Nicolas, C.; Glinel, K.; Picart, C.; Auzely-Velty, R. *Biomacromolecules* **2009**, *10*, 2875.
(4) Cui, D.; Szarpak, A.; Pignot-Paintrand, I.; Varrot, A.; Boudou, T.; Detrembleur, C.; Jerome, C.; Picart, C.; Auzely-Velty, R. *Advanced Functional Materials* **2010**, *20*, 3303.
(5) Cui, D.; Jing, J.; Boudou, T.; Pignot-Paintrand, I.; De Koker, S.; De Geest, B. G.; Picart, C.; Auzély-Velty, R. *Advanced Materials* **2011**, *23*, H200.
(6) Boudou, T.; Kharkar, P.; Jing, J.; Guillot, R.; Pignot-Paintrand, I.; Auzely-Velty, R.; Picart, C. *Journal of Controlled Release* **2012**, *159*, 403.
(7) Winter, H. H.; Chambon, F. *J. Rheol. (N. Y.)* **1986**, *30*, 367.
(8) Lin, Y. G.; Mallin, D. T.; Chien, J. C. W.; Winter, H. H. *Macromolecules* **1991**, *24*, 850.
(9) Desbrieres, J. *Polymer* **2004**, *45*, 3285.

Chapter 3

Cyclodextrin/Paclitaxel complex in biodegradable capsules for breast cancer treatment

3.1. Résumé (fr)

Ce chapitre porte sur le développement de capsules destinées à la vectorisation d'un agent anti-cancéreux, le paclitaxel (PTX). L'encapsulation de PTX est obtenue par complexation hôte-invité avec la β-cyclodextrine (β-CD) greffée sur l'acide hyaluronique (HA), constituant la paroi des capsules. La structure torique de la β-CD délimite une cavité dont la particularité est d'être hydrophobe. La partie extérieure est au contraire hydrophile et confère à la β-CD une bonne solubilité dans l'eau. L'existence de la cavité hydrophobe permet d'héberger une molécule de PTX partiellement, ce qui permet d'augmenter sa solubilité en milieu aqueux d'un facteur 100 (solubilité du PTX seul dans l'eau = 0.4 μM). Dans ce travail, nous avons cherché à combiner la complexation hôte-invité et les propriétés de transport des capsules pour former un nouveaux système de délivrance du PTX.

Le dérivé HA-cyclodextrine (HA-CD) a été préparé par une réaction de couplage de type "thiol-ène", effectuée en milieu aqueux. Cette réaction, mise au point au sein de notre laboratoire, permet le greffage simple, rapide, efficace, et dans des conditions douces de molécules variées sur des polysaccharides porteurs de fonctions alcène. Elle consiste dans le cas présent en l'addition radicalaire d'un dérivé de β-CD monofonctionnalisée avec de l'acide mercaptopropionique sur le HA modifié par des groupements pentènoate.

La complexation PTX/β-CD a été démontrée par RMN ^{1}H. Les études sur la solubilité du PTX en milieu aqueux en présence de la β-CD naturelle, du dérivé HA-CD ou d'un dérivé méthylé de la β-CD, trente fois plus soluble que la β-CD naturelle (heptakis-(2,6-di-O-methyl) β-CD (DM-β-CD)), ont montré que le dérivé HA-CD présentait un fort pouvoir solubilisant comparativement à la β-CD naturelle. Ceci a été attribué à l'augmentation de la solubilité de la cavité de CD par couplage avec l'acide hyaluronique dans la mesure où les propriétés de complexation de la CD greffée sont similaires à la CD non modifiée. Par ailleurs, cette hypothèse est confortée par le fait que la DM-β-CD présente un pouvoir solubilisant nettement supérieur à celui de la β-CD naturelle alors que leurs propriétés de complexation sont quasi-équivalentes.

Pour synthétiser les capsules à partir de HA-CD, nous avons tout d'abord vérifié sa capacité à former des films multicouches plans par complexation avec la poly(L-lysine) (PLL). Le suivi de la formation des films par microbalance à cristal de quartz avec mesure de la dissipation

(QCM-D) a montré une croissance du film HA-CD/PLL similaire à celle du film HA/PLL. Compte tenu de ce résultat et du fait que des capsules de HA/PLL peuvent être obtenues sous réserve que les couches de polymères soient réticulées chimiquement, nous avons dans une seconde phase entrepris la synthèse de capsules HA-CD/PLL en réticulant le film multicouche par couplage amine-acide en présence d'un carbodiimide hydrosoluble. L'encapsulation du PTX a été réalisée par pré-complexation préalable du PTX par le HA-CD dans la solution aqueuse utilisée lors du dépôt couche-par-couche. La quantité de PTX incorporé dans les capsules de HA-CD/PLL s'est avérée être similaire à celle obtenue avec les capsules préparées à partir de HA20C10. Les capsules de HA-CD/PLL peuvent libérer le PTX sur une période de 5 jours sans relargage rapide au début (burst effect). Des études préliminaires ont montré que les capsules inhibent la prolifération de cellules cancéreuses (cellules du cancer du sein MDA MB 231), contrairement aux capsules "contrôles" ne contenant pas de PTX.

Ces résultats ont ainsi montré la faisabilité d'obtenir de nouveaux systèmes transporteurs permettant une libération contrôlée de principes actifs peu solubles de l'eau en combinant les propriétés de complexation originales d'oligosaccharides naturels avec l'assemblage couche-par-couche en conditions physiologiques de biopolymères hydrosoluble biocompatibles sur des particules sacrificielles.

3.2. Introduction

Complexation of the anti-cancer drug paclitaxel (PTX) by β-CD or β-CD derivatives such as heptakis-(2,6-di-O-methyl) β-CD (DM-β-CD), hydroxypropyl-β-CD was investigated with the purpose to propose new PTX formulations.[1-3] β-CD can increase the solubility of paclitaxel. Moreover, the PTX/β-CD complex showed a greater antitumoral activity than the free drug at high dilution factors. It can allow the transfer of the drug from the CD cavity to tumor cells due to the reversibility of host-guest complexation.

By grafting aliphatic chains on the β-CD cavity, amphiphilic β-CD derivatives that can self-assemble into nanoparticles in aqueous solution can be obtained. New PTX formulations based on nanoparticles were thus prepared from a mixture of PTX and an amphiphilic β-CD (6-O-CAPRO-β-CD which is modified on the primary face with 6C aliphatic esters) by the nanoprecipitation technique.[4,5] Irache et al. incorporated hydroxypropyl-β-CD/PTX complexes in poly(anhydride) nanoparticles by a solvent displacement method[6,7]. These different approaches for the synthesis of CD nanoparticles showed however limitations associated with sample polydispersity, the necessity for an oil phase and/or burst effect during drug release (more than 50% PTX release was observed in the first hour[4]).

Wang et al. described the synthesis of β-CD modified chitosan-poly(acrylic acid) nanoparticles as PTX delivery systems.[8] These NPs were synthesized by the radical polymerization of acrylic acid and propenyl esterified β-CD in chitosan solution. PTX was loaded into NPs in a mixture of ethanol/water. This NPs preparation procedure is complicated, and the encapsulation efficiency was relatively low. However, the in vitro drug release profile of PTX showed a sustained manner for more than one week under simulated physiological conditions (PBS, pH 7.4) and at pH 5.7 (**Figure 3.1**).

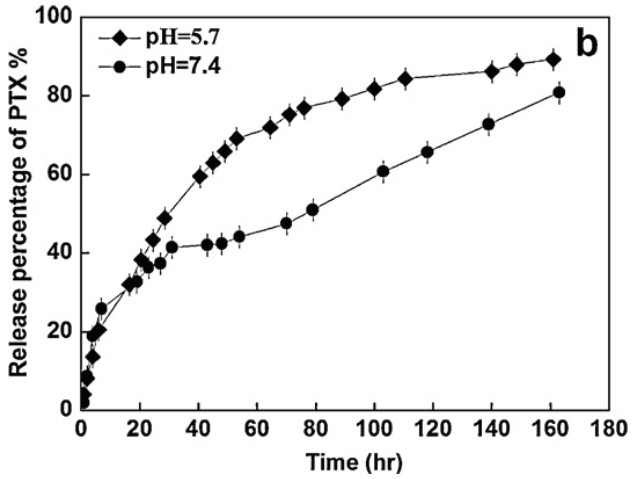

Figure 3. 1. The release profile of PTX from CS–PAACD NPs in the PBS with different pH value.[8]

These different studies show the potential of using host-guest complexation for designing hydrophobic drug carrier systems with tunable functionalities for the treatment of cancer. However, to circumvent some limitations of these systems, which are generally associated with the procedure of their preparation, new approaches to engineer CD-based carriers[9,10] would be highly desirable.

In this chapter, we design a new approach of layer-by-layer capsules containing the cyclodextrin/paclitaxel complex as drug carriers. This strategy was realized by incorporation of CD-polymers to combine the benefits of CD inclusion complexes and of biodegradable polymer matrix based on polyelectrolyte complexation.

β-cyclodextrin was grafted onto hyaluronic acid using a "thiol-click reaction" (HA-CD). The enhancement of the water-solubility of PTX through host-guest interactions with the natural β-CD, HA-CD as well as with DM-β-CD was studied.

After confirmation of assembly of HA-CD and poly(L-lysine) in multilayer films on a planar solid substrate, we investigated the generation of capsules made from (HA-CD/PLL) films and the PTX loading and release from the nanoshell. At end, we studied the capacity of (HA-CD/PLL) capsules to deliver PTX to MDA MB 231 breast cancer cells.

This study has been submitted for publication. In the complementary results, we discussed that the importance of behavious of polymers in solution in the process of formation of capsules.

3.3. Publication (submitted)

Cyclodextrin/Paclitaxel complex in biodegradable capsules for breast cancer treatment

Jing Jing, Anna Szarpak-Jankowska, Raphael Guillot, Isabelle Pignot-Paintrand, Catherine Picart and Rachel Auzély-Velty

3.3.1. Introduction

Delivery of drugs is currently a great challenge in the field of nanobiotechnology, especially for hydrophobic compounds, which constitute a great part of the currently available drugs.[11-13] Many of these compounds have been found to have limited clinical effectiveness due in part to their high toxicity, low solubility, and/or other poor pharmaceutical parameters. It has been demonstrated that conjugation of a poorly water-soluble molecule to a water-soluble polymer (called prodrug approach) can greatly enhance its aqueous solubility and reduce its cytotoxicity in vitro and in vivo.[14] Nanoparticles are alternative materials that have shown huge potential for encapsulating and delivering poorly water-soluble compounds, especially in anti-cancer therapy.[15,16] These systems provide a more flexible approach compared to prodrugs which are limited to hydrophobic drugs possessing a functionality for their chemical grafting on the polymer chain. However, even after decades of development, there are a few examples of nanotechnology therapeutic products that have been approved for clinical use.[15] One of the major obstacles is the initial burst release of the encapsulated drug which carries an increased risk of toxicity. Moreover, most of the methods to produce polymeric nanoparticles involve the use of toxic solvents and surfactants, which require intensive postprocessing purification.

Cyclodextrins (CDs) are water-soluble cyclic oligosaccharides which can include various guest molecules into their hydrophobic cavity allowing the solubilization, stabilization and transport of hydrophobic drugs.[17] Worldwide 30–40 different drugs are nowmarketed as cyclodextrin complexes.[18] Although the use of CDs as solubilizers in the pharmaceutical field has been documented for decades, more advanced CD-based drug delivery systems still need to be developed. In recent years, the nanoscale association of these host molecules with particles or polymers lead to the development of drug delivery platforms with unique stimuli-

responsiveness and adjustable drug release characteristics. By immobilizing CD on magnetic nanoparticles, it was thus shown the ability to trigger the release of hydrophobic drugs incorporated in the CD through the use of induction heating.[19] By the layer-by-layer (LbL) assembly of poly(carboxymethyl-β-cyclodextrin) complex with a small molecule and positively charged degradable poly(β-aminoesters), nanoscale coatings for small molecule delivery capable of programmable release kinetics could be obtained.[12] These surface-eroding films were prepared under mild conditions.

Extension of this technology to LbL-based hollow capsules may offer new opportunities for designing carriers with tunable functionalities in the nano/micrometer range. These capsules, also called polyelectrolyte multilayer capsules consist of two distinct compartments: the multilayer shell and the aqueous cavity. Such a structure may be advantageously used to achieve a bi-compartment delivery for both hydrophobic and hydrophilic drugs with synergistic effects for the treatment of diseases, like cancer. In general, drugs are loaded into the aqueous cavity with high loading efficiency. However, this implies that the drugs have good water-solubility and a relatively high molecular weight to avoid the leakage from the capsules. As many anticancer drugs such as paclitaxel, doxorubicin and camptothecin, are small hydrophobic molecules, it is still a challenge to load these drugs in the hydrophilic multilayer shell. Until now, few strategies have been reported for incorporation of poorly water-soluble molecules in the capsule shell. Caruso et al. reported prodrug approach in which the hydrophobic cancer drug paclitaxel (PTX) was covalently coupled to poly(L-glutamic acid) and embedded inside the capsule shell.[20] As an alternative strategy for noncovalent sequestering of hydrophobic drugs, we developed hydrophobic nanoshells based on decylamino hydrazide derivatives of hyaluronic acid (HA).[21] However, this strategy, which is based on the non-specific binding of hydrophobic molecules to alkylated HA in the shell, poses difficulty to precisely control drug release.

Here, we describe a new kind of LbL-based hollow capsules based on hyaluronic acid-cyclodextrin conjugates that combine severable favorable features as a hydrophobic drug carrier, including CD inclusion complexation, unique biological functions of hyaluronic acid (HA) and transport properties of capsules. Using paclitaxel as a model anticancer drug, we show that these systems can selectively bind the anticancer drug in the shell and release it in a selective and controlled manner to breast cancer cells.

3.3.2. Materials and Methods

Materials

The sample of bacterial sodium hyaluronate (HA) with a weight-average molecular weight of 200 kg/mol was supplied by ARD (Pomacle, France). The molecular weight distribution and the weight-average molecular weight were determined by size exclusion chromatography using a Waters Alliance chromatograph (USA) equipped with two online detectors: a differential refractometer and a light scattering detector (MALLS) from Wyatt (USA); the solutions were injected at a concentration of 1 mg/mL in 0.1 M $NaNO_3$. The polydispersity index (PDI) of the sample is $M_w/M_n \sim 1.5$. 6-monodeoxy-6-monoamino-β-cyclodextrin hydrochloride, heptakis-(2,6-di-*O*-methyl) β-CD (DM-β-CD), pentenoic anhydride, 3-mercaptopropionic acid (MPA), ethylenediaminetetraacetic acid (EDTA), phosphate buffer saline (PBS, pH 7.4), 1-ethyl-3-(3-dimethylaminopropyl) carbodiimide (EDC), *N*-hydroxysulfo-succinimide (sNHS), and all other chemicals were purchased from Sigma-Aldrich-Fluka and were used without further purification. Paclitaxel and oregon green-labeled paclitaxel (OG-PTX) were purchased from Invitrogen (USA). 2-Hydroxy-1-[4-(2-hydroxyethoxy)phenyl]-2-methyl-1-propanone (Irgacure 2959) was kindly provided by Ciba Specialty Chemicals (Basel, Switzerland). Deuterium oxide was obtained from SDS (Vitry, France). The water used in all experiments was purified by a Elga Purelab purification system, with a resistivity of 18.2 MΩ.cm. The β-cyclodextrin (β-CD) derivative monofunctionalized with MPA (CD-SH), used for the synthesis of CD-modified HA (HA-CD), was prepared in the laboratory as previously described.[22] The pentenoate-modified HA with a degree of substitution (DS; defined as the number of moles of β-CD molecules per 100 disaccharide repeating units) of 9 was synthesized as previously described.[22]

Methods

Synthesis of HA-CD

To a solution of HA-pentenoate (80 mg, 1.57×10^{-2} mmol) in ultrapure water containing Irgacure 2959 (0.05% w/v) as a photoinitiator, CD-SH (20 mg, 1.57×10^{-2} mmol) dissolved in 1 ml of water was added. The grafting of CD-SH moieties was performed under UV radiation (λ = 365 nm) for 10 min. The product was purified by diafiltration (ultramembrane Amicon YM10) with ultrapure water and was recovered by freeze-drying (95 mg). The degree of substitution of HA-CD was found to be 9 ± 1 by ^{1}H NMR (**Figure SI 3.9**).

^{1}H NMR (400 MHz, D_2O) δ (ppm): 4.95 (anomeric protons of CD), 4.55 (anomeric proton of the *N*-acetylglucosamine unit), 4.25 (anomeric proton of the glucuronic acid units), 2.8-2.5 (2 CH_2CO, CH_2-S-CH_2), 1.85 (CH_3-CO from HA), 1.7-1.2 (2 CH_2).

Synthesis of (HA-CD/PLL) capsules and quantification of OG-PTX incorporated in capsules

Microcapsules were prepared according to the method described for the synthesis of (HA/PLL) capsules using calcium carbonate particles as a sacrificial template.[23] PTX was pre-complexed with HA-CD by adding 34.2 µL of a PTX/ OG-PTX mixture (5 g L^{-1} or 5.85 mM) in methanol in the HA-CD solution (4 mL) at 1 g L^{-1}. The $CaCO_3$ particles were coated layer-by-layer by incubating them at a concentration 2 % (w/v) in solutions of HACD-PTX (at 1 g L^{-1}) and PLL (at 2 g L^{-1}), both in 0.15 M NaCl (pH 6.5). After the desired number of layers was deposited, the multilayer shell was crosslinked using EDC (400 mM) and sNHS (100 mM) in 0.15 M NaCl and the $CaCO_3$ core was removed by treatment with an aqueous solution of EDTA (0.1 M, pH 7.2). The dissolved ions resulting from the decomposition of $CaCO_3$ were then removed by dialysis against pure water, using spectra Por dialysis bags with a molecular weight cut off of 10 kDa.

The amount of OG-PTX incorporated in the capsules was determined by fluorescence intensity measurements after extraction of PTX/OG-PTX from capsules with methanol according to an established procedure[21]. The suspension of capsules (100 µL at ~ 6×10^7 capsules/mL) in PBS was centrifugated (4000 rpm, 4 min, 20 °C) and the supernatant was removed. After addition of methanol, the suspension was again centrifugated (9000 rpm, 4 min, 20 °C) and the supernatant containing OG-PTX was recovered. This process was repeated two times to ensure the full extraction of OG-PTX from the capsules. Then the solutions were analyzed using the fluorescence microplate reader (Infinite 1000, Tecan, Austria) with excitation and emission wavelengths set at 496±10 nm and 524±10 nm, respectively. To estimate the absolute OG-PTX concentration, a calibration curve for the fluorescence of OG-PTX as a function of its concentration was acquired (**Figure SI 3.10**). The effective concentration of PTX per capsule was calculated knowing the ratio of unlabeled/labeled PTX, the molecular weight of PTX and OG-PTX and the average number of capsules per mL which was determined using a Petroff-Hausser counting chamber.

Solubility studies

Two PTX stock solutions were prepared in methanol (A: 1 g L^{-1} (1.17 mM); B: 5 g L^{-1} (5.85

mM)). The solution A (1.7 µL) was added to an aqueous solutions (1 mL) of β-CD ([CD] = 6 mM), and the solution B (8.5 µL and 8.4 µL) was added to aqueous solutions (1 mL) of HA-CD ([CD] = 0.157 mM) and DM-β-CD ([CD] = 6 mM), respectively. The resulting mixtures were stirred for 4 h at room temperature and methanol was allowed to evaporate slowly under a stream of nitrogen. The suspensions were then filtered through 0.45 µm membrane filter (Millipore) and analyzed by UV spectrometry. The concentration of PTX in the solution was calculated using the Beer-Lamber law, $A = \varepsilon C l$, where A is absorbance, C is the concentration in mol/L, l is the path length of the cell (l=1.25 cm), and ε is the extinction coefficient (ε=28000).

Release kinetics of paclitaxel from (HA-CD/PLL) capsules

The suspension of PTX-loaded capsules was divided in samples of 200 µL. Each sample was dispersed in 1.5 mL PBS in an eppendorf at 37°C. Periodically (2 times per day), 1 mL release medium was removed and 1 mL fresh PBS was added to each eppendorf. At time x, one sample was treated to determine the amount of PTX retained in the capsules. PTX was extracted from the capsules with methanol and the methanolic solution was analyzed by UV spectrometry. This process was performed in duplicate.

Physicochemical characterization

^{1}H NMR spectra of CD and HA derivatives dissolved in deuterium oxide (6 mg/mL) were performed at 25 and 80 °C, respectively, using a Bruker spectrometer operating at 400 MHz.

The buildup of $(HA\text{-}CD/PLL)_i$, $(HA\text{-}CD\text{-}PTX/PLL)_i$, $(HA/PLL)_i$ films (where i denotes the number of layer pairs) was followed by in situ quartz crystal microbalance with dissipation monitoring (QCM-D, D300, Qsense, Sweden) according to the experimental protocol that has been described in our previous publications.[24,25] For SEM observations, a drop of capsules suspension is deposited on fresh clived mica and air drying. The samples were coated with a 2 nm layer of carbon and observed in secondary electron imaging mode with a FEI Quanta 250 FEG-SEM using an accelerating voltage of 3kV or sputtered with 8nm layer of Au/Pd and observed in secondary electron imaging mode with a Jeol JSM610 SEM using an accelerating voltage of 8kV.

In-vitro biocompatibility studies

Cell Culture

MDA-MB-231 cells were cultured in DMEM (Gibco, Invitrogen, USA) without pyruvate supplemented with 10 % heat-inactivated foetal bovine serum (FBS, PAA Laboratories, France), 100 U/mL penicillin G and 100mg/mL streptomycin (Gibco, Invitrogen, USA) in a 37 °C, 5% CO_2 incubator. Cells were subcultured prior to reaching 60-70% confluence. For all experiments, MDA-MB-231 cells were seeded at 5 000 cells per well in 96-well plates in 200 µL of medium and were allowed to grow for a total of four days. PTX in solution, unloaded and PTX-loaded microcapsules diluted to low (LD, 30 capsules/cell), medium (MD, 60 capsules/cell) or high density (HD, 120 capsules/cell) were added to the cells 24 h after cell plating.

Viability and proliferation assays

Cell viability was measured by 3-(4,5-dimethylthiazol-2-yl)-2,5-diphenyltetrazolium bromide (MTT, Sigma) assay. At given time intervals, 25 µL of a MTT solution (1.5 mg/mL in PBS) were added to each well. The plates were then incubated for 75 min, allowing viable cells to reduce the yellow MTT to dark-blue formazan crystals, which were subsequently dissolved in 200 µL of DMSO. Absorbance of the plate was measured using the microplate reader at 550 $\pm$ 5 nm and at 650 $\pm$ 5 nm for the reference wavelength. Cell proliferation over time was quantified by counting the total number of cells in each well. Briefly, cells were detached with 0.25 % Trypsin-EDTA solution for 5 minutes at 37 °C and then quantified using a Malassez chamber. Experiments were performed in triplicate, with three 3 wells per condition in each experiment.

Immuno-stainings

Cells were fixed in 3.7 % formaldehyde in PBS for 20 min and permeabilized for 4 min in TBS (0.15 M NaCl, 50 mM Tris-HCl, pH 7.4) containing 0.2 % Triton X-100. Slides were blocked in TBS containing 0.1 % BSA for 1 h, and were then incubated with monoclonal anti-tubulin (Sigma) (1:200) antibodies in TBS with 0.2 % gelatin for 30 min. AlexaFluor-643 goat anti-mouse IgG (Invitrogen) was then incubated for 30 min. Finally, nuclei were stained using Hoechst 33342 (Invitrogen) at 5 µg/mL for 10 min. The plates were viewed under confocal microscopy (LSM 700, Zeiss) using a 63X objective. Images were acquired with Zen 2010 software.

Statistical analysis

All the results are expressed as mean values ± standard error of the mean (SEM). Statistical comparisons were based on an analysis of variance (ANOVA) for pairwise comparisons ($p < 0.05$ was considered significant).

3.3.3. Results and discussion

To prepare capsules able to selectively entrap hydrophobic molecules within the nanoshell through host-guest complexation, HA modified by β-cyclodextrin was layer-by-layer assembled with poly(L-lysine) (PLL), a biocompatible and biodegradable polypeptide, on sacrificial colloidal particles (**Figures 3.2.A and B**). HA was selected as a polyanion due to its interesting biological properties. Indeed, HA is a natural glycosaminoglycan, which can be specifically recognized by the CD44 receptor that is over-expressed by several cancer cells.[26-29] For example, to develop breast cancer-targeted drug delivery systems, HA have been previously reported as targeting ligand for HA-paclitaxel conjugates,[30] HA-grafted liposomes,[29,31] as well as HA-coated poly(D,L-lactide-co-glycolide) nanoparticles[32].

Moreover, we previously demonstrated that by using calcium carbonate particles and carefully optimizing the assembly conditions, stable non-aggregated (HA/PLL) capsules can be obtained after crosslinking of the (HA/PLL) film through EDC/sNHS mediated amidation.[23]

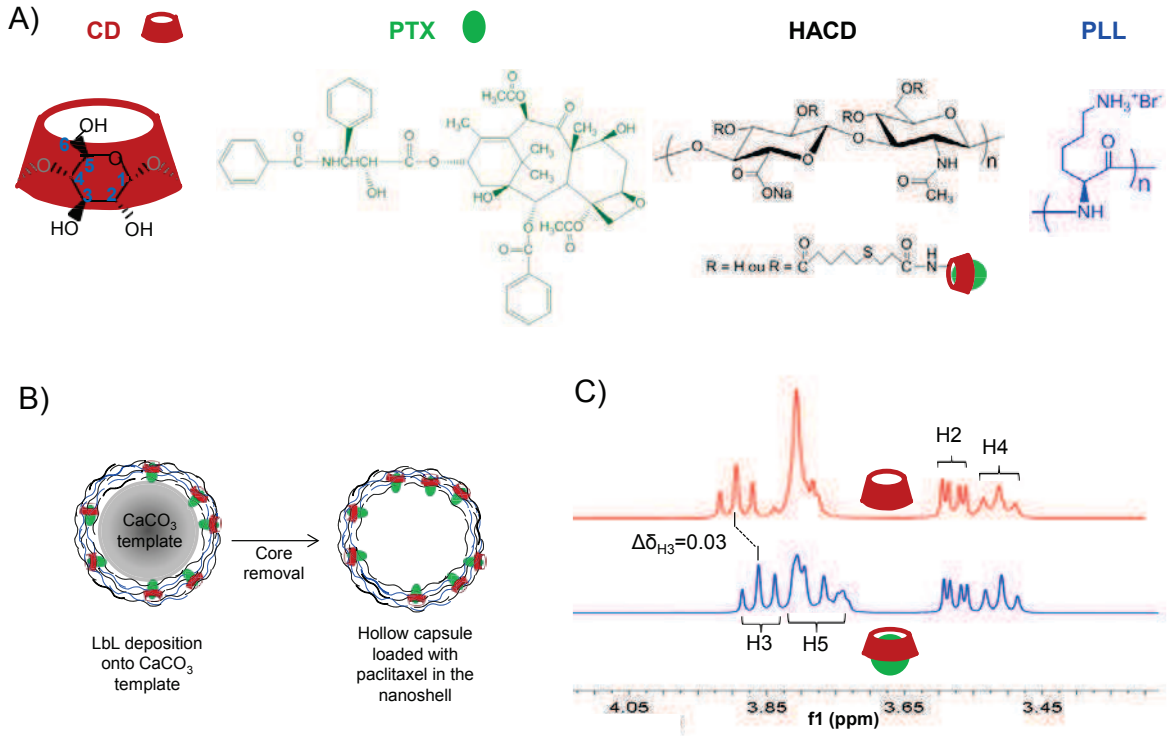

Figure 3. 2. Strategy for the synthesis of capsules with host-guest complexes in the nanoshells. A) Structure of β-CD, paclitaxel and of the biopolymers (HA-CD and PLL) forming the nanoshell. B) Schematic representation of the fabrication of stable (HA-CD/PLL) capsules by crosslinking the (HA-CD/PLL) multilayer wall before dissolution of the calcium carbonate core templates. C). Partial ^{1}H NMR spectra (400 MHz, 25 °C, D_2O) of (a) β-CD (10 mM) and (b) a mixture of β-CD (10 mM) and paclitaxel added at a concentration 2.5 µM.

HA was functionalized by β-cyclodextrin using a "thiol-ene reaction". We recently reported the potential of this coupling strategy for the modular functionalization of polysaccharides.[22] The reaction consisted in the radical addition in aqueous solution of a β-cyclodextrin derivative monofunctionalized with mercaptopropionic acid onto pentenoate-modified HA. A quantitative coupling yield was obtained, leading to a HA-CD derivative with a DS of 9 from ^{1}H NMR analysis (**Figure SI 3.9**). ^{1}H NMR spectroscopy was also used to demonstrate the complexation of PTX by the natural β-CD cavity (**Figure 3.2.C**). It is observed here that PTX induces large shifts in the NMR signals of the H-3 and H-5 protons located in the cavity, in contrast to the H-2 and H-4 protons located outside the cavity, which clearly demonstrates the formation of an inclusion complex. This allows to improve the solubility of paclitaxel in water.[2] In fact, PTX is characterized by a low solubility in water (0.4 µM or 0.34 µg/mL),[33] due to its high hydrophobicity. Therefore, PTX is difficult to administer and requires solubilization in a Cremophor® EL (CrEL, a polyoxyethylated castor oil) and ethanol mixture

(Taxol®), which often leads to adverse side effects such as hypersensitivity reactions[34]. The enhancement of the water-solubility of PTX through host-guest interactions with the natural β-CD, HA-CD as well as with the heptakis-(2,6-di-*O*-methyl) β-CD (DM-β-CD), which has a 30 fold higher aqueous solubility,[35] is shown in **Figure 3.3**.

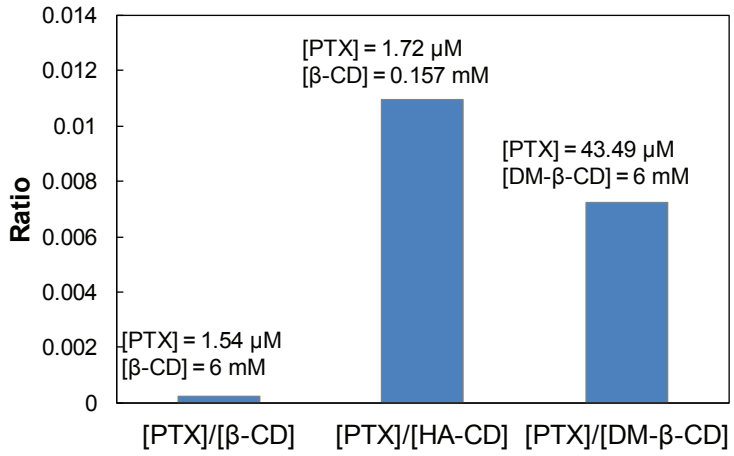

Figure 3. 3. Complexation of PTX by HA-CD in aqueous solution: dependence of paclitaxel solubility in aqueous solutions containing natural β-CD, HA-CD and DM-β-CD.

In the case of the natural β-CD, the water-solubility of PTX is increased ~ fivefold for a PTX:β-CD molar ratio of 2.57×10^{-4} ([β-CD] = 6 mM), whereas in the case of HA-CD, the same increase is achieved for a PTX:β-CD molar ratio of 1.10×10^{-2} ([β-CD] = 0.16 mM). As the inclusion performances of the natural β-CD and grafted β-CD are of the same order of magnitude, the extremely high solubilization potential obtained with HA-CD is related to the high solubility in water of the host polysaccharide. As shown in **Figure 3.3**, a similar conclusion could be drawn comparing the solubilization power of the natural β-CD with that of DM-β-CD.

Assembly of HA-CD (with and without PTX) and PLL in multilayer films was confirmed by following (HA-CD/PLL) film deposition on a planar solid substrate by QCM-D (**Figure 3.4**). Film growth was found to be exponential and very similar to that of HA/PLL[23]. Exponential growth could be related to the diffusion of PLL within the film architecture as previously observed for HA/PLL films[36].

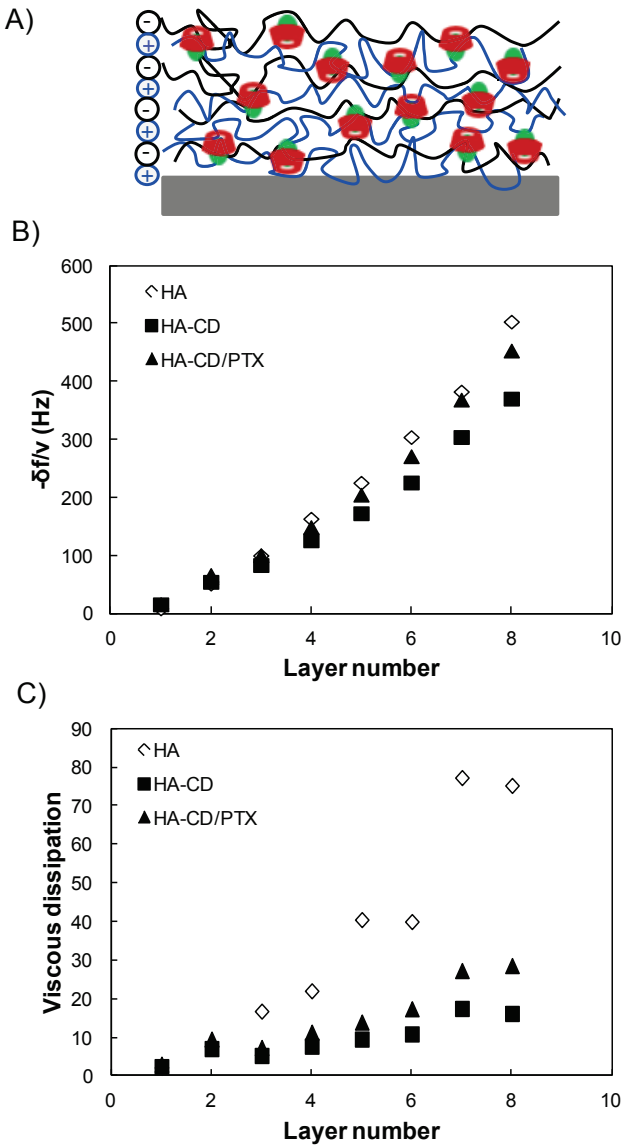

Figure 3. 4. Growth of (HA-CD/PLL) films with and without PTX in 0.15 M NaCl (pH 6.5) as measured by QCM-D on gold coated crystal. A) Schematic representation of a layer-by-layer self-assembled film of HA-CD/PLL. B) Differences in the QCM frequency shifts measured at 15 MHz are plotted for each polyanion and PLL layer. Data are given at 15 MHz for HA-CD (■) and HA-CD/PTX (▲) as compared to unmodified HA (◇). C) Viscous dissipations for each polyanion and PLL layer.

We then investigated the generation of capsules made from (HA-CD/PLL) films and the PTX loading and release from the nanoshell. To this end, Oregon Green labeled PTX (OG-PTX) was pre-complexed with HA-CD, and the resulting HA-CD/PTX complex was assembled layer-by-layer with PLL on calcium carbonate microparticles. After shell cross-linking by amide bond formation between HA and PLL and core dissolution by treatment with an aqueous solution of EDTA,[23] we successfully obtained hollow capsules. Observations of the OG-PTX-loaded capsules made of four (HA-CD/PLL) layer pairs and one HA layer in PBS

solution by CLSM confirmed their spherical shape with a size of 4.2 ± 0.2 µm (measured on three different capsule batches) and green capsule shells (**Figure 3.5**).

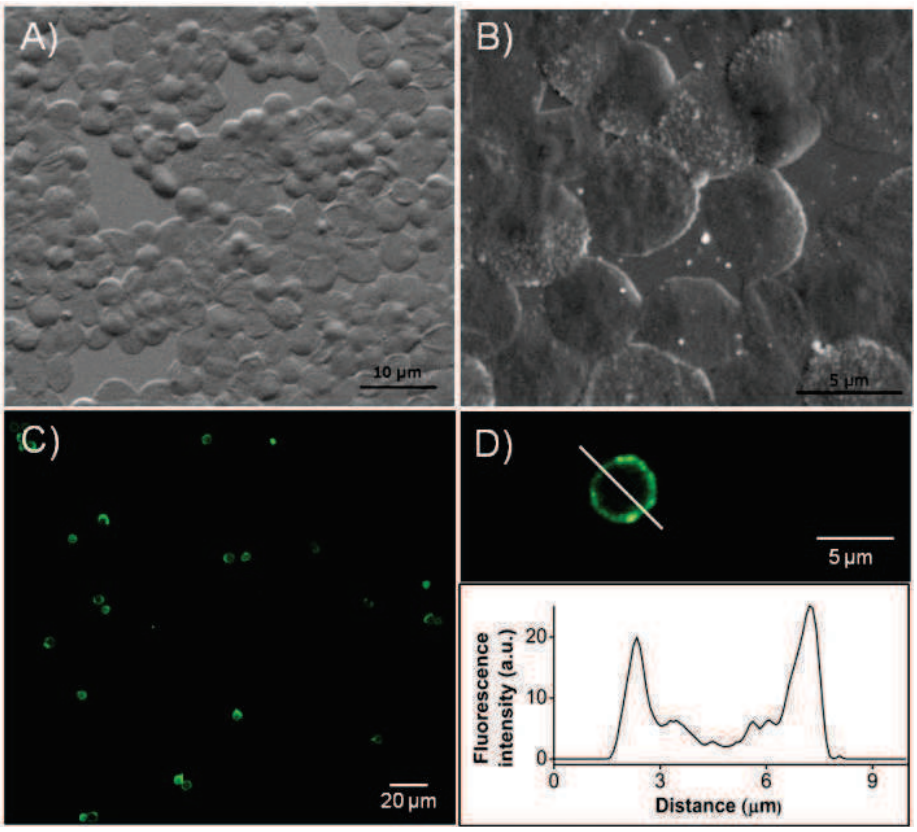

Figure 3. 5. Microscopy observations of $((HA\text{-}CD/PTX)/PLL)_4/HA$ capsules. A) and B) SEM observations of the dried hollow capsules. C) CLSM images of capsules exhibiting a localized green fluorescence in their nanoshell due to complexation of OG-PTX by CD molecules in the nanoshell. D) Magnified image of a capsule and corresponding fluorescence intensity profile along its diameter, confirming the selectivity of OG-PTX incorporation in the nanoshell.

Importantly, the intensity profile along a diameter confirmed the selective incorporation of OG-PTX in the shell, as well as its impressive stability after core removal. Furthermore, fluorescence microscopy revealed that the drug-loaded capsules were well-dispersed in phosphate buffered saline. The SEM images also indicate diameters in the order of ~ 5 µm for the dried capsules (**Figure 3.5**).

We quantified the amount of PTX entrapped in the capsules by fluorescence intensity measurements using OG-PTX. After extraction of PTX from the nanoshell with methanol,[21] the effective concentration of PTX in 100 µL of a capsule suspension at 6×10^7 capsules per mL was found to be 0.914 µM, thus corresponding to ~13 fg of PTX per capsule. New batches of PTX-loaded capsules were then treated over time in order to examine the release of PTX under simulated physiological conditions (PBS, pH 7.4, 37 °C).

As can be seen from **Figure 3.6**, PTX was released according to a two-step process with about 20 % of the drug released in the first ~ 4 h, after which there was a steady and controlled increase in release for up to 120 h. This sustained release profile, making PTX available within a period of five days, is attributed to the CD moieties which entrap the drug. Indeed, addition of DM-β-CD in the aqueous suspension of capsules triggered payload release with about 80 % of PTX released in ~ 20 h (**Figure SI 3.11**). The very small initial burst may be due to PTX encapsulated in the layers close to the surface rather to non-specific adsorption of PTX to HA. Indeed, a similar profile could be obtained in conditions limiting this potential phenomenon, i.e. by decreasing the [PTX]/[HA-CD] ratio during LbL film deposition. Taken together, these results highlight the ability of the multilayer shell to retain the vast majority of PTX within the capsule, which could potentially limit toxicity.

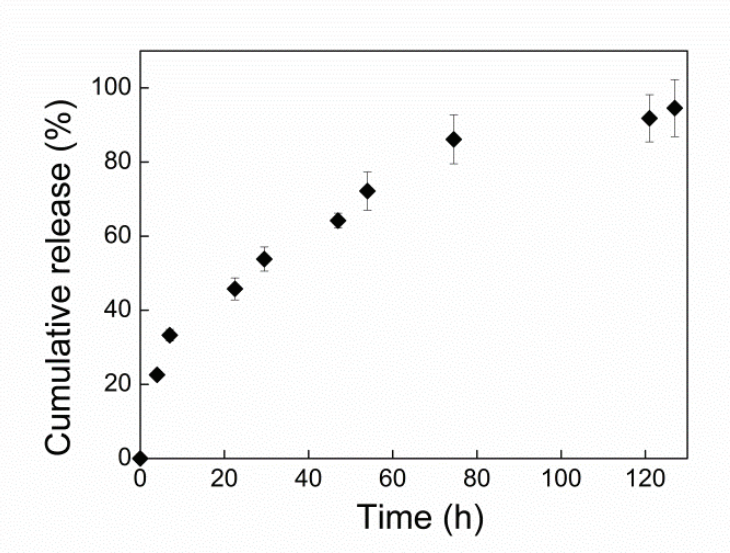

Figure 3. 6. *In vitro* release profile of paclitaxel from the ((HACD-PTX)/PLL)$_4$/HA capsules in PBS.

We then investigated the capacity of (HA-CD/PLL)$_4$-HA capsules to deliver PTX to MDA-MB-231 breast cancer cells, a cell line known to be sensitive to PTX[37]. After extraction of PTX from the nanoshell, the effective concentration of PTX in 100 µL of a microcapsule suspension at 6×10^7 microcapsules/mL was found to be of 0.914 µM, thus corresponding to ~13 fg of PTX per microcapsules. This value was taken as the highest positive reference for tests using PTX in solution (= sPTX). Unloaded and PTX-loaded capsules at different densities were added to MDA-MB-231 cell culture and observed over three days. The cytotoxicity of the capsules was evaluated by counting the cell number and by measuring the cell viability using a MTT assay[21]. Unloaded microcapsules added at increasing

concentrations to the cells did not induce any cytotoxic effect, even when added at high density (HD, ~120 caps./cell) to the cell culture (**Figures 3.7.A,A'** and **SI 3.12**). Addition of PTX in solution (**Figures 3.7.B,B'**) lead to a significant decrease of cell number and cell metabolic activity, as anticipated.

Notably, the PTX-loaded capsules exhibited an important effect on MDA-MB-231 cells (**Figures 3.7.C,C'**), strongly limiting their proliferation and metabolic activity. At day 3, the number of cells cultivated in the presence of the PTX-loaded capsules was between 7.2 to 8.6 fold lower than the cells cultivated in the absence of capsules or in the presence of unloaded capsules. MDA-MB 231 are known to express CD44,[27,30] one of the hyaluronan receptor. Indeed, we verified that CD44 is highly expressed by the cancer cells (**Figure SI 3.13**).

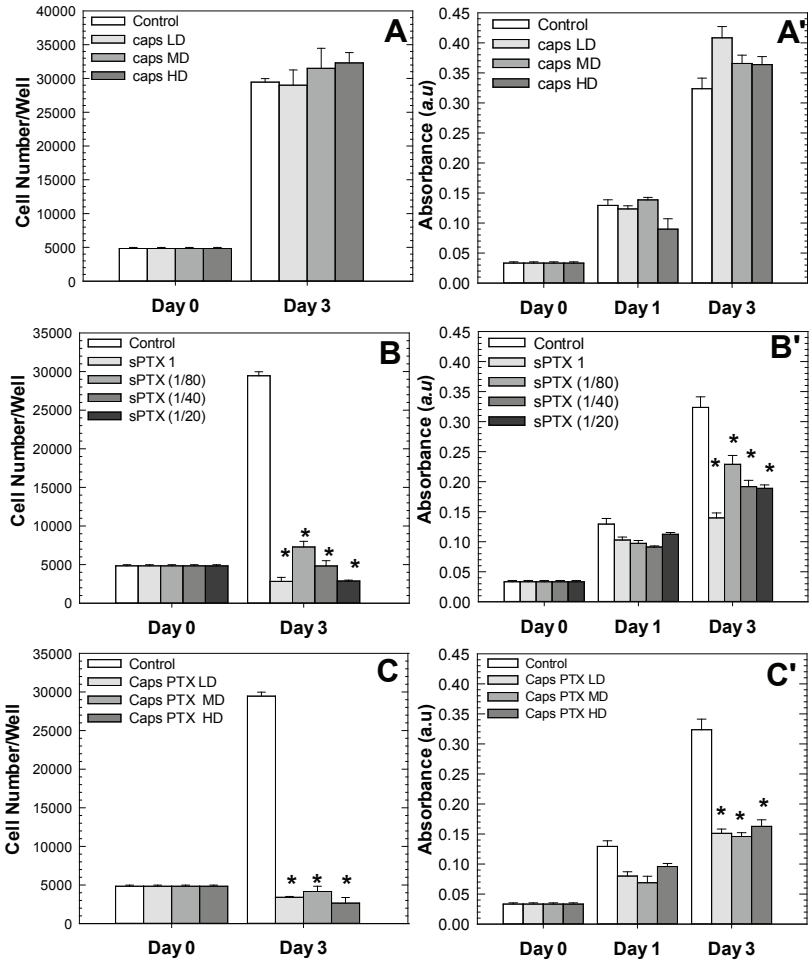

Figure 3. 7. MDA-MB-231 cell response to unloaded microcapsules in solution, to PTX in solution and to PTX-loaded $(HA\text{-}CD/PLL)_4/HA$ microcapsules. MDA-MB-231 cell number and MTT metabolic activity were quantified after one and 3 days in the presence of (A,A') unloaded microcapsules added at increasing concentrations (LD, MD or HD), (B,B') with PTX added in solution to the cells at increasing concentration (i.e. 1/80, 1/40 and 1/20 corresponding to LD, MD and

HD); (C,C') PTX-loaded microcapsules added at increasing densities (LD, MD or HD) in the culture medium. Data represent mean ± SEM of three wells. Experiments have been performed in triplicate. *,$p < 0.05$.

In the presence of $(HA\text{-}CD/PLL)_4/HA$ capsules, we noted that the capsules were in close contact with the MDA-MB 231 cells and that several capsules interacted with the cells (**Figures 3.8.A,A'**).

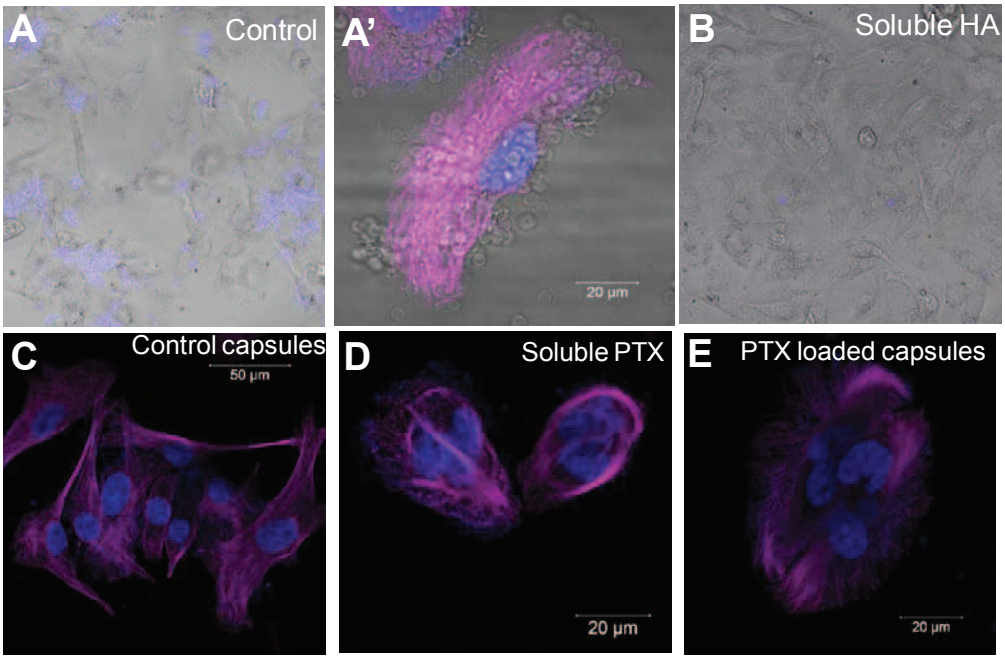

Figure 3.8. Microscopic observations of capsule/MDA-MB 231 cell interactions after 24 of culture. (A,A') Interaction of HA-containing capsules with MDA-MB-231 cells (nuclei stained in blue, β-tubulin in pink). (B) The interaction is inhbited by adding soluble HA to the culture medium.(C-E) Immuno-staining of β-tubulin (pink) and nuclei (blue) in representative MDA-MB-231 cells after 24 h of culture (C) in growth medium, (D) in contact with soluble PTX at 0.914 µM and (E) in contact with PTX-loaded microcapsules at MD density (60 capsules/cell).

When soluble HA was added to the culture medium, the interaction was fully inhibited (**Figure 3.8.B**). Thus, the interaction of the HA containing capsules and the cancer cells appears to be specifically mediated by the CD44 receptor.

MDA-MB231 cells are also known to secrete hyaluronidase, an enzyme known to specifically degrade hyaluronan,[38] which is known to be overexpressed in malignant breast cancer cells[39]. Hyaluronidase is often used as a marker for tumor detection.[40] It may also well be that the cells locally degrade the HA-containing microcapsules.

Next we investigated the effect of PTX on cell internal organization. Indeed, PTX is known to drastically affect cell internal structures, especially nucleus and microtubule organization[41].

We thus examined by immuno-staining the organization of β-tubulin and of the nucleus (**Figures 3.8.C-E**). On control cells (no capsules or unloaded capsules), the nuclei were intact and the microtubule network was well organized (**Figures 3.8.C** and data not shown). When PTX was added in the solution, bundles of microtubules were visible and the nuclei were fragmented (**Figure 3.8.D**). In the presence of PTX-loaded capsules, the fragmentation of the nuclei was particularly visible at high density and bundles of microtubules were also visible after one day of culture (**Figure 3.8.E**). This stabilization of the microtubules resulted in defects in the cell mitosis and the presence of large, multinucleated cells. As a consequence, these deficiencies in cell division lead to a very low cell proliferation, as shown by the proliferation assay (**Figure 3.7**).

All together, our data suggest that the mechanism of action of the PTX-loaded capsules is based on the combined action of several phenomena: specific interactions with MDA-MB 231 cancer cells via the CD44 receptor, passive transfer of PTX from the CD cavities to the hydrophobic lipid membrane of the cells, and local degradation of the capsules by hyaluronidase enzyme secreted by these cells.

3.3.4. Conclusion

In summary, we designed and prepare under mild physiological conditions a new kind of LbL capsules containing the hydrophobic anticancer drug paclitaxel in the shell. The synthesis of these capsules relied on the very high affinity of PTX to hyaluronic acid grafted with β-CD through inclusion complexation and the ability of HA-CD-PTX to be layer-by-layer assembled with poly(L-lysine) on sacrificial colloidal particles. These capsules, combining the inclusion capacity of β-CD and the unique biological properties of HA, exhibited controlled release properties and were effective at killing breast cancer cells. This cytotoxicity seems to be the result of favourable effects related to HA which can specifically interact with the cancer cells overexpressing the CD44 receptor, and be degraded by the hyaluronidase enzyme secreted by these cells. All together, these results indicate that these HA-CD based capsules have potential in controlled delivery of hydrophobic drugs to cancer cells.

3.4. Supporting information

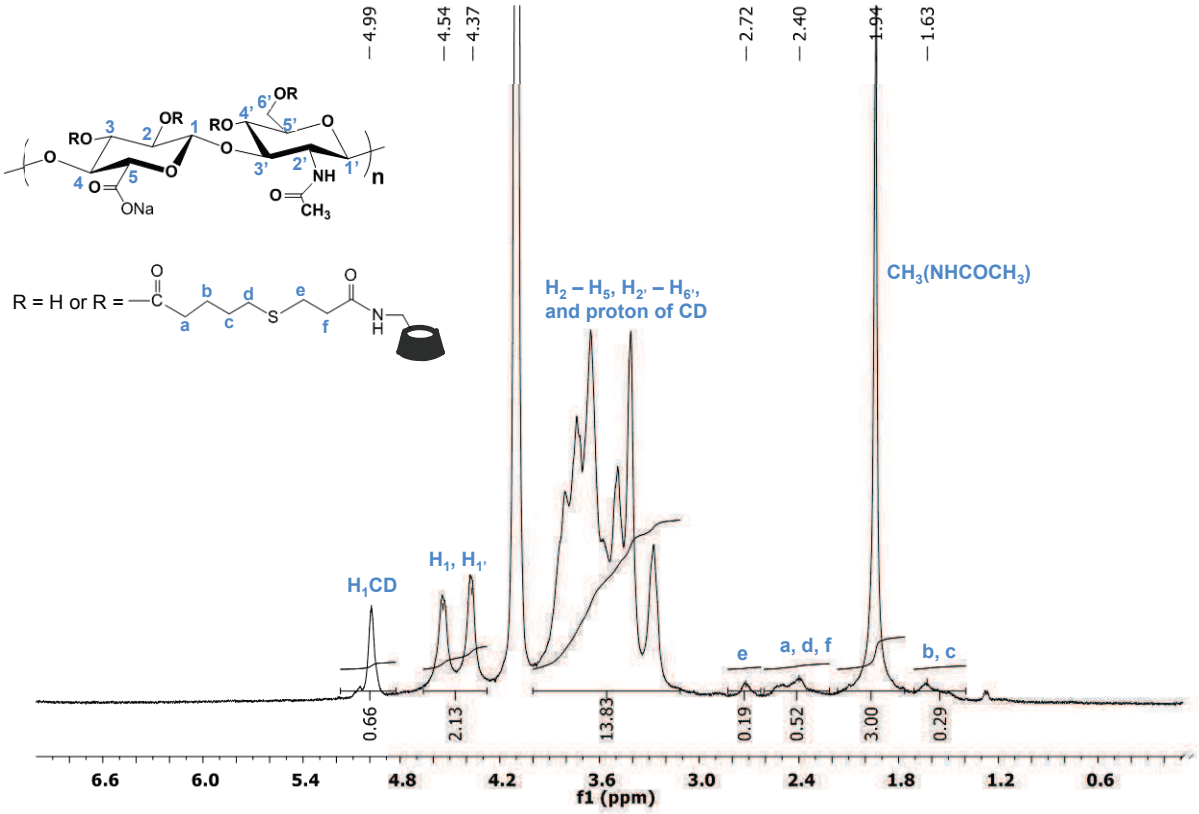

Figure SI 3. 9. ^{1}H NMR spectrum (400 MHz, 80 °C, 6 mg/mL in D_2O) of cyclodextrin-modified hyaluronic acid (DS = 9).

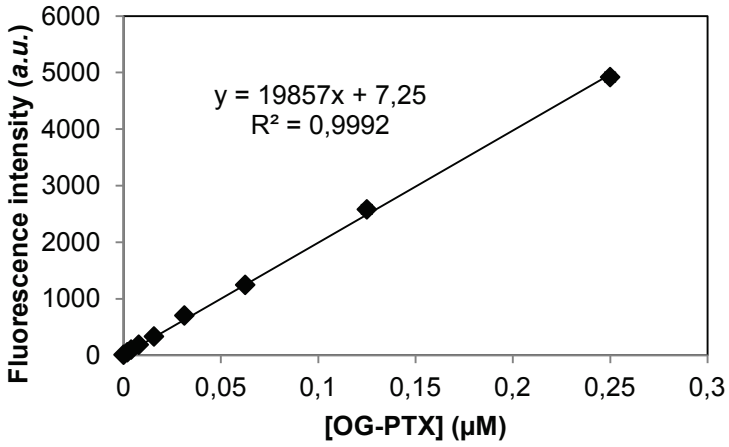

Figure SI 3. 10. Calibration curve for the fluorescence of OG-PTX in methanol as a function of its concentration in solution.

The suspension of PTX-loaded capsules was divided in samples of 200 µL. Each sample was dispersed in 1.5 mL PBS in an eppendorf at 37°C. At time t = 7 h, 1 mL of PBS release medium was removed and a solution (1 mL) of DM-β-CD ([DM-β-CD] = 6 mM) was added. After one night, a sample was treated by methanol to extract PTX from the capsules. The analysis of the methanolic solution by UV spectrometry indicated that about 80 % of PTX was released (experiment performed in triplicate). In order to establish the concentration of DM-β-CD required for full complexation of PTX entrapped in the capsule shell, we determined the amount of PTX left in the 200 µL of capsules suspension.

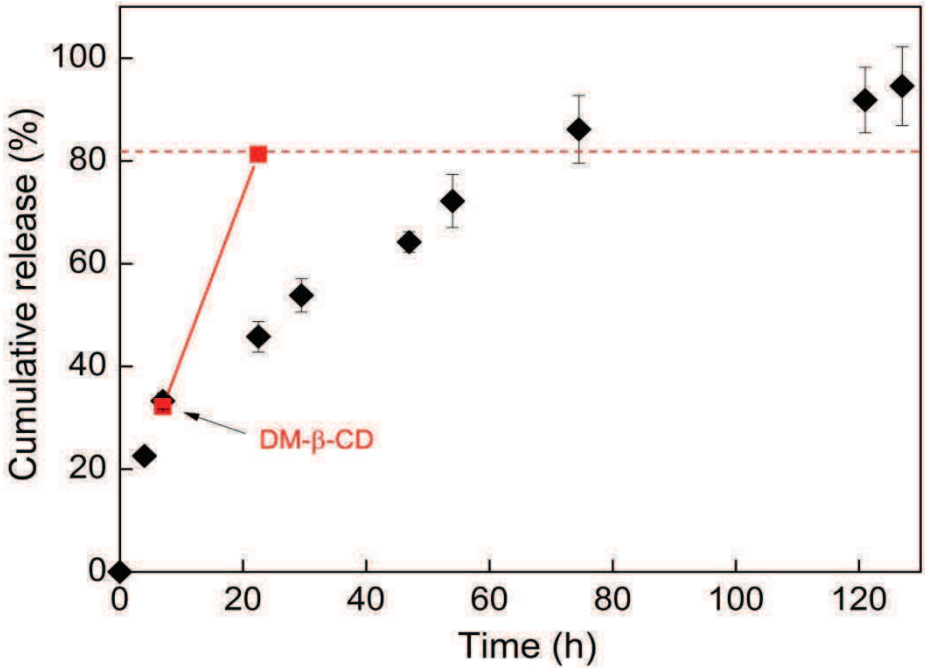

Figure SI 3. 11. In vitro release profile of paclitaxel from the $((HACD\text{-}PTX)/PLL)_4/HA$ capsules triggrered by addition of DM-β-CD ([DM-β-CD] = 6 mM) at t = 7h (red curve).

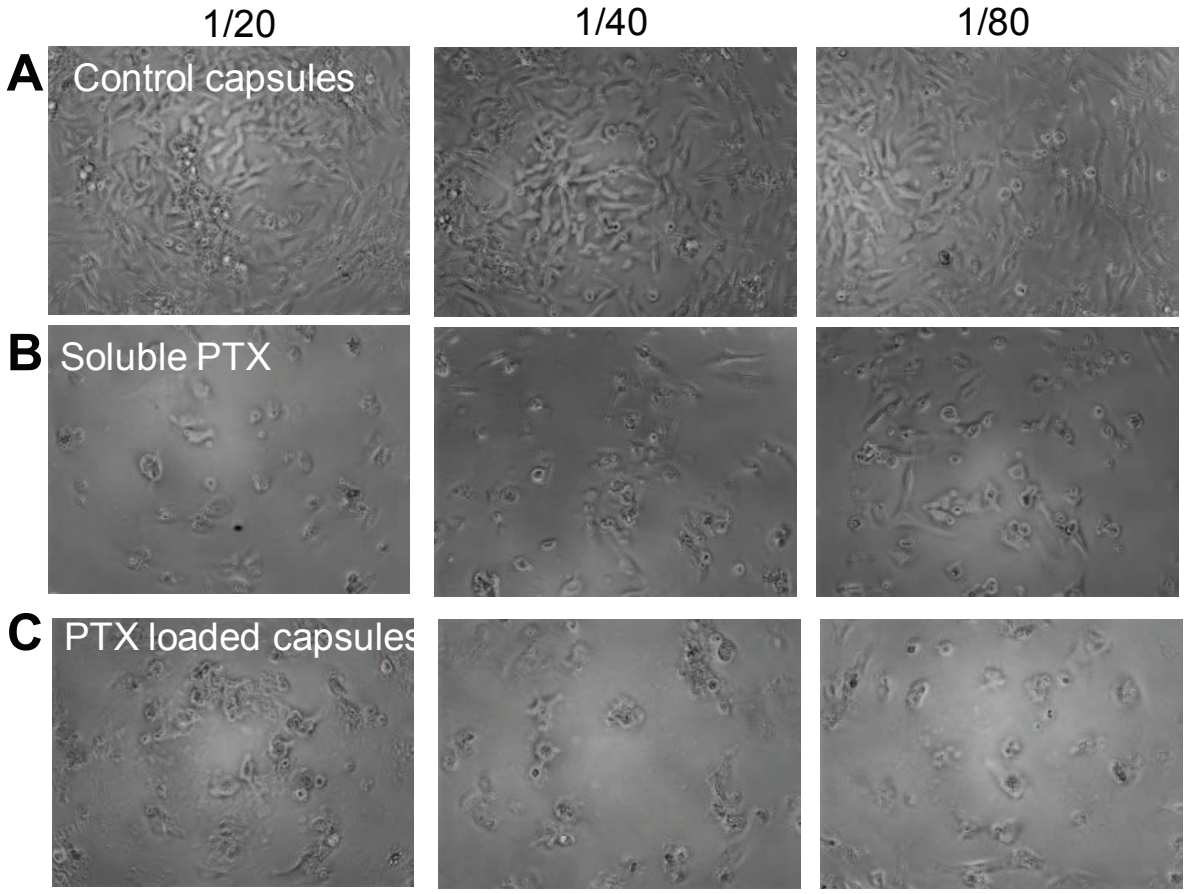

Figure SI 3. 12. Brightfield images of MDA-MB-231 cells after 3 days of culture (A) in contact with unloaded microcapsules at increasing density, (B) in growth medium in the presence of soluble PTX, (C) in contact with PTX-loaded microcapsules at increasing densities.

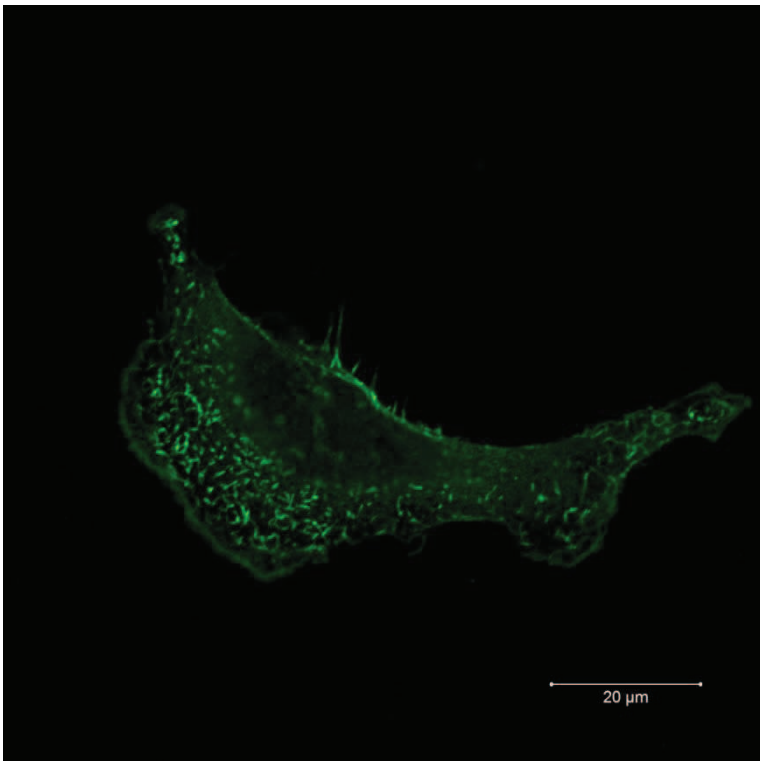

Figure SI 3.13. Immuno-staining of the CD44 receptor in MDA-MB-231 cells.

3.5. Complementary results

- Synthesis of cyclodextrin grafted HA (HA-CD)

HA-CD was synthesized by a mild and rapid method which was developed in our laboratory[22]. Pentenoate-modified HA (HA_{pt}) was reacted with thiol-functional CD by thiol-ene coupling reactions using UV light (λ = 365 nm) in the presence of the water-soluble photoinitiator Irgacure 2959 (**Scheme CR 3.1**). The molar mass of HA is M_w = 200000 g/mol.

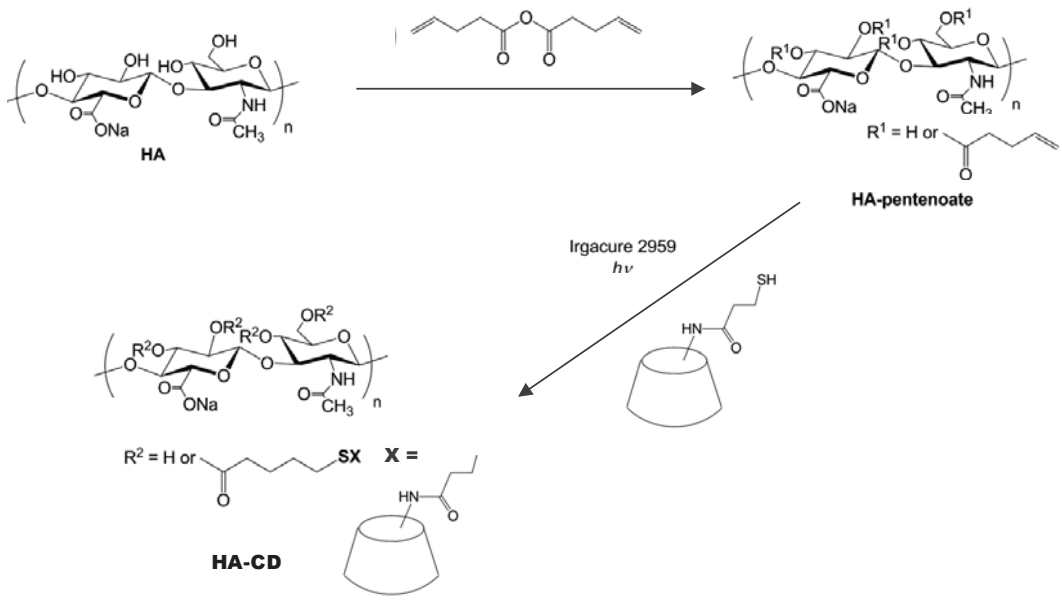

Scheme CR 3. 1. Synthesis of HA-CD by thiol-ene chemistry.

We synthesized three samples of HA-CD (see **Table CR 3.1**). Their structure was confirmed by ^{1}H NMR which also allowed to determine the degree of substitution.

Table CR 3. 1. Chemical characteristics (degree of substitution, DS) of HA-CD samples synthesized by thiol-ene chemistry.

Reference	HA_{pt}	HA-CD	
	DS^{a}_{pt}	$DS_{CD}{}^{a}$	$DS_{pt}{}^{a}$
HA-CD1	20	10	10
HA-CD2	20	15	5
HA-CD3	9	9	0

[a] derived from ^{1}H NMR integration.

The product HA-CD1 was not perfectly soluble in water. This may be attributed to the presence of pentenoate groups along the HA-chains. These hydrophobic groups may include into the CD cavities, resulting in the formation of intra- or interchain associations. We then synthesized HA-CD2 with a lower DS in pentenoate groups. This derivative appeared to be soluble in water. However, when we added this solution to $CaCO_3$ particles to prepare capsules, formation of aggregates could be observed quasi-instantaneously by optic microscopy (**Figure CR 3.14. A, B**). This was attributed to the formation of inclusion complexes between the pentenoate groups and the CD cavities, favoring associations between the polysaccharide chains. To decompose these associations, we added sodium adamandane acetate (ADAc) (4 molar equivalent of ADAc with respect to CD) in the solution of HA-CD2 and the mixture was left under stirring overnight. Adamandane is known to be a good guest

molecule for β-CD.[42] When we added the HA-CD/ADAc mixture to the suspension of $CaCO_3$ particles, no aggregate was observed (**Figure CR 3.14.C**). However, after addition of the second layer of poly(L-lysine), aggregates appeared (**Figure CR 3.14.D**). This phenomenon may be due to the fact that upon rinsing the particles during the LbL assembly, part of ADAc molecules is removed from the solution. As a result, new associations between the HA chains can be formed again. The aggregates became much bigger after the deposition of the next HA-CD layer (**Figure CR 3.14.E**).

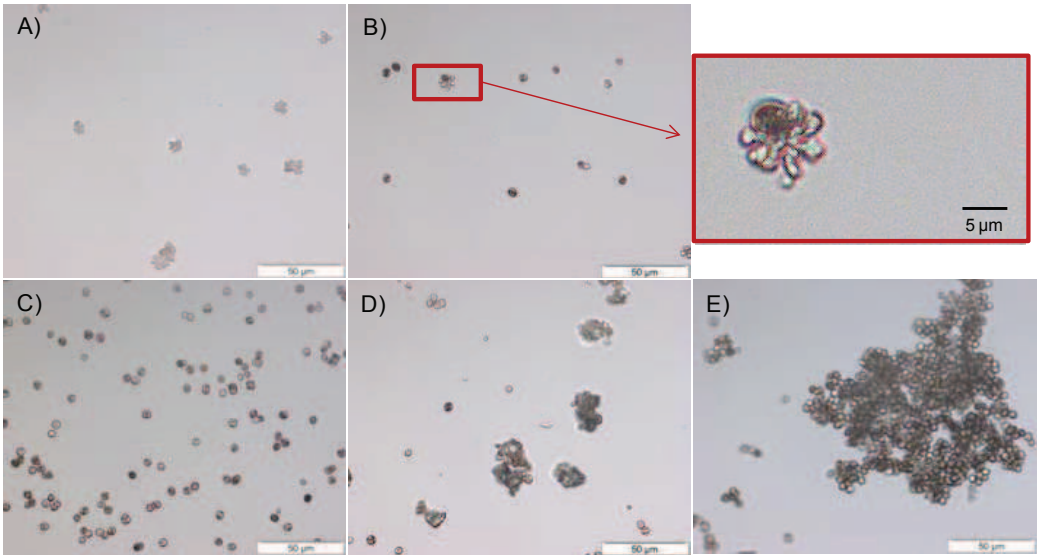

Figure CR 3. 14. Optical microscopy observation after depositing of the first layer of HA-CD2 onto $CaCO_3$ template (A) and (B); in the presence of sodium adamandane acetate (C); continued to deposit the second layer of PLL (D); continued to deposit the third layer of HA-CD (E).

Finally, we synthesized HA-CD3 in which all pentenoate groups were converted into thioethers by the radical addition of the CD-thiol derivative; with this compound, we could successfully prepare capsules.

This work showed that the behaviour of polymers in solution has a crucial role in the process of formation of capsules. The polysaccharide chains must be perfectly soluble in water to be able to cover the template as a layer, allowing the deposition of the next layers to obtain nanoshells.

3.6. Conclusion

Using hyaluronic acid modified by β-CD (HA-CD), we have succeeded to incorporate PTX selectively in the nanoshell of capsules through inclusion complexation. These PTX-loaded capsules exhibited controlled release profile and were effective to reduce the proliferation and metabolic activity of MDA MB 231 cells. This cytotoxicity seems to be the result of favourable effects related to HA which can specifically interact with the cancer cells overexpressing the CD44 receptor. The combination of cyclodextrin/drug complexation and LbL polyelectrolyte capsules offers a novel plateform for hydrophobic drug delivery.

References

(1) Alcaro, S.; Ventura, C. A.; Paolino, D.; Battaglia, D.; Ortuso, F.; Cattel, L.; Puglisi, G.; Fresta, M. *Bioorg. Med. Chem. Lett.* **2002**, *12*, 1637.

(2) Hamada, H.; Ishihara, K.; Masuoka, N.; Mikuni, K.; Nakajima, N. *J. Biosci. Bioeng.* **2006**, *102*, 369.

(3) Dordunoo, S. K.; Burt, H. M. *Int. J. Pharm.* **1996**, *133*, 191.

(4) Bilensoy, E.; Gurkaynak, O.; Ertan, M.; Sen, M.; Hincal, A. A. *J. Pharm. Sci.* **2008**, *97*, 1519.

(5) Bilensoy, E.; Guerkaynak, O.; Dogan, A. L.; Hincal, A. A. *Int. J. Pharm.* **2008**, *347*, 163.

(6) Agueeros, M.; Ruiz-Gaton, L.; Vauthier, C.; Bouchemal, K.; Espuelas, S.; Ponchel, G.; Irache, J. M. *Eur. J. Pharm. Sci.* **2009**, *38*, 405.

(7) Agueeros, M.; Zabaleta, V.; Espuelas, S.; Campanero, M. A.; Irache, J. M. *Journal of Controlled Release* **2010**, *145*, 2.

(8) Wang, X.; Chen, C.; Huo, D.; Qian, H.; Ding, Y.; Hu, Y.; Jiang, X. *Carbohydrate Polymers* **2012**, *90*, 361.

(9) Yameogo, J. B. G.; Geze, A.; Choisnard, L.; Putaux, J.-L.; Gansane, A.; Sirima, S. B.; Semde, R.; Wouessidjewe, D. *Eur. J. Pharm. Biopharm.* **2012**, *80*, 508.

(10) Choisnard, L.; Geze, A.; Vanhaverbeke, C.; Yameogo, J. B. G.; Putaux, J.-L.; Brasme, B.; Jullien, L.; Boullanger, S.; Elfakir, C.; Wouessidjewe, D. *Biomacromolecules* **2011**, *12*, 3031.

(11) Agarwal, A.; Lvov, Y.; Sawant, R.; Torchilin, V. *Journal of Controlled Release* **2008**, *128*, 255.

(12) Smith, R. C.; Riollano, M.; Leung, A.; Hammond, P. T. *Angewandte Chemie, International Edition* **2009**, *48*, 8974.

(13) Wang, Y.; Yan, Y.; Cui, J.; Hosta-Rigau, L.; Heath, J. K.; Nice, E. C.; Caruso, F. *Advanced Materials* **2010**, *22*, 4293.

(14) Duncan, R. *Adv. Drug Delivery Rev.* **2009**, *61*, 1131.

(15) Farokhzad, O. C.; Langer, R. *ACS Nano* **2009**, *3*, 16.

(16) Loomis, K.; McNeeley, K.; Bellamkonda, R. V. *Soft Matter* **2011**, *7*, 839.

(17) Uekama, K.; Hirayama, F.; Irie, T. *Chem. Rev. (Washington, D. C.)* **1998**, *98*, 2045.

(18) Devi, N. K. D.; Rani, A. P.; Javed, M. M.; Kumar, K. S.; Kaushik, J.; Sowjanya, V. *Pharmacophore* **2010**, *1*, 155.

(19) Hayashi, K.; Ono, K.; Suzuki, H.; Sawada, M.; Moriya, M.; Sakamoto, W.; Yogo, T. *ACS Appl. Mater. Interfaces* **2010**, *2*, 1903.

(20) Yan, Y.; Ochs, C. J.; Such, G. K.; Heath, J. K.; Nice, E. C.; Caruso, F. *Advanced Materials (Weinheim, Germany)* **2010**, *22*, 5398.

(21) Cui, D.; Jing, J.; Boudou, T.; Pignot-Paintrand, I.; De Koker, S.; De Geest, B. G.; Picart, C.; Auzély-Velty, R. *Advanced Materials* **2011**, *23*, H200.

(22) Mergy, J.; Fournier, A.; Hachet, E.; Auzely-Velty, R. *J. Polym. Sci., Part A: Polym. Chem.* **2012**, *50*, 4019.

(23) Szarpak, A.; Cui, D.; Dubreuil, F.; De, G. B. G.; De, C. L. J.; Picart, C.; Auzely-Velty, R. *Biomacromolecules* **2010**, *11*, 713.

(24) Richert, L.; Lavalle, P.; Payan, E.; Shu, X. Z.; Prestwich, G. D.; Stoltz, J.-F.; Schaaf, P.; Voegel, J.-C.; Picart, C. *Langmuir* **2004**, *20*, 448.

(25) Schneider, A.; Vodouhe, C.; Richert, L.; Francius, G.; Le, G. E.; Schaaf, P.; Voegel, J.-C.; Frisch, B.; Picart, C. *Biomacromolecules* **2007**, *8*, 139.

(26) Auzenne, E.; Ghosh, S. C.; Khodadadian, M.; Rivera, B.; Farquhar, D.; Price, R. E.; Ravoori, M.; Kundra, V.; Freedman, R. S.; Klostergaard, J. *Neoplasia (Ann Arbor, MI, U. S.)* **2007**, *9*, 479.

(27) Draffin, J. E.; McFarlane, S.; Hill, A.; Johnston, P. G.; Waugh, D. J. J. *Cancer Res.* **2004**, *64*, 5702.

(28) Luo, Y.; Prestwich, G. D. *Bioconjugate Chem.* **1999**, *10*, 755.

(29) Qhattal, H. S. S.; Liu, X. *Mol. Pharmaceutics* **2011**, *8*, 1233.

(30) Luo, Y.; Ziebell, M. R.; Prestwich, G. D. *Biomacromolecules* **2000**, *1*, 208.

(31) Surace, C.; Arpicco, S.; Dufay-Wojcicki, A.; Marsaud, V.; Bouclier, C.; Clay, D.; Cattel, L.; Renoir, J.-M.; Fattal, E. *Molecular Pharmaceutics* **2009**, *6*, 1062.

(32) Hyung, W.; Ko, H.; Park, J.; Lim, E.; Park, S. B.; Park, Y.-J.; Yoon, H. G.; Suh, J. S.; Haam, S.; Huh, Y.-M. *Biotechnology and Bioengineering* **2007**, *99*, 442.

(33) Sharma, U. S.; Balasubramanian, S. V.; Straubinger, R. M. *Journal of Pharmaceutical Sciences* **1995**, *84*, 1223.
(34) Gelderblom, H.; Verweij, J.; Nooter, K.; Sparreboom, A. *European Journal of Cancer* **2001**, *37*, 1590.
(35) Auzely-Velty, R.; Djedaieni-Pilard, F.; Desert, S.; Perly, B.; Zemb, T. *Langmuir* **2000**, *16*, 3727.
(36) Picart, C.; Mutterer, J.; Richert, L.; Luo, Y.; Prestwich, G. D.; Schaaf, P.; Voegel, J. C.; Lavalle, P. *Proceedings of the National Academy of Sciences of the United States of America* **2002**, *99*, 12531.
(37) Frasci, G.; Comella, P.; D'Aiuto, G.; Budillon, A.; Barbarulo, D.; Thomas, R.; Capasso, I.; Casaretti, R.; Daponte, A.; Caponigro, F.; Gravina, A.; Maiorino, L.; Carateni, G.; Gentile, A.; Comella, G. *Breast Cancer Research and Treatment* **1998**, *49*, 13.
(38) Menzel, E. J.; Farr, C. *Cancer Letters (Shannon, Ireland)* **1998**, *131*, 3.
(39) Tan, J.-X.; Wang, X.-Y.; Li, H.-Y.; Su, X.-L.; Wang, L.; Ran, L.; Zheng, K.; Ren, G.-S. *International Journal of Cancer* **2010**, *128*, 1303.
(40) Li, Y.; Li, L.; Brown, T. J.; Heldin, P. *International Journal of Cancer* **2007**, *120*, 2557.
(41) Yeung, T. K.; Germond, C.; Chen, X.; Wang, Z. *Biochemical and Biophysical Research Communications* **1999**, *263*, 398.
(42) Charlot, A.; Heyraud, A.; Guenot, P.; Rinaudo, M.; Auzely-Velty, R. *Biomacromolecules* **2006**, *7*, 907.

Chapter 4

Tunable self-assembled nanogels composed of well-defined thermoresponsive hyaluronic acid - polymer conjugates

4.1. Résumé (fr)

Ce chapitre présente une nouvelle classe de nanogels à base d'acide hyaluronique (HA), capables d'encapsuler des molécules hydrophobes selon un procédé simple en milieu aqueux. Ces nanogels sont obtenus par auto-association en milieu aqueux de dérivés de HA modifié par un copolymère thermosensible de diéthylèneglycolméthacrylate et d'oligoéthylèneglycolméthacrylate (poly(DEGMA-co-OEGMA)), induite par une élévation de la température à 37 °C. Le copolymer poly(DEGMA-co-OEGMA) a été synthétisé selon le procédé de polymérisation RAFT (Reversible Addition Fragmentation chain Transfer). En variant la proportion des monomères DEGMA et OEGMA, il est possible d'ajuster la valeur de la LCST (Lower Critical Solution Temperature) sur une large gamme de températures allant de 28 à 90 °C. Dans ce travail, le copolymère utilisé (DEGMA:OEGMA = 95:5) possède une LCST de 32°C. La température de transition « pelote-nanoparticule » des dérivés HA greffés de chaînes poly(DEGMA-co-OEGMA) avec des degrés de substitution (DS, nombre de substituants en moyenne toutes les cents unités de répétition) compris entre 3 et 6, a été déterminée en mesurant le point de trouble des solutions par spectroscopie UV. Au-dessus de cette température (voisine de 35 °C pour les trois copolymères « hybrides »), le HA-poly(DEGMA-co-OEGMA) conduit en quelques secondes à la formation de nanoparticules (ou nanogels). Ces valeurs ont pu être confirmées par des analyses par calorimétrie différentielle à balayage. La taille des nanogels dépend du DS du copolymère hybride. Des mesures de diffusion dynamique de la lumière ont montré qu'elle augmente avec le DS.

Ces nanoparticules peuvent solubiliser le Nile Red par simple ajout de quelques microlitres de solution de Nile Red dans l'éthanol à la solution de HA-poly(DEGMA-co-OEGMA) (1 mL) et chauffage à 37°C. L'incorporation du Nile Red dans les nanogels a été mise en évidence par microscopie de fluorescence qui fait apparaître des tailles homogènes. Afin d'évaluer la capacité des nanogels à transporter des agents anti-cancéreux faiblement solubles dans l'eau et à les délivrer dans des cellules cancéreuses, les particules de gel ont été chargées en paclitaxel (PTX). Nous avons choisi le HA-(poly(DEGMA-co-OEGMA)) ayant un DS de 3 pour faire les tests avec des cellules CD44+ et CD44- (cellules du cancer ovarien SKOV-3, surexprimant le récepteur CD44, et cellules de carcinome colique n'exprimant pas le CD44 à leur surface, respectivement). Les nanogels chargés en PTX ont montré une cytotoxicité plus élevée vis-à-vis de la lignée SKOV-3 par comparaison avec la lignée HCT-8/E11, mais

également avec le PTX seul et l'Abraxane® (nanoparticule de paclitaxel lié à de l'albumine sérique humaine). Ces résultats suggèrent que ces nanogels pourraient s'avérer être des candidats intéressants pour la libération thérapeutique dans le traitement de cancer.

4.2. Introduction

Cellular HA receptors CD44 and RHAMM are overexpressed in many types of cancer cell, demonstrating enhanced binding and internalization of HA[1,2]. Consequently, to increase the concentration of anticancer agent at the target site and decrease it elsewhere in the body, two platforms have been exploited so far: i) direct conjugation of cytotoxic drugs to low-molecular-mass HA, when HA itself functions as a carrier and a 'homing device'; and ii) physical incorporation of a drug within a nanoparticulate carrier to which HA is attached as a targeting coating.

In both cases, we talk about HA based architectures of submicrometer size, as only nanoobjects can circulate long enough in the blood vessels without elimination by the the reticuloendothelial system (RES), accumulate in tumor tissue by the enhanced permeability and retention (EPR) effect, and finally be internalized by cells through the endocytic pathway. The literature studies reported below demonstrate selective accumulation of the HA nanocarriers in tumor tissues likely due to the combination of the EPR effect and the HA targeting property. However, accumulation in the RES organs (liver and spleen) is also observed because HA molecules expose the nanocarriers to the HA receptors identified in these organs.

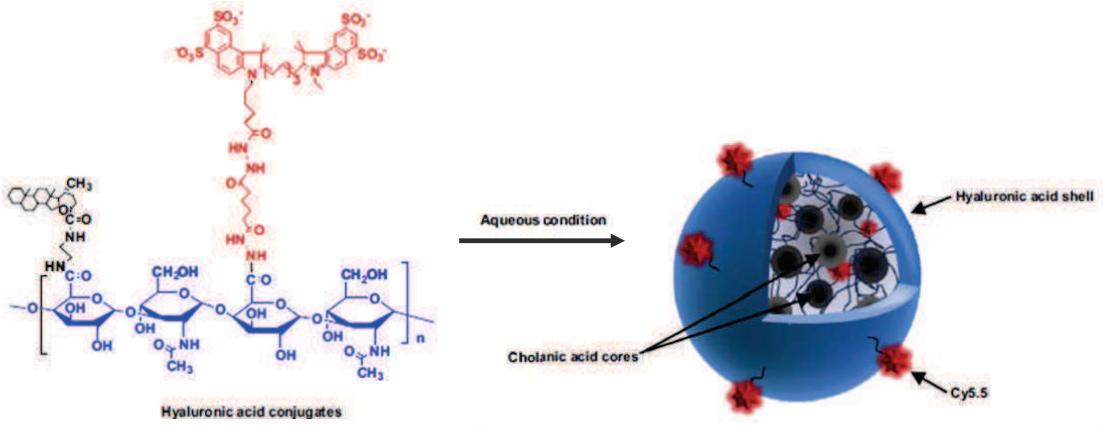

Figure 4. 1. Structure of Cy5.5-labeled hyaluronic acid nanoparticles in aqueous solution.[3]

Kim et al. investigated the in vivo biodistribution of amphiphilic hyalulronic acid-5β-cholanic acid (HA-CA) self-assembled conjugates labeled with near-infrared fluorescence dye cyanine 5.5 (Cy5.5) (**Figure 4.1**).[3,4] It was demonstrated that Cy5.5-labeled HA NPs (average diameter = 350-400 nm) are efficiently taken up by SCC7 cancer cells (squamous cell carcinoma cell) which overexpress CD44. When the NPs were systemically administrated into

the tail vein of tumor-bearing mice, most of the nanoparticles were found in tumor and liver sites (**Figure 4.2**). When comparing with pure HA polymer (Mw = 234400 g/mol), the fluorescence intensity of NPs at the tumor site was 4-fold higher which suggests that the preferentially accumulation of NPs in tumor tissues is due to a combination of passive targeting and active targeting mechanisms. For pure HA polymers, the fluorescence intensity quickly vanished in the body after injection, indicating fast clearance from the body.

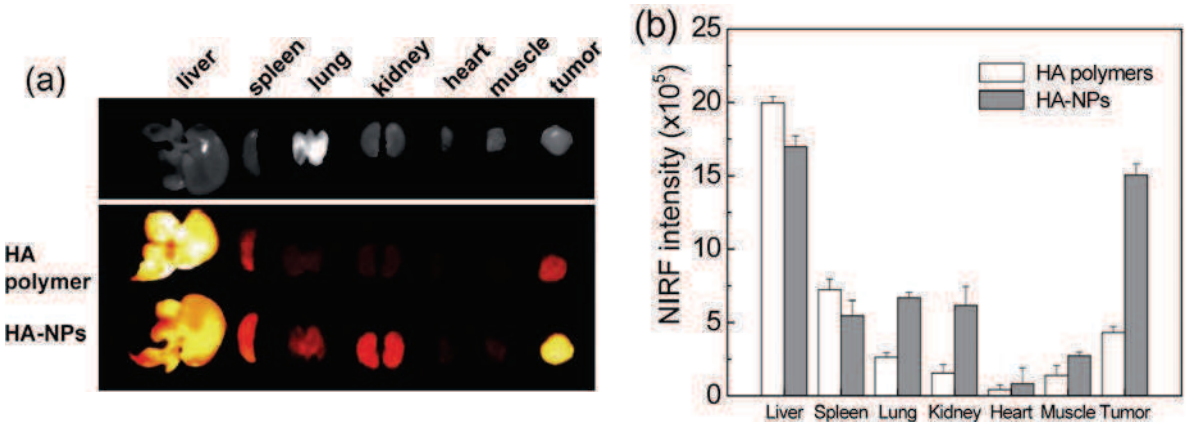

Figure 4. 2. (a) Near-infrared fluorescence (NIRF) images of dissected organs harvested from SCC7 tumor-bearing mice after 48 h post-injection. (b) Quantification of the ex vivo tumor targeting characteristics of HA-NPs in SCC7 tumor-bearing mice. All data represent mean ± SE (n = 3).[4]

Another example was reported by Yadav et al. [5] who synthesized doxorubicin (DOX)-loaded HA self-assembled NPs based on HA-poly(ethylene glycol)-b-polycaprolactone copolymer chains (HA-PEG-PCL).[5] In vivo tumor growth inhibition study was carried out in ehrlich ascites tumor (EAT) tumor-bearing mice model and compared with NPs made of methoxy poly(ethylene glycol)-b-polycaprolactone (MPEG-PCL)). The mean tumor volume of mice after 20 days of treatment with the DOX-loaded HA-PEG-PCL NPs (average diameter = 100-200 nm) was 3.2, 2.6, and 1.8 times lesser when compared with the mice treated with PBS buffer, plain DOX, and DOX-loaded MPEG-PCL NPs respectively (**Figure 4.3**). Significant higher accumulation at the tumor site and tumor growth inhibition by HA-PEG-PCL NPs was probably due to the combination of two mechanisms, i.e. selective uptake by EAT cells via receptor-mediated endocytosis and EPR effect. The receptor-mediated endocytosis was promoted by the HA moiety on the NPs, which was supposed to facilitate the recognition of NPs by EAT; after cell surface binding, the NPs might be internalized into the targeted cells. In order to evaluate the potential significance of the NPs uptake by various tissues, the biodistribution of these NPs was examined in mice. The percentage of distribution to tissue in different organs for the free drug and the drug encapsulated in NPs shown higher

concentration in tumor in comparison with the pure DOX and DOX-loaded MPEG-PCL NPs. But liver and kidney accumulation were observed in all cases (free DOX, DOX-loaded HA-PEG-PCL NPs and DOX-loaded MPEG-PCL NPs).

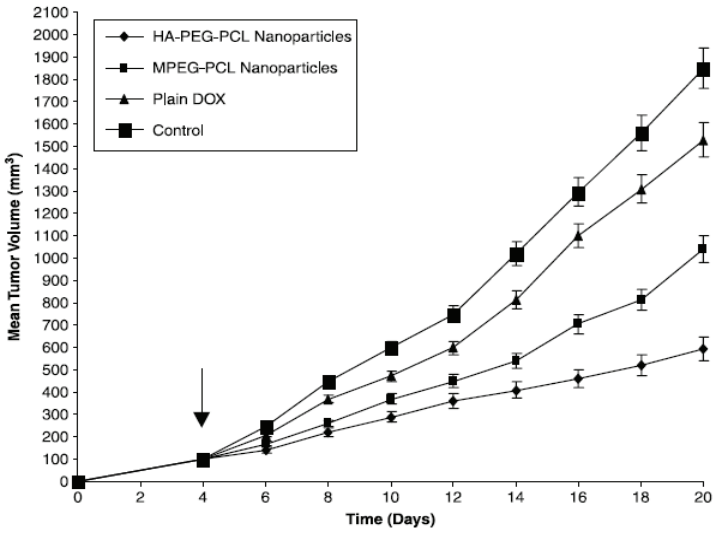

Figure 4. 3. In vivo tumor growth inhibition study of various formulations in EAT-bearing mice.[5]

These in vivo examples show the benefits of NPs based on HA for the treatment of tumors. Further investigations are also needed to avoid undesirable accumulation in the liver and the spleen if these organs are not the targets for the treatment. More sophisticated intelligent systems based on HA are still required to navigate bioactive molecules to the target organs/ tissues and cells. HA has a great potential to achieve this goal and combat tumor progression and metastasis.

In this chapter, we introduced a new class of nanogels based on hyaluronic acid which is able to encapsulate hydrophobic molecules in a simple process in aqueous solution. These nanogels were obtained by self-assembly of HA derivatives modified with a thermoresponsive copolymer. Different derivatives by varying the copolymer degree of substitution were synthesized. Their LCST, critical aggregation concentration and size were investigated. In order to evaluate the potential of the nanogels for the delivery of hydrophobic anti-cancer drugs and examine the role of HA in nanogels to cancer cells, we studied *in vitro* cell viability assay by using two types of cancer cells: human ovarian cancer cells (SKOV-3 cells which are positive for the CD44 receptor) and human colorectal cancer cells (HCT-8/E11 cells which are negative for the CD44 receptor). This work has been reported in Journal of Materials

Chemistry, B. In the complementary part, we present the differential scanning calorimetry results for different thermoresponsive HA derivatives.

4.3. Publication (J. Mater. Chem. B, DOI: C3TB20283F)

Tunable self-assembled nanogels composed of well-defined thermoresponsive hyaluronic acid - polymer conjugates

Jing Jing, David Alaimo, Elly De Vlieghere, Christine Jérôme, Olivier De Wever, Bruno G. De Geest, and Rachel Auzély-Velty

Controlled release technology is expected to have a profound impact in many biomedical fields including anti-cancer therapy.[6,7] Over the past decade, various self-assembled nanoparticulate carriers such as liposomes, polymeric micelles, and nanoparticles have been widely explored to improve the water solubility of chemotherapeutic agents, to reduce their cytotoxicity and to enhance their therapeutic effectiveness.[7,8] Among these nanomaterials, self-assembled gel nanoparticles (also called nanogels) made of hydrophobically modified biopolymers are particularly attractive for drug delivery.[9,10] Their size can be easily varied from one hundred to several hundred nanometers, their interior network comprising hydrophobic domains can be used to incorporate poorly water-soluble drugs and their hydrophilic shell can be exploited to control their biological fate and targeting ability. In this regard, several studies have focused on the use of hyaluronic acid (HA) for the design of anti-cancer drug carriers due to its interesting biological properties. Indeed, HA is a natural glycosaminoglycan, specifically recognized by the CD44 receptor that is over-expressed by several cancer cells including human breast epithelial cells[11] and human ovarian tumor cells[12]. In this context, self-assembled hydrogels nanoparticles based on the grafting of bulky hydrophobic groups (5β-cholanic acid,[13,14] pyrene,[15] poly(lactic-co(glycolic acid) (PLGA),[16] poly(ethylene glycol)- polycaprolactone[17]) on HA were developed for targeted delivery of hydrophobic anticancer drugs.

These nanoparticles showed enhanced tumor targeting ability and therapeutic efficacy, compared to the free anti-cancer agent. These important features make nanogel particles promising platforms for drug delivery with the possibility to introduce other functionalities to improve their performances. In particular, one of the limitations of these systems lies in the incorporation of drugs, which involves the use of organic solvents to solubilize the polymers, or high energy input (i.e. sonication or high shear homogenisation) with potential risk of contamination or degradation of the HA-conjugate.

In this paper we report on a novel mild and straightforward procedure for the encapsulation of hydrophobic molecules that circumvent the above mentioned issues. Our method relies on the temperature-triggered self-assembly of tunable thermosensitive HA derivatives. Such temperature-triggered approach allows solubilizing all components at room temperature, while drug loaded nanogel particles are spontaneously formed above a specific temperature (obviously below the physiological temperature of 37 °C), termed the lower critical solution temperature or LCST. Above this LCST, hydrophobic domains are formed that allow the accumulation of hydrophobic drugs.

The synthesis route for the thermosensitive HA derivatives described in this paper, is based on a combination of reversible addition-fragmentation chain transfer (RAFT) polymerization allowing to obtain well-defined thermosensitive polymers with tunable LCST and, thiol-click chemistry for their subsequent grafting on HA. The thermo-responsive properties of the HA-conjugates as well as the morphology and size of the obtained nanogels were investigated. Finally, these systems were screened in an in vitro setting for the delivery of the hydrophobic cancer drug paclitaxel to ovarian cancer cells that overexpress the CD44 receptor. We compared the cytotoxicity of PTX-loaded HA NPs with that of Abraxane, a commercially available and highly potent PTX nanoformulation that is clinically used in treatment of ovarian cancer,[18] to verify the potential of the nanogels in drug delivery.

Structures of the thermosensitive HA precursors, final HA-conjugates, HA-based nanogels and synthetic approach are shown in **Scheme 4.1**. The copolymer used for the modification of HA was prepared from diethyleneglycolmethacrylate (DEGMA) and oligoethyleneglycolmethacrylate (OEGMA). This copolymer belongs to a new class of thermoresponsive polymers which have emerged as a promising alternative to poly(*N*-isopropylacrylamide) due to their biocompatibility– similarly as common poly(ethyleneglycol) (i.e. PEG or PEO) – and their tunable LCST by varying the DEGMA to OEGMA monomer composition.[19,20] The copolymer, further denoted as poly(DEGMA-co-OEGMA) was synthesized in a 95:5 ratio of DEGMA to OEGMA by the RAFT polymerization method[21] using 2,2′-azobis(2-methylpropionitrile) (AIBN) as initiator and 4-cyano-4-(phenylcarbonothioylthio)pentanoic acid as chain transfer agent (CTA). The RAFT method offers the advantage of high end-group fidelity. Moreover, this end-group can easily

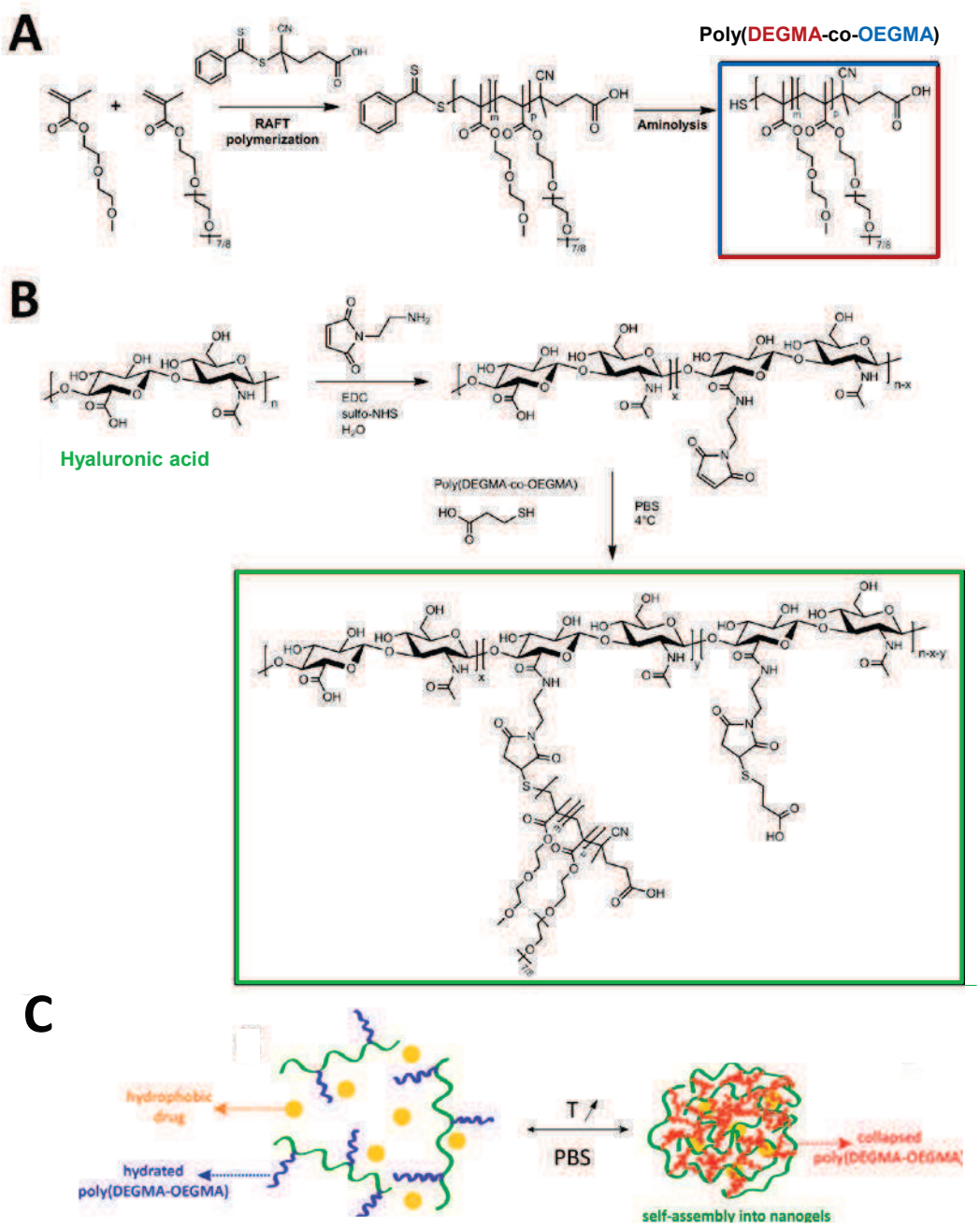

Scheme 4. 1. (A) Synthesis of poly(DEGMA-OEGMA) by the RAFT polymerization method. (B) Synthesis of thermosensitive HA conjugates by grafting poly(DEGMA-co-OEGMA) (blue chains) onto HA (green chains). (C) Schematic representation of temperature-triggered self-assembly (blue chains becoming red) of the HA-conjugates into nanogels that allow accumulation of hydrophobic compounds (yellow discs).

be converted to a thiol that can then be readily conjugated to maleimides via Michael addition to construct complex structures.[22] Experimental details are listed in Supporting Information. A good correlation between the targeted degree of polymerization (DP) and the experimental molecular weight determined via size exclusion chromatography (SEC) as well as the narrow

polydispersity (i.e. PDI ~ 1.1) indicates excellent control over the RAFT polymerization. The LCST in water of poly(DEGMA-co-OEGMA) (1 g/L) was determined by measuring the turbidity as a function of the temperature and was found to be 32 °C, which is in accordance to the values reported in literature.[19] Subsequently, poly(DEGMA-co-OEGMA) was grafted onto HA (M_w = 200000 g/mol). Therefore, 10% of the HA carboxylic acid groups were first modified with aminoethylmaleimide (AEM) via carbodiimide mediated amide-coupling. After purification, the resulting HA-AEM was reacted with poly(DEGMA-co-OEGMA) on which the RAFT end-group was converted to a thiol by aminolysis using *n*-butylamine. By varying the poly(DEGMA-co-OEGMA) to HA-AEM ratio, HA-poly(DEGMA-co-OEGMA) conjugates with different degree of substitution (DS; defined as the number of poly(DEGMA-OEGMA) chains per 100 disaccharide repeating units) were synthesized. After 12 h reaction, an excess of mercaptopropionic acid (MPA) was added to convert the remaining maleimide units to a carboxylic acid. The conjugates were subsequently purified via dialysis and their structural integrity was ascertained using ^{1}H NMR analysis (**Figure SI 4.6** in Supporting Information). This revealed a DS of 3, 4 and 6 for the respective conjugates, which corresponds to approximately 60 % of the targeted DS. Successful grafting was further confirmed by FT-IR spectroscopy (**Figure SI 4.7** in Supporting Information). In the IR spectra of the HA conjugates, a significant change in the relative intensities of the band at 1720 cm^{-1} corresponding to the carbonyl stretching of the methacrylate comonomer units and of the band at 1602 cm^{-1} attributed to the asymmetric carbonyl stretch from the carboxylate group of HA can be observed with an increasing degree of substitution.

The thermo-responsive properties of the HA-poly(DEGMA-co-OEGMA) conjugates are shown in **Figure 4.4.A**. The LCST values of the respective HA-poly(DEGMA-co-OEGMA) conjugates, as determined via turbidity measurements, were all situated around 35 °C, independent on the degree of substitution of the conjugates. Dynamic light scattering performed at 40 °C revealed a monomodal distribution of the hydrodynamic radius (R_h) of the temperature-induced assemblies (**Figure 4.4.C**). These data demonstrate that poly(DEGMA-co-OEGMA) modified HA is able to assemble into nanogel structures by a temperature-induced mechanism. This was additionally supported by comparing the two-dimensional ^{1}H-^{13}C HSQC NMR spectra of HA-poly(DEGMA-co-OEGMA) recorded at different temperatures (**Figure SI 4.8** in Supporting Information). A drastic decrease of the intensity of

the proton signals of the grafted copolymer could be observed by heating the samples from 25 to 40 °C.

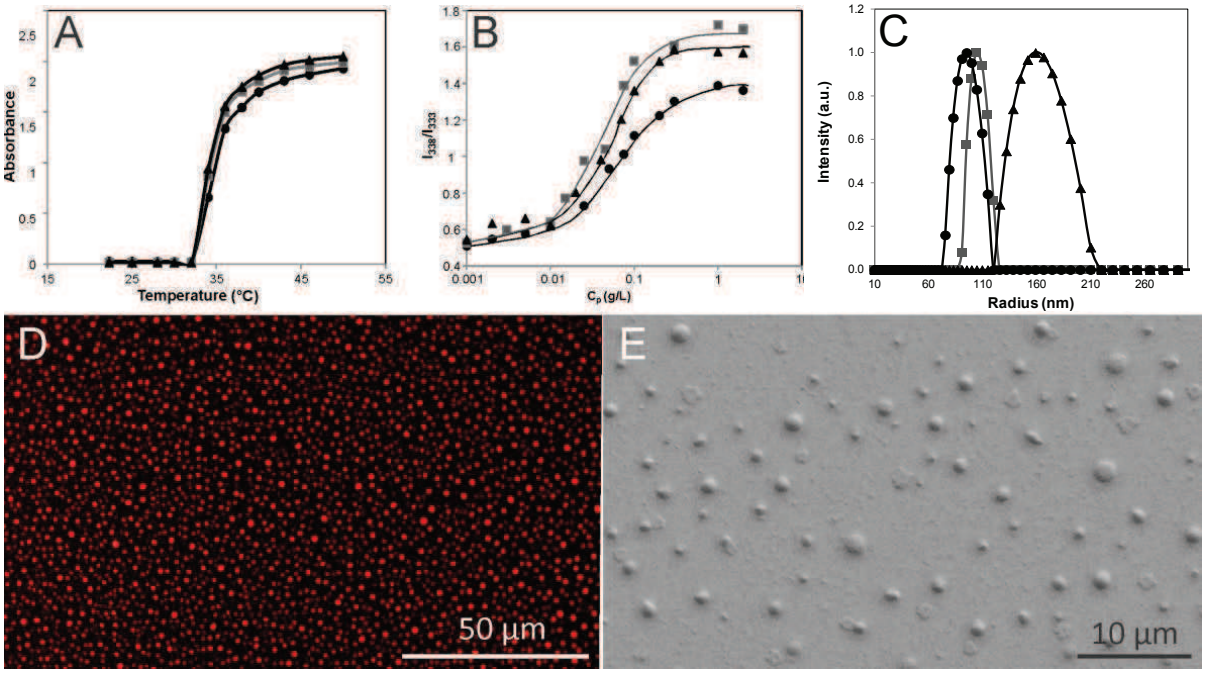

Figure 4.4. Temperature-responsive behavior of the HA-poly(DEGMA-co-OEGMA) conjugates in PBS (pH 7.4 and 0.15 M NaCl). (A) Transmittance plots as a function of temperature for HA-poly(DEGMA-co-OEGMA) with a DS of respectively 3 (●), 4 (■) and 6 (▲) at a concentration C_p = 5 g/L. (B) Intensity ratios (I_{338}/I_{333}) calculated from pyrene excitation spectra for HA-poly(DEGMA-co-OEGMA) with a DS of respectively 3 (●), 4 (■) and 6 (▲). (C) DLS size distribution of HA-poly(DEGMA-co-OEGMA) nanogels at 40 °C (C_p = 0.5 g/L). The average R_h values are 95 nm (DS 3), 105 nm (DS 4) and 159 nm (DS 6). (D) Fluorescence microscopy image at 40 °C of HA-poly(DEGMA-co-OEGMA) nanogels (DS 3) loaded with Nile Red (C_p = 2 g/L). (E) Scanning electron microscopy image of HA-poly(DEGMA-co-OEGMA) nanogels (C_p = 2 g/L; DS 4).

In contrast, the HA proton signals which were masked by the copolymer proton signals at 25 °C became clearly visible at 40°C, thereby allowing assignment of the protons/carbons of the HA backbone. Interestingly, the R_h was found to vary between 95 and 159 nm, depending on the DS of the HA-poly(DEGMA-co-OEGMA) conjugates, with a higher DS leading to higher R_h. This is in contrast to structures assembled from HA modified with bulky hydrophobic groups (such as e.g. 5β-cholanic acid).[13] Indeed, the type of assembly formed by hydrophobically modified polyelectrolytes (such as HA) is reported to strongly depend on whether inter- or intra-chain hydrophobic association occurs.[23] Polyelectrolytes with bulky hydrophobic groups and/or a high degree of substitution exhibit a strong tendency towards intra-molecular association, resulting in single-molecule assemblies.

The HA-poly(DEGMA-co-OEGMA) conjugates reported in the present paper have long temperature-sensitive pending moieties that are likely to entangle with each other when surpassing the LCST, forming both intra- and inter-chain entanglements. Therefore, we speculate that with increasing DS, the extend of inter-chain binding increases, leading to increase in size of the formed nanogels. Here we have deliberately chosen to use a low DS to obtain nanogels which are predominantly composed of HA, as we aim to exploit further on the CD44-receptor binding properties of HA. Additionally, when attempting to graft an elevated amount of poly(DEGMA-co-OEGMA), phase-separation between poly(DEGMA-co-OEGMA) and HA in the reaction mixture is likely to occur.

Importantly, these nanogels are stable over time (when kept above the LCST) and do not further aggregate. Additionally, nanogel formation was found to be reversible as the solutions turned clear upon cooling and became turbid upon re-heating. The critical aggregation concentration (CAC) of the HA-poly(DEGMA-co-OEGMA) conjugates was determined by fluorescence spectroscopy using pyrene as fluorescent probe.[24] Pyrene was simply added as concentrated ethanolic solution to the respective HA-poly(DEGMA-co-OEGMA) solutions. **Figure 4.4.B** shows the ratio of the fluorescence intensity emitted at λ=338 nm and λ=333nm. These curves were recorded, in phosphate buffered saline (i.e. pH 7.4 and 0.15 M NaCl) at 37 °C, thus reflecting physiologically relevant conditions. The CAC was estimated from the threshold concentration (as shown in **Figure SI 4.9** in Supporting Information) that yielded self-assembled nanogels and yielded values of 0.02 g/L for HA-poly(DEGMA-co-OEGMA) conjugates with a DS of respectively 3, and 0.01 g/L for a DS of 4 and 6. The slight decrease in CAC with increasing DS, might contribute to the hypothesis that a higher DS of pending poly(DEGMA-co-OEGMA) moieties facilitates the formation of inter-chain entanglements.

The formed nanogels were visualized by adding Nile Red (as concentrated ethanolic solution) to a solution of HA-poly(DEGMA-co-OEGMA) followed by imaging on a fluorescence microscope equipped with a controlled heating stage set at 40 °C. Nile Red exhibits a dramatic increase in fluorescence intensity when it is accommodated in a hydrophobic environment compared to a hydrophilic environment.[25] As shown in **Figure 4.4.D**, spherically shaped particles are formed that exhibit strong fluorescence. These findings demonstrate that the HA-poly(DEGMA-co-OEGMA) nanogels can encapsulate hydrophobic molecules in the hydrophobic domains that are formed above the LCST of the HA-poly(DEGMA-co-OEGMA) conjugates. Further proof of the formation of solid nanogels was

obtained from scanning electron (SEM) analysis by drying at 45 °C a heated (also at 45 °C) droplet of HA-poly(DEGMA-co-OEGMA) in pure water (to avoid recrystalization of PBS salts) onto mica, followed by SEM imaging. **Figure 4.4.E** shows the formation of slightly deflated spherical particles. Control experiments with non-modified HA that was deposited onto mica under identical conditions as the nanogels did not show the formation of particles (**Figure SI 4.10** in Supporting Information).

In the last part in this work, we evaluated the potential of the nanogels for the delivery of hydrophobic anti-cancer drugs. As these nanogels are based on HA, which binds to the CD44 receptor, they hold potential for targeted delivery to ovarian cancer cells that often overexpress this receptor. First we incubated human ovarian cancer cells (SKOV-3 cells; these are positive for the CD44 receptor as confirmed by Western blotting (**Figure SI 4.11** in Supporting Information) with Nile Red loaded nanogels at 37 °C, to assure the HA-poly(DEGMA-co-OEGMA) conjugates to be in the self-assembled nanogel state. For these biological experiments we have chosen HA-poly(DEGMA-co-OEGMA) conjugates with a DS of 3 as these yielded the smallest particles which would favor their cellular internalization. As shown by fluorescence microscopy (**Figure 4.5.A**), the Nile Red payload is being internalized by the SKOV-3 cells.

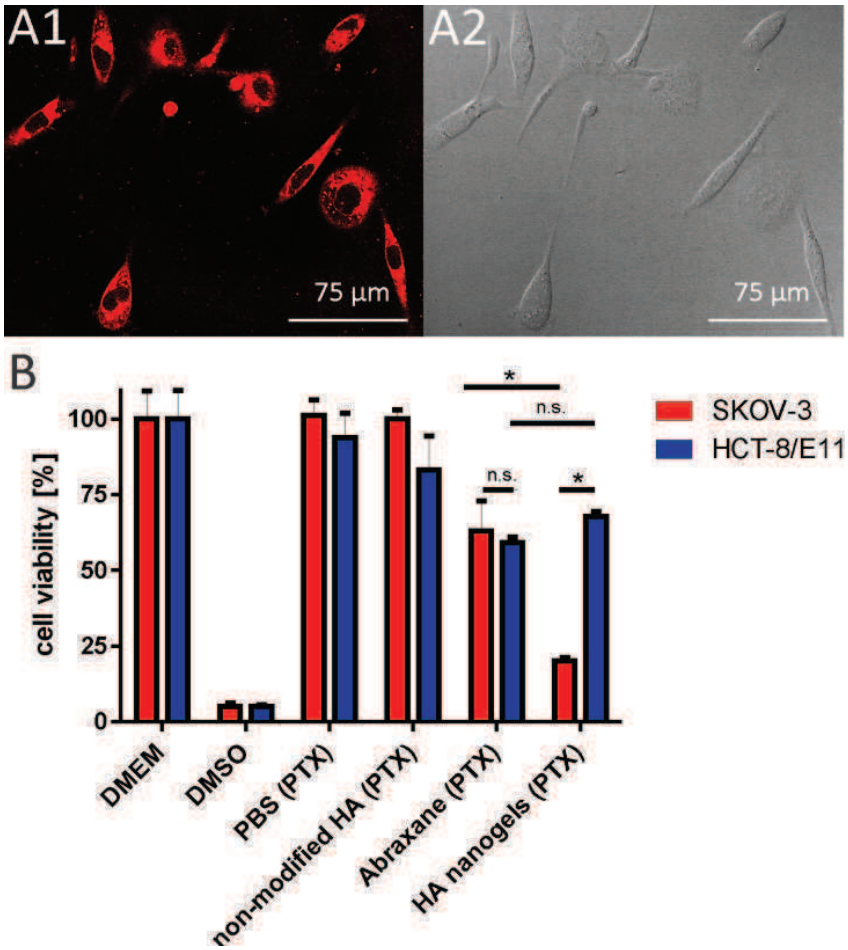

Figure 4.5. (A) Confocal microscopy images of human ovarian cancer cells (SKOV-3) incubated with Nile Red loaded HA-poly(DEGMA-co-OEGMA) (DS 3) nanogels. The panel A1 depicts the red fluorescence channel and the panel A2 depicts the DIC channel. (B) Cell viability of SKOV-3 and HCT/8E-11 cells treated with controls and the respective PTX formulations. (n=5; *: $p<0.001$; n.s.: not statistically significant)

Secondly, we loaded the HA-poly(DEGMA-co-OEGMA) nanogels with paclitaxel in identical fashion as we did for pyrene and Nile Red earlier in this paper, i.e. by simply adding a concentrated methanolic solution of PTX to a HA-poly(DEGMA-co-OEGMA) solution at room temperature followed by increasing the temperature to 37 °C. We opted for a PTX concentration of 30 µM in the HA-poly(DEGMA-co-OEGMA) stock solutions, resulting in an effective PTX concentration of 25 µM in the HA-poly(DEGMA-co-OEGMA) nanogels (Entrapment efficiency = 80 %, see Supporting Information). Next we evaluated whether formulating PTX in HA-poly(DEGMA-co-OEGMA) nanogels enhances the potency of PTX as well as providing a higher selectivity towards CD44 positive cells. Therefore in a first

series of preliminary experiments we used Abraxane to determine the optimal concentration range of PTX to eradicate SKOV-3 cells in an *in vitro* setting.

These experiments indicated that Abraxane treatment of SKOV-3 cells for 2.5 h followed by replacement of the medium and one week culturing and finally MTT analysis of the cell viability, induced a 40% reduction of the cell viability for a PTX concentration of 0.1 µg/mL (**Figure 4.5.B**). Subsequently, we treated SKOV-3 cells with PTX loaded HA-poly(DEGMA-co-OEGMA) nanogels at a PTX concentration of 0.1 µg/mL. As controls we took PTX in PBS, PTX in PBS mixed with native – non-modified – HA and Abraxane. Note that for these experiments always identical concentrations of PTX were used. Pure culture medium (DMEM) and DMSO were used as respectively negative and positive control. Furthermore, besides SKOV-3 cells, that overexpress the CD44-receptor, we also used HCT-8/E11 cells that do not overexpress the CD44 receptor (as verified by Western blotting (**Figure SI 4.11** in Supporting Information). As shown in **Figure 4.5.B**, encapsulation of PTX in HA-poly(DEGMA-co-OEGMA) nanogels strongly enhances the potency of PTX compared to PTX in PBS or PTX mixed with native HA. Firstly, PTX loaded HA-poly(DEGMA-co-OEGMA) nanogels are even more potent than Abraxane. Secondly, when comparing the effect of PTX treatment on SKOV-3 and HCT-8/E11 cells a reduction of potency of the PTX loaded HA-poly(DEGMA-OEGMA) nanogels is observed while the potency of Abraxane treatment is similar for both cell lines. **Figure SI 4.12** in Supporting Information shows cell viability data recorded for PTX concentrations of 0.1 µg/ml and 0.2 µg/ml, respectively, demonstrating that the same extend of SKOV-3 cell eradication, requires a two-fold increase of PTX concentration formulated as Abraxane, relative to PTX loaded in HA-poly(DEGMA-co-OEGMA) nanogels. Taken together, these findings suggest that formulating PTX in the thermosensitive HA-nanogels allows significant dose sparing which is highly important in reducing cytotoxic side-effect to healthy tissues.

Summarizing, we have shown for the first time that grafting thermosensitive polymers onto hyaluronic acid allows temperature-triggered assembly into nanogels, with the particle size depending on the degree of substitution. Hydrophobic molecules (dyes and drugs) could be loaded into these nanogels by simple mixing. Nanogel-mediated delivery of the hydrophobic anti-cancer drug paclitaxel showed enhanced potency and selectivity in the eradication of CD44 positive human ovarian cancer cells *in vitro*. These results suggest that these nanogel carriers hold great potential for the delivery of chemotherapeutics in anti-cancer therapy.

Future work will focus on in vivo delivery of PTX loaded nanogels to xenografted ovarian tumours.

4.4. Supporting information

Materials

The sample of bacterial sodium hyaluronate (HA) with a weight-average molecular weight of 200 kg/mol was supplied by ARD (Pomacle, France). The molecular weight distribution and the weight-average molecular weight of this HA sample were determined by size exclusion chromatography using a Waters GPC Alliance chromatograph (USA) equipped with a differential refractometer and a light scattering detector (MALLS) from Wyatt (USA); the solution was injected at a concentration of 5×10^{-4} g/mL in 0.1 M $NaNO_3$. The polydispersity index (PDI) of the sample is $M_w/M_n \sim 1.5$. 4-Cyano-4-(phenylcarbonothioylthio)pentanoic acid, di(ethylene glycol) methyl ether methacrylate (DEGMA), oligo(ethylene glycol) methyl ether methacrylate (OEGMA, M_n = 475 g mol^{-1}), 2,2′-azobis(2-methylpropionitrile) (AIBN), *N*-(2-aminoethyl)maleimide trifluoroacetate salt (AEM), 3-mercaptopropionic acid (MPA) and, all other chemicals were purchased from Sigma-Aldrich-Fluka and were used without further purification. The water used in all experiments was purified by a Elga Purelab purification system, with a resistivity of 18.2 MΩ cm.

Methods

^1H NMR spectra were recorded on a Bruker spectrometer operating at 400 MHz with deuterium oxide (D_2O) or deuterated chloroform ($CDCl_3$) (SDS, Vitry, France) as a solvent.

Two-dimensional HSQC experiments were acquired using 2K data points and 256 time increments. The phase sensitive (TPPI) sequence was used and processing resulted in a 1K×1K (real-real) matrix. Chemical shifts are given relative to external tetramethylsilane (TMS = 0 ppm) and calibration was performed using the signal of the residual protons or carbons of the solvent as a secondary reference. Fourier transform infrared spectroscopy (FT-IR) measurements were performed on a RX1 spectrometer (Perkin Elmer, UK) with horizontal ATR accessory. For each sample, 32 scans were recorded between 4000 and 400 cm^{-1} with a resolution of 2 cm^{-1} using Spectrum software V 5.0.0. The spectrum analysis was performed by using Origin 7.0 software.

The molecular weight and polydispersity index of the block copolymer was measured by size-exclusion chromatography (tetrahydrofuran, flow rate: 1 mL/min) at 40 °C with a Waters 600 liquid chromatrograph equipped with a differential refractometer and a light scattering detector (MALLS) from Wyatt.

The transmittance of the polymer solutions at 500 nm was measured on a Varian Cary 50 UV/Vis Spectrophotometer equipped with a temperature controller.

Pyrene emission spectra were measured on a Perkin Elmer luminescence LS 50B spectrometer between 360 and 500 nm. Pyrene solubilized in ethanol was added up to a concentration of 10^{-7} M in the polymer solution and excited at 334 nm. The I_1/I_3 ratio of the intensities of the first and the third peaks of fluorescence spectrum of pyrene was used to study the formation of hydrophobic domains resulting from the association of the copolymer chains.

Dynamic light scattering (DLS) experiments were carried out using an ALV laser goniometer, which consists of a 22 mW HeNe linear polarized laser operating at a wavelength of 632.8 nm, an ALV-5000/EPP multiple τ digital correlator with 125 ns initial sampling time, and a temperature controller. The accessible scattering angles range from 50 to 140°. The aqueous solutions of the HA-poly(DEGMA-co-OEGMA) conjugates (0.5 g/L in PBS) were filtered directly into the glass cells through 0.22 μm MILLIPORE Millex LCR filter. Data were collected using digital ALV Correlator Control software and the counting time for measuring the elastic or the quasi-elastic scattering intensities varied for each sample from 180 to 300 s. The relaxation time distributions, $A(t)$, were in the sequence obtained using CONTIN analysis of the autocorrelation function, $C(q,t)$. Diffusion coefficients D were calculated from following equation:

$$\frac{\Gamma}{q^2}\Big|_{q\to 0} = D \qquad (1)$$

where Γ is relaxation frequency ($\Gamma = \tau^{-1}$), and q is the wave vector defined as following equation:

$$q = \frac{4\pi n}{\lambda}\sin\left(\frac{\theta}{2}\right) \qquad (2)$$

where λ is the wavelength of the incident laser beam (632.8 nm), θ is the scattering angle, and n is the refractive index of the media. Consequently, the hydrodynamic radius (R_h) was calculated from the Stokes-Einstein relation as follows:

$$R_h = \frac{k_B T}{6\pi\eta\Gamma} q^2 = \frac{k_B T}{6\pi\eta D} \qquad (3)$$

where k_B is the Boltzmann constant, T is the temperature, and η is the viscosity of the medium.

Confocal Laser Scanning Fluorescence Microscopy (CLSM) was performed on a Leica SP5 confocal microscope equipped with a 63x oil immersion objective.

Synthesis of Poly(DEGMA-co-OEGMA)

A mixture of 4-cyano-4-(phenylcarbonothioylthio)pentanoic acid (0.114 g, 0.4066 mmol), DEGMA (8 g, 42.50 mmol), OEGMA (1.06 g, 2.23 mmol) and AIBN (0.004 g, 0.024 mmol) was dissolved in toluene (20 mL) and N_2 gas was purged for 30 min to the solution. The reaction vessel was sealed and then put into a pre-heated oil bath at 80 °C for 21 h 30. The resulting mixture was precipitated in cold diethyl ether (200 mL) to give the random copolymer as a waxy liquid in 82 % yield (6.56 g). SEC (THF) M_n: 16900 g/mol. PDI: 1.1. ^{1}H NMR (400 MHz, $CDCl_3$) δ (ppm) : 7.47, 7.38 (H of aromatic ring), 4.11 (CH_2OCO), 3.69-3.57 (CH_2O), 3.40 (CH_3O), 1.92-1.63 (CH_2), 1.26-0.88 (CH_3).

Synthesis of HA-poly(DEGMA-co-OEGMA)

The first step consisted in the aminolysis reaction of poly(DEGMA-co-OEGMA) with *n*-butylamine, which leads to thiol-capped copolymer chains. Thus, the copolymer (1 g) was introduced in a flask placed under a nitrogen atmosphere. CH_2Cl_2 (10 mL) was added, and after complete dissolution of the polymer, *n*-butylamine (10 mL, 0.1 mol) was added to the solution. The reaction mixture was stirred for 10 min at room temperature. During this period, the originally pink solution became pale yellow. A waxy liquid (0.80 g) was recovered by precipitation in diethyl ether. The thiol-capped copolymer was then reacted with HA-AEM (DS = 10). This derivative was prepared by dissolving HA (0.60 g, 1.49 mmol) in pure water to a concentration of 6 g/L. *N*-(2-Aminoethyl)maleimide trifluoroacetate salt (0.285 g, 1.12 mmol) and *N*-hydroxysulfosuccinimide sodium salt (0.162 g, 0.75 mmol) were added to this solution. The pH of the reaction medium was then adjusted to 4.75. Next, an aqueous solution of *N*-(3-dimethylaminopropyl)-*N*′-ethylcarbodiimide hydrochloride (0.054 g, 0.28 mmol) was added slowly to the mixture. The pH of the reaction medium was maintained at 4.75 by addition of 0.5 M HCl. The reaction was allowed to proceed at room temperature until no further change in pH was observed (i.e. 4 hours). The modified HA was purified by

diafiltration through a membrane Amicon YM 30. The diafiltration was stopped when the filtrate conductivity was lower than 10 µS. Next, the solution of the HA-AEM derivative was diluted with pure water to obtain a final volume of 360 mL, and divided into portions of 60 mL (i.e. into portions of 0.1 g of HA-AEM). After addition of a 10-fold concentrated solution of PBS (6.6 mL) to one of the portions, poly(DEGMA-co-OEGMA) (0.412 g, 0.024 mmol) was added and the mixture was stirred at 4 °C (pH 7.4) for 12 h. After addition of MPA (21 µL, 0.24 mmol) and stirring again at 4 °C for 6 h, the HA-poly(DEGMA-co-OEGMA) was purified by diafiltration through a membrane Amicon YM 30. The product was then recovered by freeze-drying as a white powder in (0.340 g) with a DS in copolymer chains of 6 from ^{1}H NMR integration.

The synthesis of the other poly(DEGMA-co-OEGMA) samples with DS=3 and 4 was performed using a similar procedure, with different amounts of the copolymer, i.e. 0.206 and 0.288 g, respectively, per HA-AEM portion.

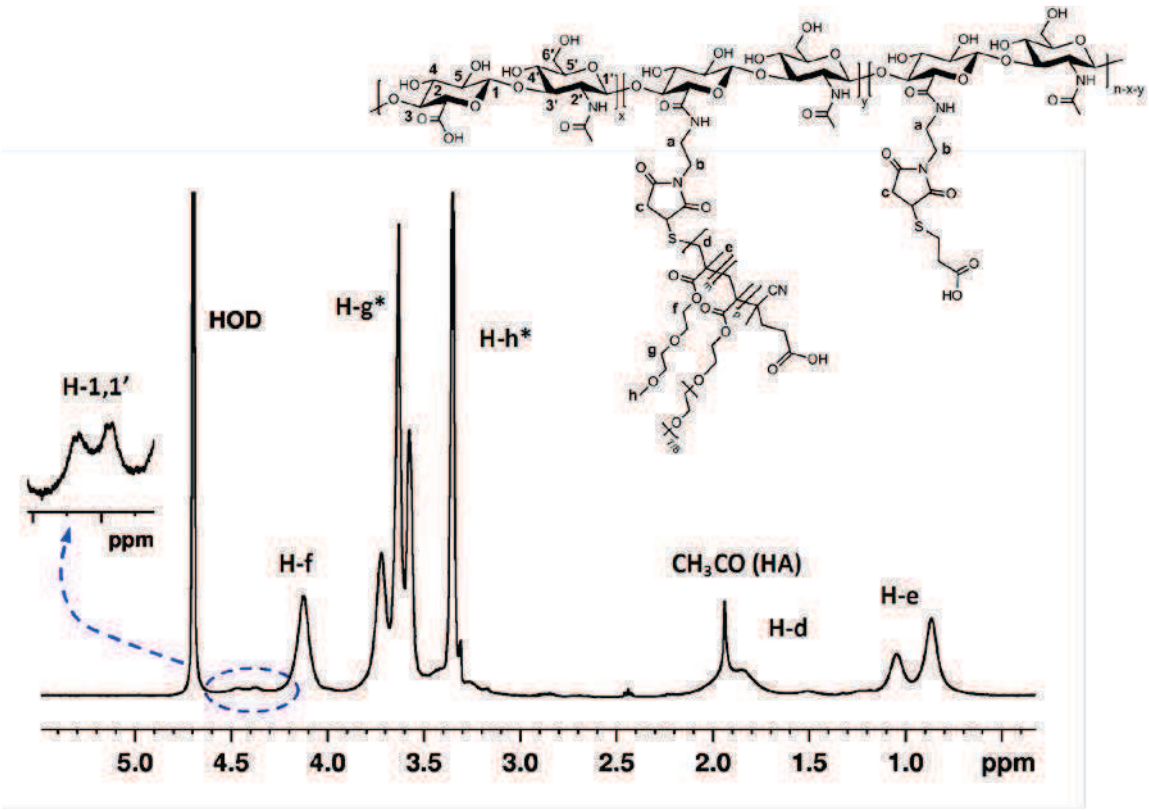

Figure SI 4. 6. ^{1}H NMR spectrum (400 MHz, 6 mg/mL in D_2O, 25 °C) of HA-poly(DEGMA-co-OEGMA), DS = 6. *These signals mask the H-2, H-2', H-3, H-3', H-4, H-4', H-5, H-5' and H-6 proton signals of HA.

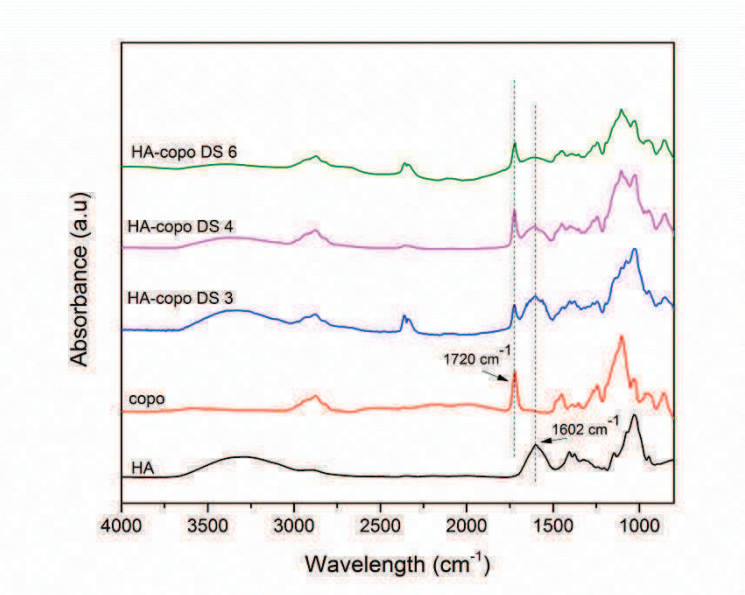

Figure SI 4.7. FT-IR spectra of initial HA, poly(DEGMA-co-OEGMA) and of the HA-copolymer with DS = 3, 4 and 6.

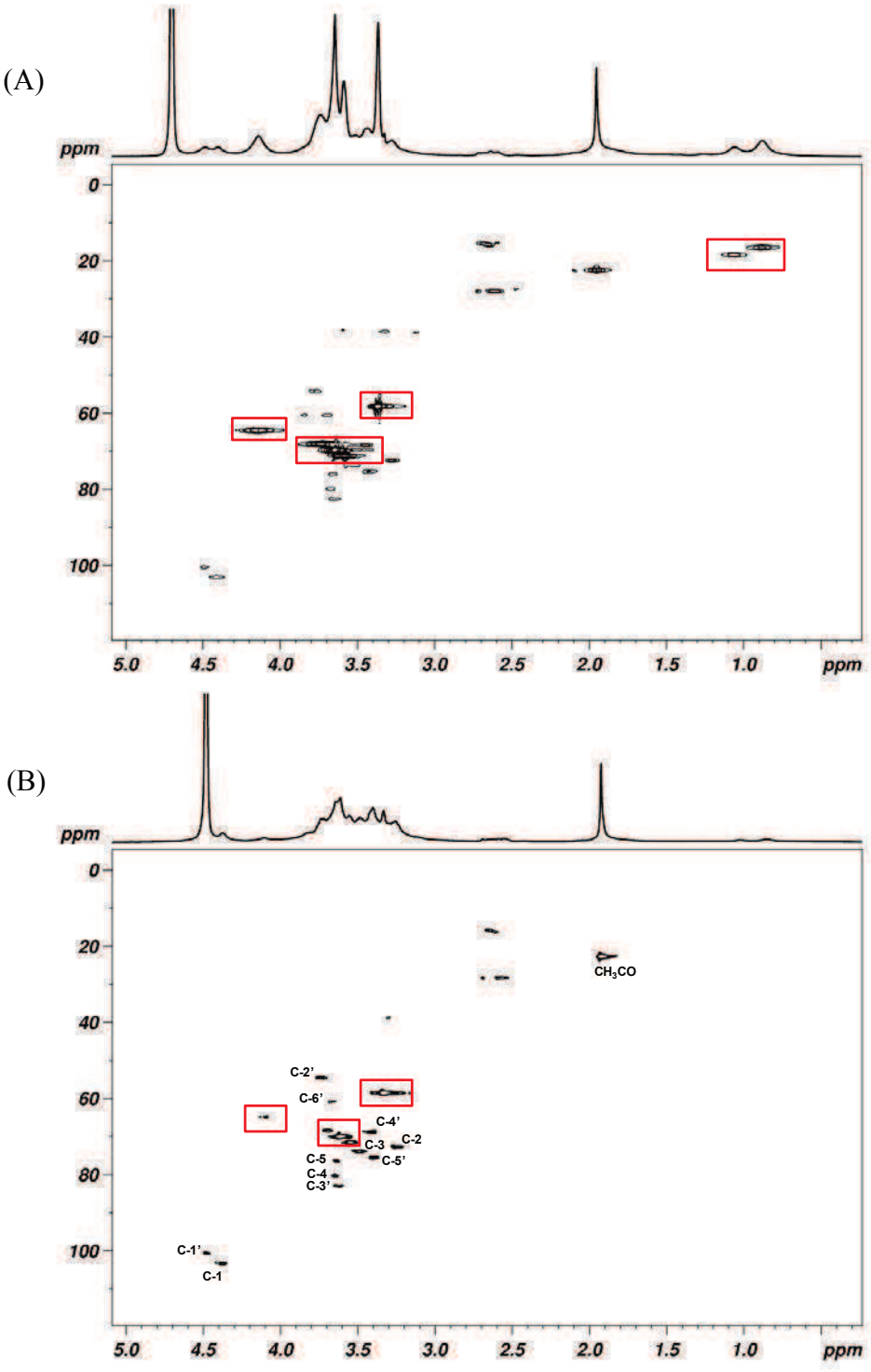

Figure SI 4.8. 1D ^{1}H NMR and 2D ^{1}H-^{13}C HSQC NMR spectra (400/100 MHz, 20 mg/mL in D_2O) of HA-poly(DEGMA-co-OEGMA) with DS = 3 at 25 °C (A) and 40 °C (B). The HA protons located in the δ 3.1-3.6 ppm region, which were masked by the copolymer proton signals in the 1D spectrum at 25 °C, became clearly visible at 40°C due to the decrease of the proton signals of the copolymer. The assignment of the carbon signals of HA is given in spectrum B and the cross-peaks corresponding to the copolymers are marked in red.

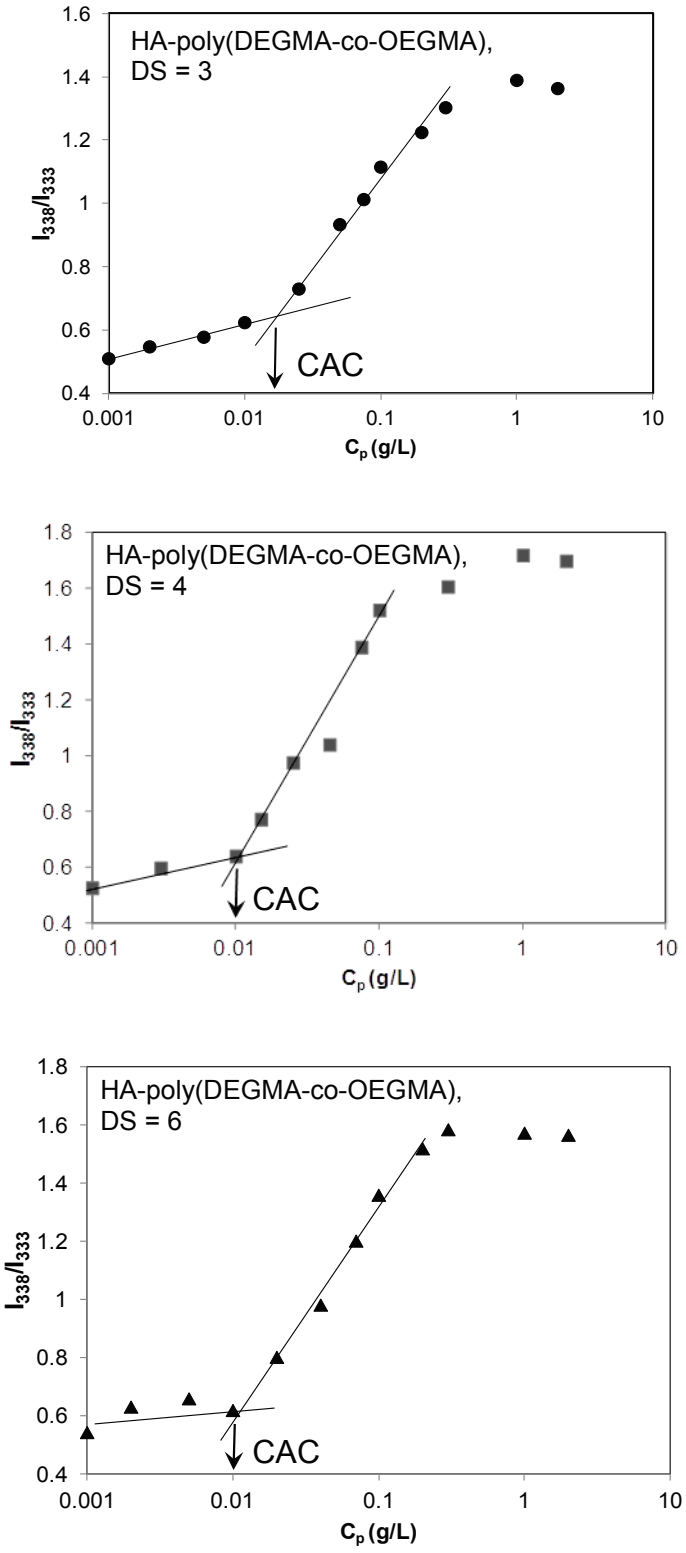

Figure SI 4. 9. Plots of the intensity ratios of I_{338}/I_{333} for three different HA-poly(DEGMA-co-OEGMA) from pyrene excitation spectra as a function of concentration.

Scanning electron microscopy observation of nanogels.

Drops of solutions in pure water of respectively poly(DEGMA-co-OEGMA) modified HA and non-modified HA, pre-heated at 45 °C were deposited onto mica-coated copper stubs (also pre-heated at 45 °C) and allowed to air drying at 45 °C. The samples were coated by 2 nm of electron beam evaporation carbon and observed in secondary electron imaging mode with a Zeiss ultra 55 FEG-SEM (CMTC-INPG, Grenoble) at an accelerating voltage of 3 kV, using an in-lens detector.

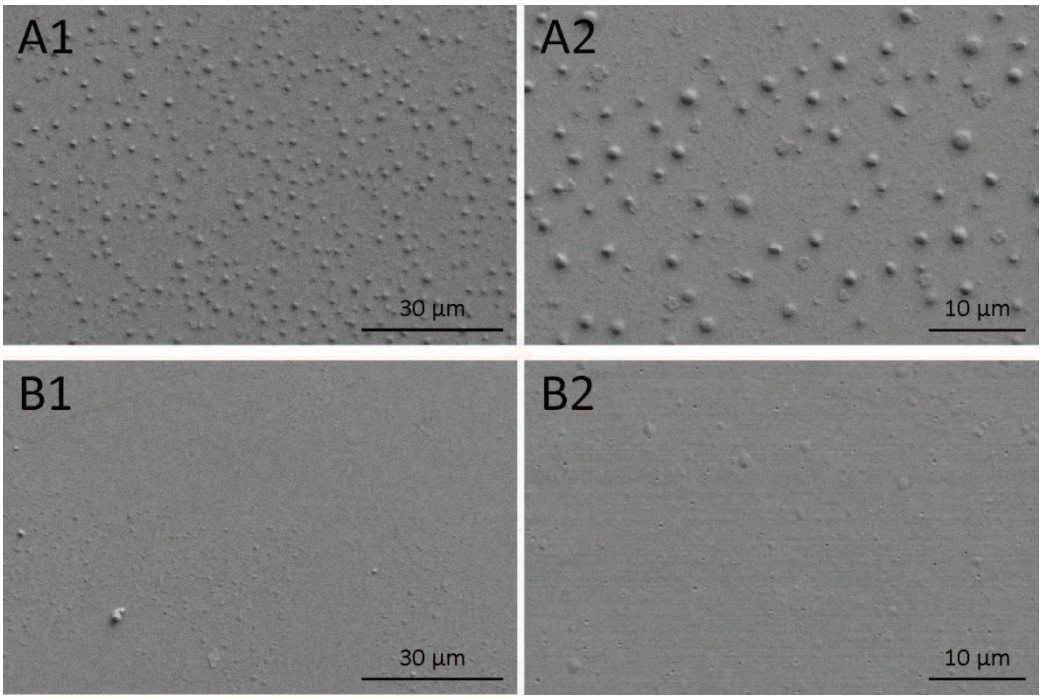

Figure SI 4. 10. Scanning electron microscopy images of (A) poly(DEGMA-co-OEGMA) modified HA (DS 4) and (B) non-modified HA.

Encapsulation of hydrophobic molecules in thermosensitive HA Nanogels.

To a solution (0.5 mL) of HA-poly(DEGMA-co-OEGMA) (DS = 3) at 2 g/L at room temperature, a solution of Nile Red in ethanol (1 mg/mL or 3.14 mM) was added to obtain a NR concentration of 10 µM. The mixture was stirred in a water bath at 40 °C and ethanol was allowed to evaporate slowly under a stream of nitrogen.

To solutions (0.5 mL) of HA-poly(DEGMA-co-OEGMA) (DS = 3) at 2 g/L at room temperature, a solution of paclitaxel in methanol (1 mg/mL or 1.17 mM) was added to obtain PTX concentrations of 80, 60, 30 and 20 µM. The mixtures were stirred in a water bath at 40 °C and methanol was allowed to evaporate slowly under a stream of nitrogen. The solutions containing PTX at 30 and 20 µM remained clear whereas that containing PTX at 60 and 80

μM contained small particles in dispersion. *In vitro* cell experiments were thus conducted using the 30 μM sample for which the entrapment efficiency (EE) was found to be 80 %. It was determined by centrifugation (10000 rpm for 10 min) to remove non-encapsulated PTX and quantification by high-performance liquid chromatography (HPLC) of PTX loaded in the nanogels. To this end, PTX was extracted from the nanogels with acetonitrile. Isocratic reverse-phase HPLC was performed using a Nucleodur C18 column at 25 °C. The mobile phase consisted of acetonitrile/water (45:55, v/v) with a flow rate of 0.9 mL/min. The signals were recorded by UV detector at 227 nm. A calibration line was conducted to determine the PTX concentration in the range of 0.1–40 μM, and the r^2-value of peak area against PTX concentration was at least 0.999.

The encapsulation efficiency was calculated based on the following equation :

$$EE\ (\%) = \text{weight of PTX in nanogels/weight of the feeding PTX} \times 100\%$$

***In vitro* cell culture assays.**

Cell lines. Human colorectal cancer cell line HCT-8/E11,(Vermeulen, S.J.; Bruyneel, E.A.; Bracke, M.E.; Debruyne, G.K.; Vennekens, K.M.; Vleminckx, K.L.; Berx, G.J.; Vanroy, F.M.; Mareel, M.M. *Cancer Research* 1995, **55**, 4722-4728) and human ovarium cancer cell line SKOV-3 (ATCC, Manassas, VA) were maintained in DMEM (Invitrogen, Carlsbad, CA) supplemented with 10% FBS and antibiotics.

Protein analysis. For Western blot analysis cell lines were harvested in Laemmli lysis buffer. Cell lysates (25 μg) were suspended in reducing sample buffer and boiled for 5 minutes at 95 °C. Samples were run on 8% SDS-PAGE, transferred to PVDF membranes, blocked in 5% non-fat milk in PBS with 0.5% Tween-20, and immunostained with the following primary antibodies: mouse monoclonal anti-CD44s (clone BBA10) (R&D systems, Minneapolis, MN), and mouse monoclonal anti-tubulin (Sigma-Aldrich, St.-Louis, MO). **Figure SI 4.11** shows a photograph of the obtained blots.

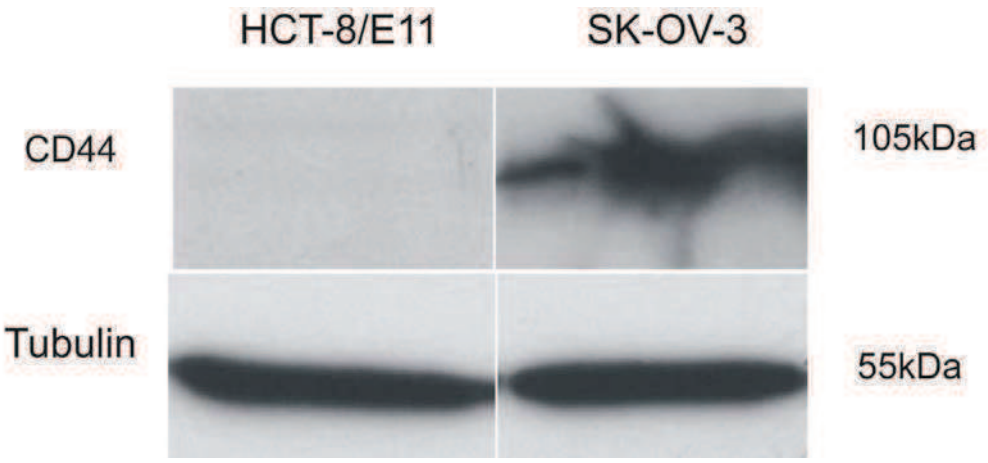

Figure SI 4.11. Western blot analysis of cell lysates.

Cell viability assay. Cells were seeded at a density of 10000 cells / well into 24-well plates. After 24 h, cells were treated for 2.5 h with PTX dispersed in PBS, PTX mixed with non-modified HA, PTX formulated as Abraxane (purchased from Celgene) and PTX formulated in thermosensitive HA nanogels. The latter formulation was kept at 40 °C to assure the presence of nanogels. The cells were thermostated at 37 °C during the addition of the respective samples, again to assure the HA to be preset as nanogels. All experiments were run in five fold. Cultures were washed and conditioned with fresh medium for 6 days. The effect on cell viability was determined using the 3-(4, 5-dimethylthiazol-2-yl)-2, 5-diphenyltetrazolium bromide (MTT) metabolic viability assay. This is a sensitive, quantitative and reliable assay that measures the conversion of the yellow MTT substrate into a dark blue formazan salt by cellular dehydrogenases. Optical densities were obtained by measuring the dissolved formazan crystals with a spectramax paradigm multi-mode microplate detection platform (Molecular devices, Sunnyvale, CA) at 570 nm. **Figure SI 4.12** shows a resume of the cell viability data obtained from adding different concentrations of PTX.

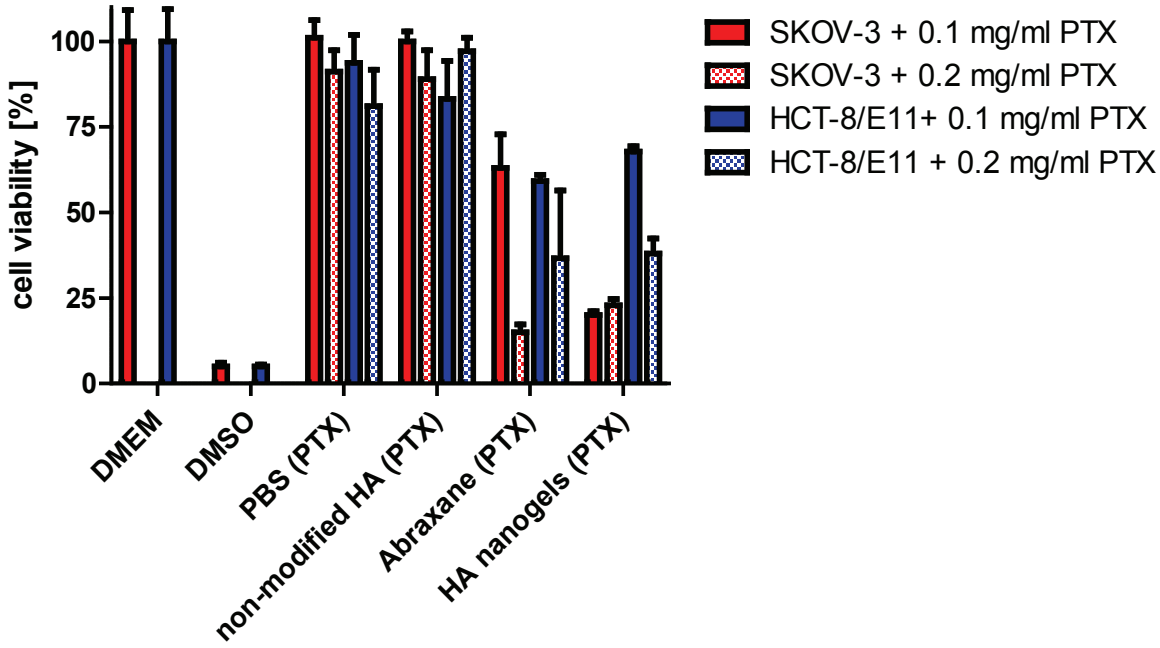

Figure SI 4. 12. Cell viability of SKOV-3 and HCT/8E-11 cells treated with controls (no PTX added) and the respective PTX formulations.

4.5. Complementary results

- Analysis of the thermal behavior of aqueous solutions of the HA-poly(DEGMA-co-OEGMA) derivatives by differential scanning calorimetry

In order to have a better insight into the self-association mechanism of the HA-poly(DEGMA-co-OEGMA) copolymer, differential scanning calorimetry (DSC) experiments were performed on solutions of the HA-poly(DEGMA-co-OEGMA) derivatives having different DS. The samples prepared in PBS were analyzed on a microDSCIII (Setaram). The difference in heat flow between the sample and the reference (PBS solution) was observed by increasing the temperature from 10 °C to 60 °C at a rate of 0.25 °C/min and then, decreasing the temperature from 60 °C to 10 °C.

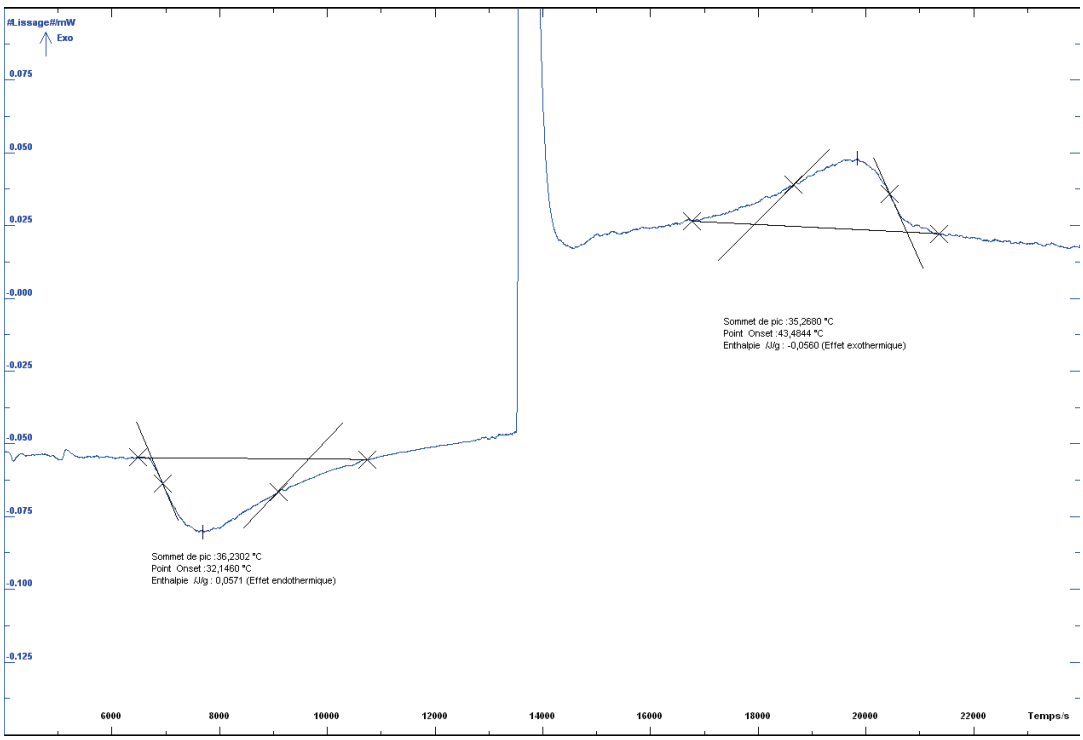

Figure CR 4. 13. DSC curve of HA-poly(DEGMA-co-OEGMA) (DS = 3) at a concentration of 5 g/L in PBS buffer. The temperature increased from 10 °C to 60 °C and then, descended from 60 °C to 10°C at 0.25 °C/min.

In all experiments, endothermic peaks were produced upon heating the solutions as a result of the self-association of the HA-poly(DEGMA-co-OEGMA) copolymers caused by the dehydration of the poly(DEGMA-co-OEGMA) chains (**Figure CR 4.13**). **Table CR 4.1.**

presents les thermodynamics characteristics of solutions of the hybrid copolymers and of the poly(DEGMA-co-OEGMA) copolymer derived from DSC measurements. We found that the temperature of the beginning of the coil-to-nanoparticle transition was identical for all the three samples (DS 3, 4 and 6) and corresponds to the LCST value of the poly(DEGMA-co-OEGMA) copolymer (32 °C). The temperature at the maximum of the endothermic peak was in good agreement with the cloud point determined from the transmittance measurements (~35°C) (Figure 4.1.A). Interestingly, the values of this temperature decreases as the DS of the hybrid copolymers increases, indicating stronger hydrophobic interactions for the HA derivatives containing higher amounts of poly(DEGMA-co-OEGMA) chains. The relative enthalpy value (ΔH value per poly(DEGMA-co-OEGMA) chain) obtained for solutions of the HA derivatives by DSC measurements was closed to the ΔH value obtained from the poly(DEGMA-co-OEGMA) copolymer ($\Delta H \sim 35$ kJ mol^{-1}).

Table CR 4. 1. Thermodynamic characteristics obtained by DSC measurements in PBS buffer from 10°C to 60°C at 0.25 °C/min.

Sample	C (g L^{-1})	T_{Tr}[a] (°C)	T_{max}[b] (°C)	ΔH[c] (J g^{-1})	$n_{copolymer}$[d] (mol)	$\Delta H/n_{copolymer}$ (J mol^{-1})[e]
HA-poly(DEGMA-co-OEGMA) **DS 3**	5	32.15	36.23	0.0571	1.63×10^{-7}	350594
HA-poly(DEGMA-co-OEGMA) **DS 4**	5	32.17	36.09	0.0643	1.83×10^{-7}	350757
HA-poly(DEGMA-co-OEGMA) **DS 6**	5	32.20	35.88	0.0745	2.10×10^{-7}	355365
	10	31.30	34.83	0.1406	4.19×10^{-7}	335331
poly(DEGMA-co-OEGMA)	3	32.06	36.00	0.0623	1.77×10^{-7}	351164
	1.5	33.00	36.64	0.0322	8.87×10^{-8}	363001

[a]Temperature of the beginning of the coil-to-nanoparticle transition; [b]Temperature at the maximum of the endothermic peak; [c]Enthalpy value for 1 g of sample; [d]Amount of copolymer on mole correspond to 1 mL of sample; [e]Relative enthalpy value per one mole of copolymer.

4.6. Conclusion

We have synthetized thermoresponsive hyaluronic acid derivatives. Their LCST value revealed the LCST of grafted copolymer. At the body temperature, HA-copolymer was shown to self-assemble into nanogels with the ability to encapsulate hydrophobic molecules into their hydrophobic domain. The size of nanogel was found to vary depending on the DS of copolymer. *In vitro* cell viability studies showed that with incorporating the hydrophobic anti-cancer drug paclitaxel, the nanogels exhibited high effective and selectivity in the eradication of CD44 positive human ovarian cancer cells. These results suggest that these temperature-triggered nanogels hold great potential for hydrophobic drug delivery.

References

(1) Day, A. J.; Prestwich, G. D. *Journal of Biological Chemistry* **2002**, *277*, 4585.

(2) Hua, Q.; Knudson, C. B.; Knudson, W. *Journal of Cell Science* **1993**, *106*, 365.

(3) Choi, K. Y.; Chung, H.; Min, K. H.; Yoon, H. Y.; Kim, K.; Park, J. H.; Kwon, I. C.; Jeong, S. Y. *Biomaterials* **2010**, *31*, 106.

(4) Choi, K. Y.; Min, K. H.; Na, J. H.; Choi, K.; Kim, K.; Park, J. H.; Kwon, I. C.; Jeong, S. Y. *J. Mater. Chem.* **2009**, *19*, 4102.

(5) Yadav, A. K.; Mishra, P.; Jain, S.; Mishra, P.; Mishra, A. K.; Agrawal, G. P. *J. Drug Targeting* **2008**, *16*, 464.

(6) Farokhzad, O. C.; Langer, R. *ACS Nano* **2009**, *3*, 16.

(7) Loomis, K.; McNeeley, K.; Bellamkonda, R. V. *Soft Matter* **2011**, *7*, 839.

(8) Yallapu, M. M.; Jaggi, M.; Chauhan, S. C. *Drug Discovery Today* **2011**, *16*, 457.

(9) Park, S.-j.; Na, K. *Journal of Pharmaceutical Investigation* **2010**, *40*, 201.

(10) Oh, J. K.; Lee, D. I.; Park, J. M. *Progress in Polymer Science* **2009**, *34*, 1261.

(11) Iida, N.; Bourguignon, L. Y. W. *Journal of Cellular Physiology* **1997**, *171*, 152.

(12) Bourguignon, L. Y. W.; Zhu, H.; Chu, A.; Iida, N.; Zhang, L.; Hung, M.-C. *Journal of Biological Chemistry* **1997**, *272*, 27913.

(13) Choi, K. Y.; Chung, H.; Min, K. H.; Yoon, H. Y.; Kim, K.; Park, J. H.; Kwon, I. C.; Jeong, S. Y. *Biomaterials* **2009**, *31*, 106.

(14) Choi, K. Y.; Min, K. H.; Na, J. H.; Choi, K.; Kim, K.; Park, J. H.; Kwon, I. C.; Jeong, S. Y. *Journal of Materials Chemistry* **2009**, *19*, 4102.

(15) Yang, X.; Kootala, S.; Hilborn, J.; Ossipov, D. A. *Soft Matter* **2011**, *7*, 7517.

(16) Lee, H.; Ahn, C.-H.; Park, T. G. *Macromolecular Bioscience* **2009**, *9*, 336.

(17) Yadav, A. K.; Mishra, P.; Jain, S.; Mishra, P.; Mishra, A. K.; Agrawal, G. P. *Journal of Drug Targeting* **2008**, *16*, 464.

(18) Hawkins, M. J.; Soon-Shiong, P.; Desai, N. *Advanced Drug Delivery Reviews* **2008**, *60*, 876.

(19) Lutz, J.-F.; Hoth, A. *Macromolecules* **2006**, *39*, 893.

(20) Lutz, J.-F.; Akdemir, O.; Hoth, A. *Journal of the American Chemical Society* **2006**, *128*, 13046.

(21) Boyer, C.; Bulmus, V.; Davis, T. P.; Ladmiral, V.; Liu, J.; Perrier, S. *Chemical Reviews (Washington, DC, United States)* **2009**, *109*, 5402.

(22) Willcock, H.; O'Reilly, r. K. *Polymer Chemistry* **2010**, *1*, 149.

(23) Hashidzume, A.; Morishima, Y.; Szczubialka, K. *Handbook of Polyelectrolytes and Their Applications* **2002**, *2*, 1.

(24) Amiji, M. M. *Carbohydrate Polymers* **1995**, *26*, 211.

(25) Gautier, S.; Boustta, M.; Vert, M. *Journal of Controlled Release* **1999**, *60*, 235.

General conclusion (en)

Polysaccharides, due to their outstanding merits such as safety, non-toxicity and biodegradability, have received more and more attention in the field of drug delivery. Hyaluronic acid is a highly hydrated polysaccharide of great biological interest. It can be easily chemically modified, resulting in many kinds of functional polysaccharide derivatives. In this thesis, we have synthesized different types of HA derivatives in aqueous media. These comprise alkylated HA derivatives, HA-cyclodextrin conjugates, and hybrid copolymers made of HA and of a thermosensitive ethylene glycol copolymer.

The alkylated HA derivatives were studied in a previous work done in our laboratory. These amphiphilic polysaccharides can self-associate in aqueous solution, due to the formation of hydrophobic nanodomains of alkyl chains. The latter show good ability to incorporate hydrophobic dyes and drugs, such as nile red and paclitaxel, respectively. β-Cyclodextrin molecules were grafted onto HA by a mild and rapid "thiol-ene" reaction. The resulting HA-CD could bind several paclitaxel molecules via the pendant CD cavities. The high increase of paclitaxel solubility in water was attributed to the high hydrophilic character of HA.

Based on the ability of alkylated HA and cyclodextrin grafted HA to accomodate hydrophobic molecules paclitaxel into their hydrophobic "nanocavities", we then demonstrated the formation of polyelectrolyte multilayer capsules based on these HA derivatives. These capsules were prepared by the layer-by-layer deposition of oppositely charged polyelectrolytes on $CaCO_3$ particles, followed by decomposition of the carbonate core. These carriers have attracted a great deal of interest due to their multicompartment structure with the possibility to introduce a high degree of functionality at the nanometer scale within the shell. The loading of PTX in the nanoshell was achieved by first complexing PTX with HA derivatives in solution and then, depositing these PTX-containing polyelectrolytes alternately with poly(L-lysine) according to the layer-by-layer technique. The capsules made from alkyl HA showed durability of drug entrapment under physiological conditions after several days. Interestingly, HA-CD lead to capsules which showed sustained release of PTX within a period of five days. In the two cases, the PTX loaded capsules were found to decrease the viability and proliferation of MDA MB 231 breast cancer cells, while unloaded capsules did not impact cell viability. Due to these promising results, these hydrophobic polysaccharide nanoshells open new avenues for applications of hydrophobic drug-carrier systems in nanomedicine.

Thiol modified poly(diethyleneglycolmethacrylate - oligoethyleneglycolmethacrylate (poly(DEGMA-co-OEGMA)) was reacted with a HA-maleimide conjugate to obtain HA-poly(DEGMA-co-OEGMA). The LCST value of this HA-copolymer was determined to be around 35°C via turbidity measurements. At the body temperature, HA-copolymer was thus shown to self-assemble into nanogels with the ability to encapsulate hydrophobic molecules into their hydrophobic domain. The size of nanogel was found to vary between 190 and 320 nm, depending on the DS of the HA-poly(DEGMA-co-OEGMA) conjugates. In vitro cell culture studies showed that with incorporating the hydrophobic anti-cancer drug paclitaxel, the nanogels exhibited high efficiency and selectivity in the eradication of CD44 positive human ovarian cancer cells. These results suggest that these temperature-triggered nanogels hold great potential for the delivery of chemotherapeutics in anti-cancer therapy.

Conclusion générale (fr)

Polysaccharides suscitent un intérêt croissant dans le domaine de délivrance de médicaments en raison de leurs propriétés exceptionnels telles que la non-toxicité et la biodégradabilité. L'acide hyaluronique est un polysaccharide fortement hydraté. Grâce à sa présence naturelle dans le corps humain et aux nombreuses possibilités de modifications chimiques de ce polysaccharide, l'acide hyaluronique est un bon candidats pour la conception de transporteurs de principes actifs. Dans cette thèse, nous avons synthétisé différents types de dérivés du HA en milieu aqueux. Ceux-ci comprennent les dérivés alkylés du HA, HA-cyclodextrine conjugués et des copolymères «hybrides» composés de HA et d'un copolymère thermosensible de l'éthylène glycol.

Les dérivés alkylés du HA ont été étudiés dans les travaux précédent au sein du laboratoire. Ces polysaccharides amphiphiles peuvent s'auto-associer en solution aqueuse par la formation de nanodomaines hydrophobes par des chaînes alkyle. Le dernier présente une forte capacité d'incorporer d'une sonde fluorescente and un médicament hydrophobe, tels que le nile red et le paclitaxel, respectivement. La β-cyclodextrine a été greffé sur le HA par une réaction douce et rapide de couplage de type "thiol-ène". Le HA-CD peut encapsuler les molécules de paclitaxel par la présence de la cavité hydrophobe de cyclodextrine. La forte augmentation de la solubilité du paclitaxel dans l'eau a été attribué au caractère hydrosoluble de HA.

Basé sur la capacité d'accueillir des molécules hydrophobes paclitaxel dans leurs hydrophobes "nanocavités", nous avons ensuite montré la formation de multicouches de polyélectrolytes de capsules à partir de ces dérivés du HA. Ces capsules ont été préparés par dépôt couche par couche de polyélectrolytes de charges opposées sur les particules de $CaCO_3$, suivie de sa décomposition. La paroi de ces capsules "multicompartiments" est donc constituée d'un film multicouche de polymères permettant d'introduire diverses fonctionnalités. L'insertion des molécules paclitaxel dans la paroi des capsules a été réalisée par pré-complexation avec les dérivés du HA en solution, et ensuite déposition ces PTX-polyélectrolytes avec le poly(L-lysine) selon la technique de couche par couche. Les capsules à base de HA alkylé ont montré une durabilité d'incorporation des molécules hydrophobe dans les conditions physiologiques pendent plusieurs jours. Les molécules incorporées ne libèrent pas. Mais, les capsules à base de HA-CD ont pu libérer le PTX sur une période de 5 jours. Dans les deux cas, les capsules chargées de PTX ont été trouvés qu'elles permettent de réduire la viabilité et la prolifération

des cellules cancéreuses. Ces multicouches ouvrent de nouvelles voies vers des applications en nanomédecine, comme systèmes transporteurs de médicaments hydrophobes.

L'acide hyaluronique modifié par maleimide a été réagit avec poly(diethyleneglycolmethacrylate - oligoethyleneglycolmethacrylate (poly(DEGMA-co-OEGMA)) modifié par thiol afin d'obtenir le copolymère «hybrides» thermosensible. La valeur de la LCST de ce copolymère de HA est autour de 35 °C en déterminant par les mesures du point de trouble des solutions. Au-dessus de cette température, le HA-poly(DEGMA-co-OEGMA) conduit à la formation des nanogels avec la capacité d'encapsuler des molécules hydrophobes dans leur domaine hydrophobe. La taille des nanogels dépend du DS du copolymère hybride en variant entre 190 et 320 nm. Les nanogels chargés en PTX ont montré une cytotoxicité plus élevée avec des cellules du cancer surexprimant le récepteur CD44. Ces résultats suggèrent que ces nanogels thermosensible pourraient s'avérer être des candidats intéressants pour la libration thérapeutique dans le traitement de cancer.

Annexes

Article

Polyelectrolyte multilayer nanoshells with hydrophobic nanodomains for delivery of Paclitaxel

Journal of Controlled Release, Volume 159, Issue 3 (10 May 2012), p. 403-412.

Thomas Boudou, Prathamesh Kharkar, Jing Jing, Raphael Guillot, Isabelle Pignot-Paintrand, Rachel Auzely-Velty, Catherine Picart

Cf :

http://www.sciencedirect.com/science/article/pii/S0168365912000272

List of Figures

List of Schemes

List of Tables

Abbreviations

Abbreviation	Name
ALG	Alginate
AuNPs	Gold nanoparticles
β-CD	β-Cyclodextrin
BSA	Albumin from bovine serum
CHI	Chitosan
DC	Dendritic cell
DEGMA	Diethyleneglycolmethacrylate
DEX	Dextran
DEXS	Dextran sulphate
DM-β-CD	heptakis-(2,6-di-*O*-methyl) β-cyclodextrin
DOX	Doxorubicin
DS	Degree of substitution
EDC	1-ethyl-3-(3-dimethylaminopropyl) carbodiimide
EDTA	Ethylenediaminetetraacetic acid
EGCG	Epigallocatechin gallate
EGFR	Epidermal growth factor receptor
EPR	Enhanced Permeability and Retention
FITC	Fluorescein isothiocyanate
HA	Hyaluronic acid
HA20C10	Decylamino hydrazide hyaluronic acid (DS = 0.2)
HA-CD	β-Cyclodextrin grafted hyaluronic acid
HER2	Human epidermal growth factor receptor 2
LbL	Layer-by-Layer
LCST	Lower critical solution temperature
mAb	Monoclonal antibodies
MPS	Mononuclear phagocytic system
MTT	3-(4,5-dimethylthiazol-2-yl)-2,5-diphenyltetrazolium bromide
NP	Nanoparticle
NR	Nile red
OEGMA	Oligoethyleneglycolmethacrylate
OG-PTX	Oregon green-labeled paclitaxel
PAH	Poly(acrylic acid)
PARG	Poly-L-arginine
PBS	Phosphate buffer saline
PCL	Polycaprolactone
PEG	Poly(ethylene glycol)
PEI	Poly(ethyleneimine)
PGA	Poly(L-glutamic acid)
PLA	Poly(lactic acid)

PLL	Poly(L-lysine)
PMA	Poly(methacrylic acid)
PSS	Poly(styrene sodium sulfate)
PTX	Paclitaxel
PVPON	Poly(*N*-vinyl pyrrolidone)
QCHI	Quaternized chitosan
QD	Quantum dots
RAFT	Reversible addition fragmentation chain transfer
RES	Reticuloendothelial system
SDS	Sodium dodecyl sulfate
siRNA	Short interfering RNA
sNHS	*N*-hydroxysulfo-succinimide

Symbols

Δf	Frequency shift
ΔH	Enthalpy
K_a	association constant
M_w	Weight-average molar mass
R_h	hydrodynamic radius

List of Instruments

AFM	Atomic Force Microscopy
CLSM	Confocal Laser Scanning Microscopy
DLS	Dynamic light scattering
DSC	Differential scanning calorimetry
SEM	Scanning Electron Microscopy
QCM-D	Quartz Crystal Microbalance with Dissipation

Design and evaluation of hydrophobic drug delivery systems based on chemically modified polysaccharides: toward new approaches for anti-cancer therapy

This work focused on the design of hydrophobic drug carrier made of chemically modified polysaccharide, especially derivatives of hyaluronic acid (HA).
The layer-by-layer capsules possessing a fascinating multicompartment structure have recently as attractive vehicles used for biomedical applications. In order to encapsulate the anti-cancer hydrophobic drugs, paclitaxel (PTX), within the wall of capsules, alkylated derivatives and cyclodextrin (CD) conjugate of HA were synthesized. The alkylated HA derivatives can self-associate in aqueous solution to form hydrophobic nanodomains of alkyl chains which show good ability to incorporated hydrophobic molecules. The HA-cyclodextrin conjugates could bind selectively PTX molecules via the pendant CD cavities. The capsules were prepared by depositing these PTX-containing polyelectrolytes alternately with poly(L-lysine). When breast cancer cells were incubated with these two types of PTX-loaded capsules, their viability was found to strongly decrease.
Self-assembled nanogels based on HA were also investigated. A thermosensitive copolymer of diethyleneglycolmethacrylate and oligoethyleneglycolmethacrylate was grafted onto HA chains in order to allow temperature-induced self-assembly into nanogels with tunable size. These nanogels can be easily loaded with hydrophobic molecules and hold potential for paclitaxel delivery towards human ovarian cancer cells.

Conception et évaluation de systèmes transporteurs de principes actifs hydrophobes à base de polysaccharides modifiés: vers de nouvelles approches pour la thérapie anti-cancéreuse

Ce travail de thèse porte sur la conception de transporteur de médicament hydrophobe basé sur les polysaccharides chimiquement modifiées, notamment de dérivés d'acide hyaluronique.
Les capsules couche par couche possédant une structure multicompartiment suscitent un intérêt important pour des applications biomédicales. Afin d'encapsuler des médicaments hydrophobes anti-cancéreuse, le paclitaxel (PTX), dans la paroi de capsules, les dérivés alkylé du HA et HA-cyclodextrine (CD) conjugué ont été synthétisés. Les HA alkylés peuvent s'auto-associer en solution aqueuse pour former des nanodomaines hydrophobes par des chaînes alkyles qui montrent une bonne aptitude pour incorporer les molécules hydrophobes. Les HA-cyclodextrines peuvent encapsuler sélectivement des molécules PTX via les cavités de CD. Les capsules ont été ensuite préparées en déposant alternativement ces PTX-polyélectrolytes et le poly(L-lysine). Lorsque les cellules cancéreuses du sein ont été incubées avec ces deux types de capsules chargées en PTX, leur viabilité a diminué fortement.
Une nouvelle classe de nanogels à base de HA a été également étudiée. Ces nanogels sont obtenus avec une taille réglable par auto-association en milieu aqueux de dérivés de HA modifié par un copolymère thermosensible de diéthylèneglycolméthacrylate et oligoéthylèneglycolméthacrylate, induite par une élévation de la température. Ces nanogles sont capables d'encapsuler facilement des molécules hydrophobes. En chargeant en PTX, ces nanogles présentent un potentiel important pour transporter le PTX vers les cellules cancéreuses ovariennes.